The University Of Sheffield.

THE INFLUENCE OF RANDOM MICROSTRUCTURE ON WAVE PROPAGATION THROUGH HETEROGENEOUS MEDIA

Yilang Song

A thesis submitted for the degree of Doctor of Philosophy

Department of Mechanical Engineering

02/2015

Summary

In this thesis the influence of mechanical and geometrical properties of a heterogeneous periodic composite material (in 1D and 2D), both deterministic and stochastic in nature, on wave propagation has been analysed from the position of stop band phenomenon.

Numerical analyses have been used to identify those parameters that have the most significant effect on the wave filtering properties of the medium. The study has started on a 1D periodic laminate material. Further, a randomness has been added into the material's properties in order to study its influence on the stop band. The stop band phenomenon has also been studied on the material in a 2D case, first with periodic microstructure, then with randomness added into the microstructure to test its influence on the stop band. Special attention has been given to the prediction of the first stop band frequency with numerical analysis of an explicitly defined heterogeneous structure compared and confirmed by results obtained using gradient theory and analytical derivations.

Acknowledgement

I wish to express my sincere appreciation to those who have contributed to this thesis and supported me in one way or the other during this amazing journey.

First of all, I am extremely grateful to my main supervisor, Dr. Inna Gitman, who offered her continuous advice and encouragement throughout my PhD. I thank her for the systematic guidance and great effort she put into training me in the scientific field. I also remain indebted for her understanding and support during the times when I was really down and depressed due to personal problems.

My sincere gratitude is reserved for Professor Harm Askes for his guidance and unyielding support. His deep insights helped me at various stages of my research.

Very special thanks to the Leverhulme Trust for their financial support. With their support, a great team was united including Dr. William J. Parnell, Ruth Voisey and Ellis Barnwell from University of Manchester; Prof. Harm Askes, Dr. Inna Gitman, Dr. Terry Bennett (University of Adelaide), Kwame Koduah-Sarpong and me from University of Sheffield. I am so proud to be one of them. Besides, with the Leverhulme Trust's support, I could focus on the research without worrying to much about living cost.

I would like to thank Dr. William J. Parnell for his organisation of this group and his suggestions. He is so kind and showed tremendous patient to me during our co-working period. I would also like to thank Ruth Voisey, Ellis Barnwell and Kwame Koduah-Sarpong for their encouragement and support. With them I experienced different culture and gain great friendship.

PhD students often talk about loneliness during the course of their study but this is something which I never experienced at Sheffield. A heartfelt thanks to Zefeng Wang, Linhao Fang, Yin Xia, Jingchao Zhou, Shen Chen, Yiyin Hao, Si Chen and other friends not only for all their useful suggestions but also for being there to listen when I needed an ear.

Words cannot express the feelings I have for my parents and my brother for their constant unconditional support - both emotionally and financially. I want to thank my grandparents as well, although they have already passed away, I believe they would be more than happy to know my accomplishment.

Contents

List of Figures

List of Tables

Chapter 1

Introduction

It is well known that heterogeneous materials behave very differently from their homogeneous counterparts, particularly when they are subjected to dynamic loading. This is principally ascribed to the presence of wave dispersion in heterogeneous materials and leads to a wide variety of interesting dynamic effects. One certain well-studied phenomenon caused by wave dispersion is the presence of what are known as *stop bands* or *band gaps* (i.e., intervals of frequencies where wave propagation is not permitted). Well described in the book by Brillouin [1], the phenomenon has mainly been studied in two-phase materials with periodic structure [2–4].

1.1 Introduction of a stop band phenomenon

The stop band phenomenon was first found in ordinary crystals, when electrons propagate inside them. The atoms inside the crystals are arranged periodically and can interact with the electrons to create electron band gaps. The the stop band was found in the photonic crystals, where electromagnetic waves can interact with the composite material with dielectric properties to create photonic band gaps [5]. Following discovery of the photonic crystals, a material with an elastic wave band was found and named the phononic crystal material [6]. Phononic crystals, also named elastic band gap (EBG) materials, are heterogeneous elastic media composed of periodic arrays of inclusions embedded in a matrix. The propagation of sound and vibrations in these materials can be strictly prohibited in certain frequency ranges [4, 7, 8].

Hence, it is possible to apply phononic crystals in many circumstances. Phononic crystals can be designed as an elastic filter with 1D [9], 2D [4, 7, 10–25]or 3D [26] microstructure based on different applications. Phononic crystal has potential to be used as noise attenuation material for reducing the noise from traffic. A noted experiment in the stop band phenomenon field carried out by Martinez-Sala and co-workers [27] demonstrated the sound attenuation effect of a sculpture built by Eusebio Sempere. The phononic crystal can also be applied to manufacturing refractive acoustic devices [28]. In addition to these uses, a phononic crystal can be employed as waveguide device [29].

Two developed theories explain the stop band phenomenon in phononic crystals: Bragg scattering theory [10] and local resonance theory [30]. Based on the Bragg scattering

theory, an elastic wave passing through an elastic periodic material at certain frequencies, looses the possibility of vibration mode, thus resulting in the stop band. However, this theory presents difficulty in explaining the phenomenon at low frequencies (especially under 1kHz). Different from the above theory, Liu's local resonance theory indicates that the stop band phenomenon occurs because, at certain frequencies, scatter in the composite material has resonance and interacts with the elastic wave to prevent its propagation. This theory can properly explain the stop band at low frequencies.

1.2 Methods of studying stop band phenomena

To understand the stop band phenomenon, a number of studies have been undertaken both experimentally and theoretically. Experimentally, research is mostly focused on finding stop bands for composite materials in the two-dimensional case [8, 31–40]. Theoretically, several methods have been applied to predict stop bands for materials with both periodic and non-periodic geometrical microstructures [5, 30, 41–51]. Both strands of research are discussed in more detail below.

1.2.1 Experimental studies for stop band phenomenon

Experiments can help researchers understand the stop band phenomenon and verify and validate theoretical predictions. At the same time, experiments can be the first step in potential engineering applications of phononic crystal design. A number of experiments have been conducted by researchers [9, 52–65], and most are based on material with periodic microstructure. Experiments in the phononic crystal field can be divided into two types: acoustic wave propagation experiments and elastic wave propagation experiments.

Acoustic wave propagation experiments

In acoustic wave propagation experiments, waves are typically produced by loudspeakers and received by microphones. These experiments are generally used to discover stop bands for cylinders (made of steel, glass, PVC, and so on) that are periodically arranged in air. Vasseur et al. [8] investigated stop bands for materials with both solid and hollow copper cylinders periodically placed in air and water. The experiments indicated that the thickness of the hollow cylinder does not influence the properties of the stop band when the matrix is air, but does significantly influence them when the matrix is water. Lu et al. [66] experimented with Al/air composites, including solid, hollow, and semi-hollow-shaped Al cylinders. They found that, compared to solid and hollow cylinder systems, semi-hollow cylinder systems obtained the best stop band performance.

Elastic wave propagation experiments

In elastic wave propagation experiments, the well-known ultrasonic transmission technique is applied. Vasseur et al. [6] proved band gaps (120-270 kHz and 430-510 kHz) existence in a steel/epoxy composite (steel cylinders are arranged by triangular

array). The same material (steel/epoxy composite in which steel cylinders are arranged by square array) has been studied by Zhang et al. [40] as well. The researchers discovered two stop bands (100-200 kHz and 340-400 kHz); this result is in agreement with finite element (FE) simulation results. These two experiments [6, 40] show that fiber arrangement can affect the stop band phenomenon.

1.2.2 Theoretical methods for stop band prediction

Phononic crystals have been studied not only experimentally but also theoretically. Different methods have been proposed for calculating the frequency stop band, such as the plain-wave expansion (PWE) method [2, 3], the multiple-scattering (MS) method [5], the finite difference time domain (FDTD) method [6, 66, 67], the layered MS method [30], the Finite element method [51], and the transfer matrix method [68]. Among them, PWE, MS, and FDTD methods are most commonly used, and are examined in detail. Besides above mentioned approaches, a methodology for stop band prediction, based on gradient theory has been developed in this study and will be introduced in detail in this section as well.

Plain-wave expansion (PWE) method

The plain-wave expansion (PWE) method was first introduced to determine stop bands by Kushwaha et al. [2], who claimed to have achieved "the first full calculation of an "*acoustic*" or "*phononic*" band structure". In this work, the authors analysed the stop band phenomenon for two materials: nickel alloy cylinders (periodically arranged) in an aluminum alloy background, and aluminum alloy cylinders (periodically arranged) in a nickel alloy background. In both cases, they obtained full phononic gaps independent of wave propagation direction [2]. The PWE method can be explained as follows: expanding geometrical properties of periodic material into the Fourier series, then applying the Bloch-Floquet theorem to calculate the eigenmodes [69]. This method is explained in detail in [10].

Similarly, Sigalas and Economou [3] applied the PWE method to examine elastic waves propagating through composite material which had a host material (Lucite) embedded with periodically placed cylindrical inclusions (such as Fe, steel, Pb and Mo). In their research, Sigalas and Economou studied the influence of different inclusions on stop bands and found that, generally, stop bands are most likely to appear in materials with a light component as a host and a heavy component as inclusion. Simultaneously, they studied the influence of geometrical differences (square lattices and hexagonal lattices) on stop bands, showing that material with hexagonal lattices were more favourable for stop band creation.

Other materials, such as the carbon/epoxy composite [4], steel/epoxy composite [6] and metallic rods/air composite [7, 8], have been studied based on the PWE method. However, the PWE method can only be applied to material with a periodic structure and in infinite space. As such this presents a limitation to its applicability in terms of real life applications, where finite structure of non-periodic properties are of interest.

Multiple-scattering (MS) method

The multiple-scattering (MS) method was originally developed to calculate the propagation of electrons. The elastic wave propagation in phononic crystals can be treated as an analogy to the propagation of electrons in an electronic structure. Hence, the MS method has been transferred to calculate frequency stop bands in phononic crystals [5].

The fundamental concept of the MS method is that for any scatter in a system, the incident wave can be treated as a sum of scattered waves from other scatters in the same system plus an external field. Based on this idea, a total field can be determined and the transmission coefficient can be calculated. The MS method is discussed in detail in [5].

Biwa et al. [70] applied this method to predict stop bands for an SiC/Ti-alloy composite with periodic and random fiber arrangements. In this work, they found that stop bands occurred at $kd = \pi$ and $kd = 2\pi$ (where k is the wave number and d is the distance between fiber centres) with square fiber arrangement and $kd = 4\pi/3$ and $kd = 2\pi$ with hexagonal fiber arrangement. However, in this work, no significant stop band was observed in composites with randomly arranged fibers. Based on the MS method, Kobayashi et al. [71] studied the same material (SiC/Ti-alloy composite) in finite length periodic material. In this research they indicated that stop bands appeared in a finite length of the material at the same frequency ($kd = \pi$ and $kd = 2\pi$). In the same paper [71], the authors compared the influence of the material's length to stop bands. This comparison showed that the longer the material is (26 fibers arrangement comparing to 10 fiber arrangement in the material), the more significant the stop band phenomenon will appear.

Finite difference time domain (FDTD) method

The finite difference time domain (FDTD) method has been applied in photonic [72–76] and acoustic fields [77–79] successfully and has been introduced to calculate stop band in phononic crystals. The FDTD method can a) obtain field results in both time and frequency domains; b) do finite length material simulation which can be compared to experiments directly [80]; and c) calculate stop bands for composites not only with periodic microstructure but also random microstructure [5]. The FDTD method is based on a discrete time and space domain, as discussed in [5].

Vasseur et al. [6] applied the FDTD method to calculate stop bands for a steel/epoxy composite (solid/solid system) with periodically arranged steel cylinders. After simulation, the researchers obtained two stop bands for the steel/epoxy composite, compared them to the results generated from applying the PWE method on the same material, and found good agreement. The FDTD method was also applied by Vasseur et al. [8] to calculate stop bands for a copper/air composite (solid/fluid system). Lu et al. [66] studied the stop band phenomenon for Al semi-hollow cylinder embedded in air based on the FDTD method. They compared simulation results with solid Al/air composite and hollow cylinder (Al)/air composites, which indicated that the semi-hollow cylinder/air material exhibits a wider stop band.

Stop band prediction based on gradient theory

Previous theoretical stop band prediction methods all suffer from being complex and time consuming. In this project, to calculate the stop band more efficiently, gradient elasticity theory [81] is introduced and applied to predict the stop band (see Chapter 3 and Chapter 4) .

Gradient elasticity theory is a homogenisation method which considers not only local effects on the infinitesimal points of interest, but also the surroundings of these infinitesimal points under loading by adding extra gradient terms in Hooke's law. Using gradient elasticity theory makes it possible to predict the wave dispersion effect in material in which the classical Hooke's law does not capture the wave dispersion [82]. By considering the influence of material microstructure, which is represented by a length scale (an additional parameter preceding the extra gradient term), it is possible to use gradient theory to predict the stop band. The gradient theory is introduced in detail in Chapter 3 and followed in Chapter 4 by its application.

1.3 Material randomness and stop bands

Most of the works introduced earlier in this chapter are based on periodic material. When materials' parameters include randomness, the stop band predictions will be different. The randomness could be introduced to the material during the manufacturing process, for example in certain applications a carbon fiber composite material follows manual manufacturing process: the carbon fibers are scattered manually over the host material.

Nakashima and co-workers [51] studied the influence of randomness on 2D material's geometrical properties on the stop band. In their work, the 2D material is a rectangular material with five circle inclusions. The randomness is added to change the position of these inclusions but the position change only happens in the direction perpendicular to the wave propagation direction. The results show that, within randomness, the wave transmission is reduced as a whole compared to material without any randomness. However, the work only had three realizations with randomness which, as a sample number, is quite small. In addition, the 2D material with randomness has only one inclusion in the direction perpendicular to the wave propagation direction which means the 2D material is an inadequate representation for the material with multiple inclusions in the direction perpendicular to the wave propagation direction.

Liang and Patil [69] studied the influence of randomness on the stop band, based on fiber-reinforced composite material with quasi-random fiber arrangements. Their simulation result indicates that randomness can create a noticeable difference in wave propagation. Moreover, at some frequencies, an addition of randomness into material may change the stop band into a pass band.

To study the influence of randomness on wave propagation, such experiments have also been carried out. Vasseur and Deymier [83] conducted an experiment to study acoustic wave propagation though both periodic and random 2D composite material with circle

inclusions. Their experiment indicates that the randomness only has limited influence on wave propagation though the composite media. However, their experiment with randomness only had one realization.

In this research, randomness will be added to 1D and 2D materials to test the influence of randomness on the stop band. The randomness will be added into both the material's mechanical and geometrical properties. Additionally, the influence of different levels of randomness in the material on the stop band will be studied.

1.4 Aim and scope

The aim of this work is to understand the influence of internal (and particularly non-periodic) structure of a material on a time-harmonic elastic wave propagating through it. Specifically, it is desired to understand how mechanical and geometrical characteristics of the microstructure affect the appearance and / or other properties of stop bands.

The main objectives to achieve the aforementioned aim are presented below:

1. To analyse the stop band phenomenon in a case of one-dimensional laminate material based on classical elasticity, whereby
   (a) analyse the contrast in mechanical properties;
   (b) analyse the influence of geometrical characteristics;
   (c) analyse the influence of periodicity and non-periodicity of materials' mechanical and geometrical properties.
2. To research the stop band phenomenon analytically and numerically based on gradient elasticity in one-dimensional case.
3. To study the stop band phenomenon in two-dimensional case based on classical elasticity by
   (a) analysing the influence of periodicity and non-periodicity of materials' geometrical properties;
   (b) analysing the influence of different shapes of inclusions.
4. To analyse the stop band phenomenon numerically in two-dimensional material based on gradient elasticity.

Structure of the thesis. This thesis is divided into 6 Chapters.

Chapter 1 This chapter introduces the background of the research project and presents the aim and objectives of the research.

Chapter 2 The stop band phenomenon is first studied based on a one-dimensional periodic laminate material. By changing the materials' mechanical and geometrical

properties, the influence of the contrast of the heterogeneous components on the stop band is studied. Further, randomness is added into the materials' properties in order to study its influence on the stop band.

Chapter 3 The gradient elasticity theory is introduced to predict the stop band both analytically and numerically. Both analytical and numerical results based on gradient theory are compared with previously obtained simulation results based on classical elasticity theory for explicit heterogeneous material.

Chapter 4 The stop band phenomenon is studied on material with a two-dimensional microstructure. Following the procedure introduced for a 1D case, the stop band based on 2D material is first analysed for periodic structures. Then different levels of randomness are added into the microstructure to test the influence of randomness on the stop band. Gradient elasticity theory is also applied for the 2D case to confirm the numerical results.

Chapter 5 This chapter concludes the thesis.

Chapter 6 This chapter presents the future research plans.

Chapter 2

Influence of material properties on the stop band phenomenon based on classical elasticity in 1D

In this chapter, the key parameters that influence the stop band (Young's modulus, mass density, and a length of a unit cell) have been analysed for the one-dimensional case. To accomplish this, finite element analysis has been performed. The study was strictly focused on periodic laminates first, followed by an investigation into the influence of randomness added to materials' properties on the stop band.

2.1 Simulation method

In order to define a stop band, band zones should be introduced first. Generally, band zones refer to frequency ranges, in which the wave at all these frequencies has similar propagating behaviour. If the wave can propagate at all frequencies in a frequency range, it becomes a pass band zone, or what is known as a pass band. Otherwise, if the wave cannot propagate at all frequencies in a frequency range, it becomes a stop band zone, otherwise known as a stop band. Analytical techniques fail to produce reliable predictions of the stop / pass band zones in cases of complex (e.g. random) geometries and / or mechanical properties. Alternatively, the finite element method (FEM), which is a numerical method used to solve differential equations that can describe a wide range of physical problems, could easily describe complex geometry involving finite elements with regular shape and discrete continuous problem. Meanwhile, the FEM method is able to simulate dynamic problems with varying timeframes. Hence, in this project, the finite element method has been chosen as the method for running the simulation.

The fundamental principle of FEM is that a complex domain can be divided into regular small regions (known as finite elements), and differential equations which are used to describe these physical problems that can be approximately solved in the small region. Then all equations for small regions can be assembled to analyse the problem for the whole complex domain.

2.2 Simulation procedure

Generally speaking, a finite element simulation needs the following steps [84]:

a A geometrical structure should be created and materials' parameters should be assigned.

b The geometry and materials' parameters should be translated into a numerical model in an appropriate software, here MATLAB.

c The numerical model of the structure should be meshed by appropriate elements (such as triangle element, or square element, the latter of which will be applied in this project) depending on the requirement of the simulation interest.

d Loading and boundary conditions should be added to the structure.

e Running the simulation and recording relevant results.

f Post-processing of recorded results.

All these steps are described in detail in the following sections and one simulation example is presented in detail.

2.2.1 Simulation set-up

A test example is discussed in this section to indicate the structure and the simulation process used in this project for one-dimensional cases. A continuous longitudinal sine wave has been sent through a bar and the signal has been recorded after the wave has propagated through a testing material. By comparing the amplitude difference between the input and output waves, the influence of the material microstructure on the wave propagating through the testing material can be measured. Simulations employed in Chapter 2 all have the same overall structure and are based on the same test set-up with different material properties.

2.2.2 Structure of numerical simulation model in 1D

The numerical model is shown in Figure 2.1 with a bar of a total length $L = 220$ mm, both ends of the bar being fixed horizontally, which became the boundary condition. As shown in the figure, the bar contains four parts, indicated by A_1, A_2, B and C.

Part C (with length $L_C = 100$ mm) is the actual test material which can be heterogeneous or homogeneous depending on the particular research question. Part B (with length $L_B = 10$ mm) is made up of homogeneous material located at the left and right end of Part C. The centre of the left Part B is the source point of the waves and the centre of the right part B is the receiver point after the wave propagates through Part C. Parts A_1 and A_2 (with length $L_{A_1} = L_{A_2} = 25$ mm) attached to Parts B are perfect match layers (PML).

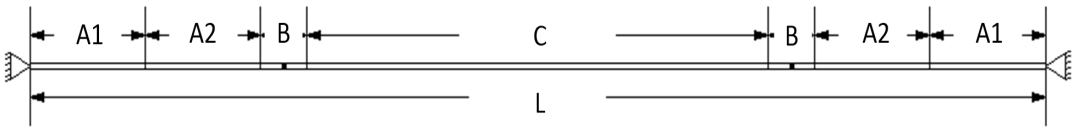

Figure 2.1: Structure of the simulation sample

Table 2.1: Length of each material in the structure

Material	A_1	A_2	B	C
Length (mm)	$L_{A_1} = 25$	$L_{A_2} = 25$	$L_B = 10$	$L_C = 100$

The perfect match layers are materials that can absorb waves without creating any reflection [85]. The PMLs (Parts A_1 and A_2) are added here to remove reflection from left Part A_2 to left Part B and reflection from right Part A_2 to right Part B. Assuming the density of material in Parts B, A_1 and A_2 to be ρ_B, $\rho_{A_2} = 10\rho_B$ and $\rho_{A_1} = 50\rho_B$ and Young's modulus of material in Parts B, A_1 and A_2 to be E_B, $E_{A_2} = 0.1E_B$ and $E_{A_1} = 0.02E_B$. To create perfect match layers, the impendence of Parts B, A_1 and A_2 should be the same and the relation is given by

$$\sqrt{\rho_B E_B} = \sqrt{\rho_{A_1} E_{A_1}} = \sqrt{\rho_{A_2} E_{A_2}} \tag{2.1}$$

Furthermore, the wave speeds in the various parts are related by

$$V_{A_2} = \sqrt{\frac{E_{A_2}}{\rho_{A_2}}} = 0.1V_B \tag{2.2}$$

$$V_{A_1} = \sqrt{\frac{E_{A_1}}{\rho_{A_1}}} = 0.02V_B \tag{2.3}$$

In this way, when the wave propagates though Part B to Part A_2 there will be no reflection; and because of low wave speed in Parts A_1 and A_2 there will be no reflection from either end of the model before the simulation is complete. Theoretically, Parts A_1 and A_2 can combine into one part with an appropriate property and will not influence the entire simulation. However, if the difference of wave speed between Part B and PML is too large the noise of simulation will have a significant influence on the results. Hence, in this project, perfect match layers are divided into Parts A_1 and A_2 to reduce the noise of the simulation.

In this study, the value of damping and Poisson's ratio of all materials are considered to be zero to simplify simulation.

2.2.3 Simulation process and transmission coefficient

The stop band frequency is assessed by the transmission coefficient (T). There are different definitions of a "stop band". In this project we assume that when T is less than 5% the wave propagation in the material can be interpreted as *"stopped"* and the frequency of the wave fulfilling this condition is deemed to fall within the stop band. To determine the stop band frequency, it is necessary to evaluate wave propagation for a range of frequencies.

For each transmission coefficient of one test material at one frequency, two simulations have been undertaken; one with homogeneous material in Part C which is then taken to be the same as material in Part B; and one with heterogeneous material in Part C. In simulation, the homogeneous material normally chosen has the average material property for testing heterogeneous material. For both simulations, a continuous sine wave with a single frequency has been used: set force $F_g = A_g \sin(\omega t)$ at the source point where A_g is amplitude, ω is angular frequency and t is time. Furthermore, the boundary condition and initial condition can be formulated as b.c., $u(0) = u(L) = 0$; i.c., $t = 0, v(x) = u(x) = 0$ (u is displacement and v is velocity). U is the displacement recorded at the receiver point: U_h for homogeneous material simulation and U_c for heterogeneous material simulation. The displacements are recorded since the wave approached the receiving point until the simulation ends. Then a Fourier transform has been applied to U_h and U_c, and the amplitude of the propagated wave at incident wave frequency was obtained, indicated by the Fourier-transformed signal by A_h and A_c. In this study, the signal received at the recording point usually contains more than 30 periods and is convergence (for heterogeneous testing material). Hence, when applying the Fourier transform,the influence of the leakage is minor. The transmission coefficient of the test material at the given frequency is then defined as

$$T = \frac{A_c}{A_h} \tag{2.4}$$

The transmission coefficient defined by Eq. (2.4) thus describes the amplitude change of the wave after it propagates through the test material C at a given single frequency. As such, for a particular frequency a conclusion can be made as to whether it falls within the stop band or pass band.

Hence, the entire simulation process for one test material at one frequency can be divided in to steps:

- Step 1, set up the geometry model.
- Step 2, calculate materials' mechanical properties for all parts in the model for homogeneous simulation and heterogeneous simulation.
- Step 3, run finite element simulation and perform Fourier transform to gain amplitude A_h of the wave propagating through the homogeneous material.

- Step 4, run finite element simulation and perform Fourier transform to gain amplitude A_c of the wave propagating through the heterogeneous material.
- Step 5, calculate the transmission coefficient using Eq. (2.4).

To determine the stop band for one heterogeneous material, simulations covering a certain range of frequencies are needed. One transmission coefficient will be obtained for one frequency. Transmission coefficients for all test frequencies can indicate the stop band and pass band in the testing frequencies.

In Steps 3 and 4, as mentioned earlier, to run finite element simulation, the geometry model must be meshed with finite elements. In this chapter, because all simulations were limited to 1D situation, the finite element was selected to be a bar element, which has only one degree of freedom.

Additionally, when running a finite element simulation, a time integration procedure is needed. In this study, the Newmark time integration procedure [84] was applied to all simulations in 1D and 2D situations. The Newmark integration method can be expressed by equations as:

$$^{t+\Delta t}\dot{U} = {}^{t}\dot{U} + [(1-\delta)\,{}^{t}\ddot{U} + \delta\,{}^{t+\Delta t}\ddot{U}]\Delta t \tag{2.5}$$

$$^{t+\Delta t}U = {}^{t}U + {}^{t}\dot{U}\Delta t + [(0.5-\eta)\,{}^{t}\ddot{U} + \eta\,{}^{t+\Delta t}\ddot{U}]\Delta t^2 \tag{2.6}$$

where U is displacement, $\dot{U}$ is velocity, $\ddot{U}$ is acceleration, t is the present time step, Δt is the time interval, $t+\Delta t$ is the next time step, and δ and η are parameters which can decide the accuracy and stability of the integration.

When δ is equal to 0.5 and η is equal to 0.25 the integration is unconditionally stable. Hence, in this study, the value of δ was set to 0.5 and the value of η was set to 0.25 in all simulations.

2.2.4 Simulation example for one frequency and convergence study

Following the process introduced in Section 2.2.3, one example is presented to explain the transmission coefficient calculation at one frequency for a periodic laminate material consisting of two different components. The convergence study of the simulation will be discussed in this section as well.

The whole structure is as shown in Figure 2.1: a bar with total length $L = 220$ mm, $L_{A_1} = L_{A_2} = 25$ mm, $L_B = 10$ mm and $L_C = 100$ mm. The microstructure of the heterogeneous material (Part C) is shown in Figure 2.2, with an alternating pattern of material component 1 (M_1) and material component 2 (M_2). This could be treated as a 1D representation of a matrix material, with inclusions embedded in the matrix. The volume fraction of M_1 is $v = 50\%$. The total length of one layer of M_1 and one layer of M_2 is the length of the unit cell (L_{unit}), which is equal to 10 mm. Hence, Part C contains 10 layers arranged periodically.

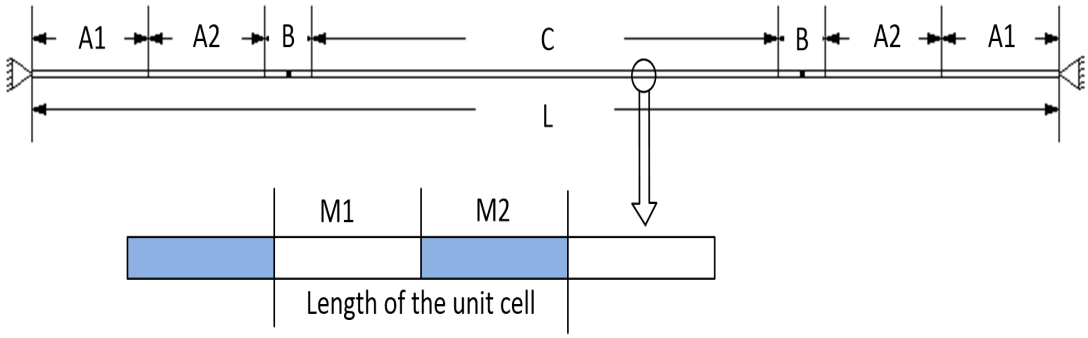

Figure 2.2: Structure of the heterogeneous material (Part C)

As mentioned in the Introduction, the stop band phenomenon only exists in heterogeneous material. Hence, the differences between material components' properties is the key area to study in terms of the stop band phenomenon.

Assuming the Young's modulus of M_1 is $E_1 = 2 \times 10^{11}$ Pa and the Young's modulus of M_2 is E_2. The ratio between E_1 and E_2 is denoted as $\beta_E = E_2/E_1$. Similarly, assume mass density of M_1 is $\rho_1 = 8 \times 10^3$ kg/m^3 and density of M_2 is ρ_2. The ratio between ρ_1 and ρ_2 can be denoted as $\beta_\rho = \rho_2/\rho_1$. For all simulations in Section 2, the mechanical properties of M_1 are kept the same.

As discussed in Section 2.2.3, two simulations are needed to calculate the transmission coefficient at one frequency. In the first simulation, Part C is set to be homogeneous material, which is the same as Part B. Material properties of Part B are calculated by the average of M_1 and M_2. In the second simulation, Part C is set to be heterogeneous material but Part B is kept as the same homogeneous material used in the first simulation.

In the FE-based calculation, the size of finite elements becomes an important factor which can have a huge impact on the simulation accuracy. A convergence study was implemented to ensure that the simulation had acceptable accuracy. In this study, dynamic loading was applied to simulate wave propagation. Hence, the size of the finite elements should be able to capture the movement of the wave, which means the size of the finite elements should be significantly smaller than the wavelength. Based on engineering experience, the finite element length should be 10 times smaller than a wavelength, which means using at least 10 elements to describe a single wave [84]. The wavelength λ can be calculated by Eq.(2.7), in which V is wave speed and f is frequency.

$$\lambda = \frac{V}{f} \tag{2.7}$$

For this convergence study, assume the homogeneous material placed in Part C is steel ($E_1 = 2 \times 10^{11}$ Pa and $\rho_1 = 8 \times 10^3$ kg/m^3); the longitudinal elastic wave speed in the material can be calculated by Eq. (2.8), which equals 5×10^3 m/s.

$$V = \sqrt{\frac{E}{\rho}} \tag{2.8}$$

For one-dimensional simulation, the maximum testing angular frequency that will be used in this section is set to be 4.5×10^6 rad/s. Based on Eq. (2.7), if the wave speed is fixed, the maximum frequency will lead to minimum wavelength. Hence, if the finite element size fulfills the requirement at the maximum frequency, it will fulfill the requirements of the lower frequencies as well. At the maximum testing frequency, the wavelength is calculated as 6.98 mm. As mentioned before, finite element length should be at least 10 times smaller than the wavelength; thus, the finite element length for the first simulation was chosen to be 0.5 mm. For the first simulation, a continuous sine wave was sent in at the source point at the left B part, and displacements were recorded at the recording point in the right B part (then transferred to amplitude). Several simulations were performed with the same material and loading properties but with decreasing finite element length (all simulations had the same time step as well) to study the convergence. The total length of the model was $L = 220$ mm in all simulations but the finite element length decreased from 0.5 mm to 0.025 mm in different simulations (the number of elements increased from 440 to 8800). The results are shown in Table 2.2. They illustrate that the differences between the recorded amplitudes for simulations 3, 4 and 5 are tiny. Hence, the simulation results converge when the finite element length is less than 0.1 mm. In this study, to ensure simulation accuracy, finite element length in all one-dimensional simulations is chosen to be 0.05 mm.

Table 2.2: Convergence study of finite element length change

Simulation	Length of finite element (mm)	Recording amplitude	Number of elements
1	0.5	7.98×10^{-7}	440
2	0.2	5.12×10^{-7}	1100
3	0.1	5.18×10^{-7}	2200
4	0.05	5.17×10^{-7}	4400
5	0.025	5.17×10^{-7}	8800

Because this study includes wave propagation, the convergence study of time discretisation is needed as well. Similar to finite element length, if the discrete time step can ensure accuracy at the maximum frequency it will fulfill the requirements of lower frequencies as well. According to Bathe [84], the time step should be at least 20 times smaller than the period of the wave. For maximum testing angular frequency 4.5×10^6 rad/s, the period is 1.4×10^{-6} s. The first time step was then set to be 5×10^{-7} s and the time step was reduced in further simulations. The results of the time step convergence study are shown in Table 2.3. The difference between the recording amplitude of

simulation 8 and 9 was minor. In this study, to ensure the simulation accuracy, the time step was set to be 1×10^{-8} s.

Table 2.3: Convergence study of time step change

Simulation	time step (s)	Recording amplitude
6	5×10^{-7}	4.22×10^{-9}
7	1×10^{-7}	4.96×10^{-7}
8	5×10^{-8}	5.12×10^{-7}
9	1×10^{-8}	5.17×10^{-7}

Hence, the time step in the simulation was set to be 1×10^{-8} s and finite element length was 0.05 mm, which establishes 4400 finite elements for the one-dimensional model.

For homogeneous material, no reflection occurs inside the material when waves pass though it, and the wave received at the recording point should be exactly the same as the wave sent at the source point. Thus waves will not interact with each other when they pass though homogeneous material. Waves will not interact with reflected waves from boundaries because of the absorbing boundary conditions. Hence, when the test part is a homogeneous material, theoretically, one wave is enough to test the transmission coefficient. However, for heterogeneous material, waves will interact with each other because of reflection inside the material. For this reason, sending only one wave though the heterogeneous material will provide results limited in range of applicability. To analyse both homogeneous and heterogeneous situations, the same continuous waves should be sent at the source point for both situations, to test the transmission coefficient.

For this test example, the simulation frequency was set to be 3.18×10^5Hz (2×10^6rad/s). As introduced previously, a continuous wave is initiated at the source point, and the simulation time should be long enough to ensure sufficient periods of the wave for it to be captured at the recording point to calculate the transfer coefficient. In the test example, the mechanical properties of material 1 (M_1) (component of heterogeneous material) were as introduced earlier in this section ($E_1 = 2 \times 10^{11}$ Pa and $\rho_1 = 8 \times 10^3$ kg/m^3) and the difference ratio of M_1 and M_2 in the heterogeneous material was set to be $\beta_E = 0.25$ and $\beta_\rho = 0.1$. The mechanical properties for the homogeneous material can then be calculated as the average properties of M1 and M2: $E_B = 8 \times 10^{10}$ Pa and $\rho_B = 4.4 \times 10^3$ kg/m^3. The wavelength of the homogeneous material was found to be 13.4 mm and the simulation time was set to be 1.023×10^{-4} seconds. During the simulation time, more than 30 periods of the wave were activated at the source point and more than 20 periods of the wave were received there; this number of periods is sufficient for applying the Fourier transform to ascertain amplitude.

The first test in this section was a continuous wave propagating through homogeneous material (Part C). The displacements at the recording point are shown in Figure 2.3. Here, the recorded displacements were regular sine waves (because the displacement

changed to above zero which is the first time the wave reached the recording point). The Fourier transform is then applied to the recorded displacements and the result is shown in Figure 2.4. The maximum amplitude calculated by Fourier transform of homogeneous material was $A_h = 2.43 \times 10^{-6}$ mm.

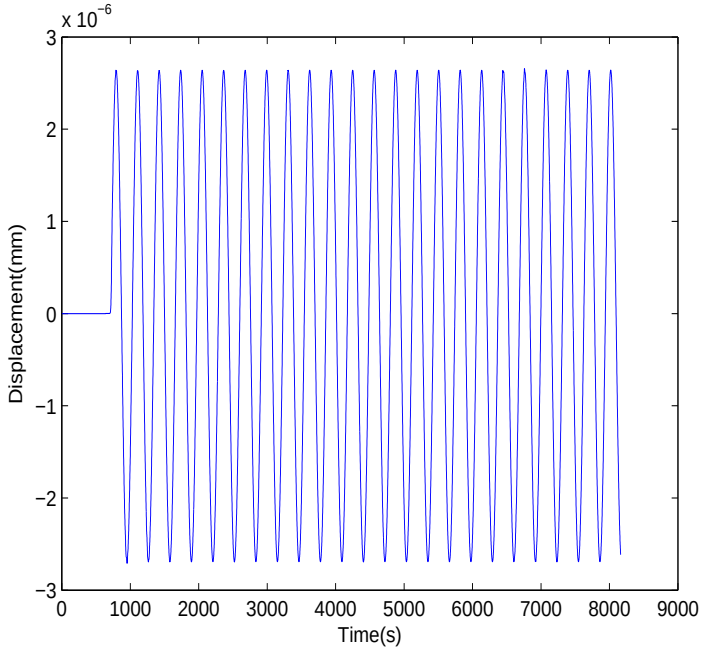

Figure 2.3: Displacements at recording point of homogeneous material example

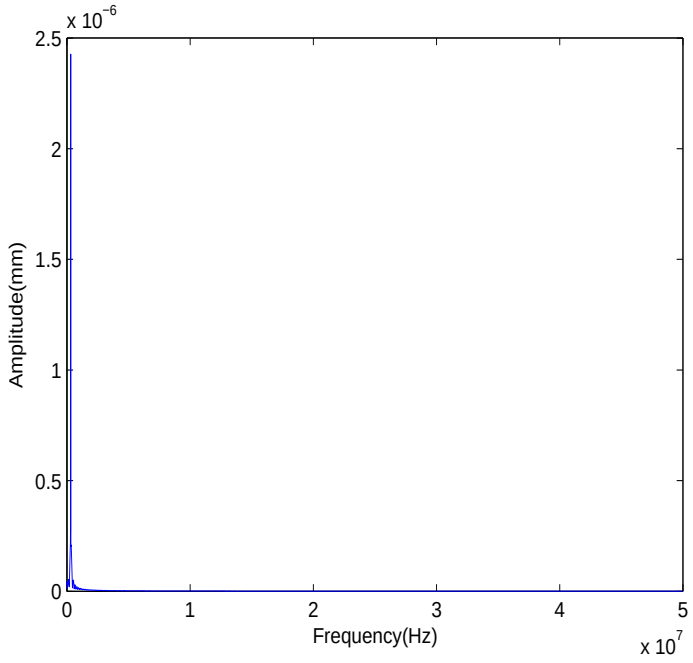

Figure 2.4: Amplitude of recorded displacements of homogeneous material example

The second test was for a continuous wave propagating though heterogeneous material (in the second simulation, Part B was the same homogeneous material as in the first simulation but Part C was replaced by a periodic laminate material). The displacements at the recording point are shown in Figure 2.5. This depicts how the recorded displacements are decreasing as the time changes. The Fourier transform was then applied to the recorded displacements; the result is shown in Figure 2.6. The maximum amplitude calculated by Fourier transform of heterogeneous material is $A_c = 3.72 \times 10^{-8}$ mm.

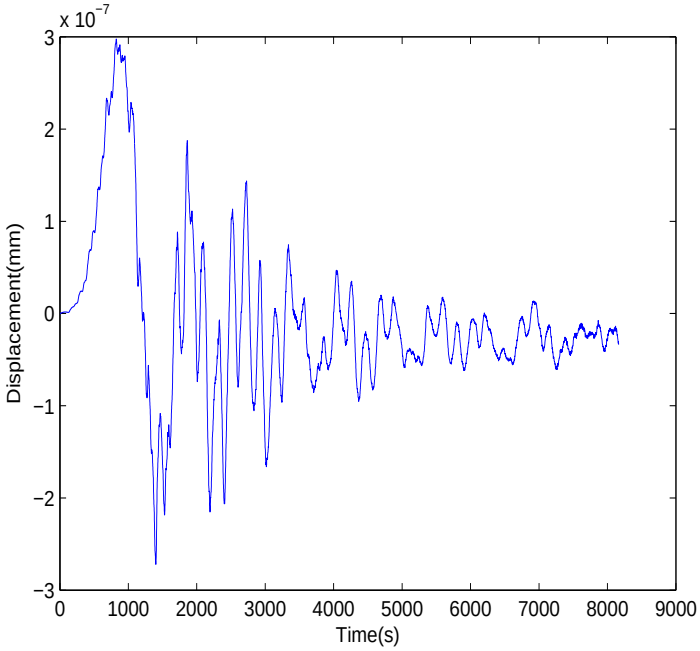

Figure 2.5: Displacements at recording point of heterogeneous material example

The transmission coefficient of the heterogeneous material under dynamic loading at this frequency then can be calculated as $T = A_c/A_h = 3.72 \times 10^{-8}/2.43 \times 10^{-6} = 1.52 \times 10^{-2}$. The value of the transmission coefficient $T = 1.52 \times 10^{-2}$ at the frequency $f = 3.18 \times 10^5$ Hz showed that the wave has difficultly propagating through the material; thus, the frequency is located within the stop band.

2.3 Stop band phenomenon in material with deterministic properties in 1D

As has been shown in the previous section, the stop band phenomenon in wave propagation will only occur when the wave propagates though heterogeneous materials. Hence, the microstructure and the mechanical properties of components of the heterogeneous material are of great importance. In this section, the influence of both the

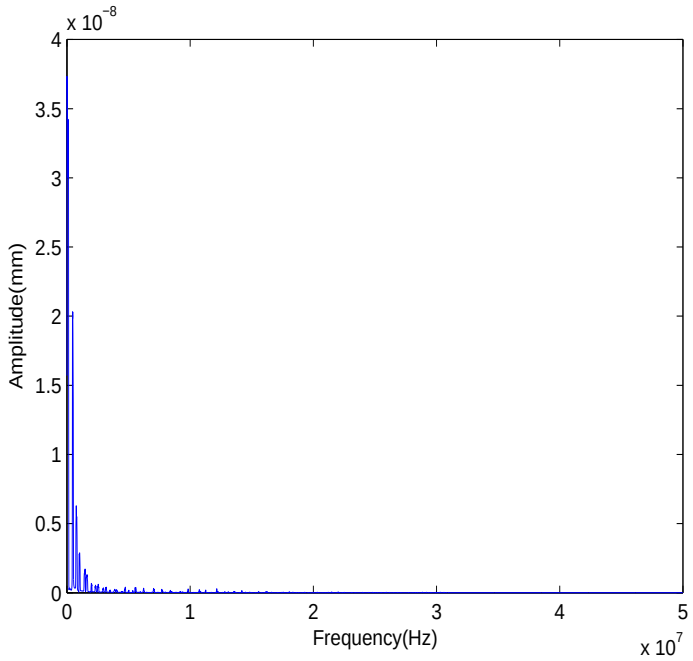

Figure 2.6: Amplitude of displacements of heterogeneous material example

material's mechanical properties and geometrical properties on the stop band will be studied.

2.3.1 Influence of Young's modulus on the stop band

The first group of tests focused on analysing the influence of Young's modulus on the stop band phenomenon. In this group of simulations, the heterogeneous material of Part C is a periodic laminate material consisting of two different components. Here four cases (Cases 1-4) were studied by varying Young's modulus ratio of M_1 to M_2 while keeping the other parameters of M_1 and M_2 equal in all four cases (see Table 2.4). For each frequency in each group of tests, the simulation procedure followed the process introduced in Section 2.2.4.

Table 2.4: Material parameters for Young's modulus influence test

Case	β_E	β_ρ	L_{unit}
1	0.5	1	10 mm
2	0.25	1	10 mm
3	0.1	1	10 mm
4	0.05	1	10 mm

In all cases, the incident wave frequency ω ranged from 1×10^5 rad/s to 4.5×10^6 rad/s with intervals of 5×10^4 rad/s. The result of case 1 (i.e. $\beta_E = 0.5$) is shown in Figure 2.7 in which the transmission coefficient T was plotted against the frequency $f = \omega/2\pi$.

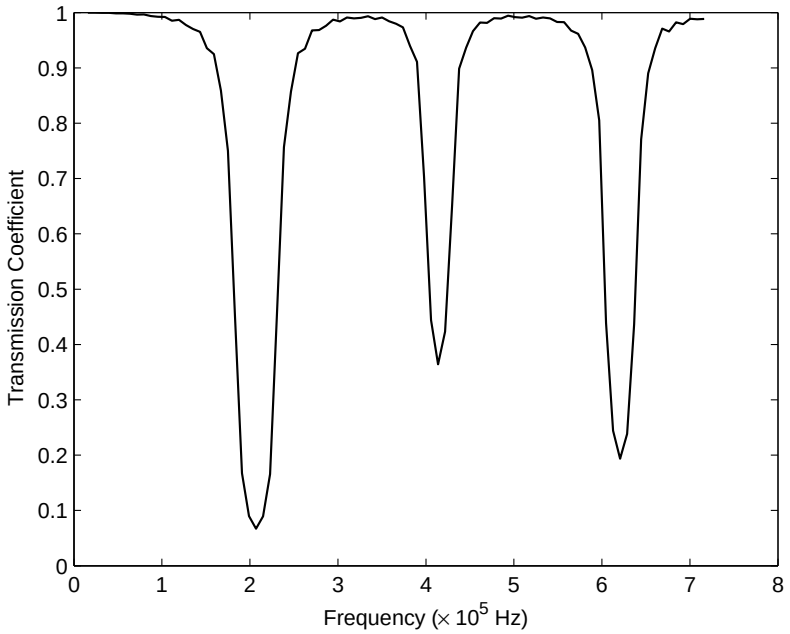

Figure 2.7: Simulation result of Young's modulus influence test while $\beta_E = 0.5$

At low frequency (less than 1.5×10^5 Hz), the transmission coefficient is almost equal to 1 which means that waves can pass through the heterogeneous material without any drop in amplitude. When increasing the test frequency, three significant drops of the transmission coefficient became apparent. In particular, initially, the transmission coefficient dropped to around 5% when the test frequency was approximately 2×10^5 Hz. This results signifies that the waves were virtually unable to propagate through the heterogeneous material at this frequency.

Figure 2.8 shows results for a range of contrasts in two material's Young's modulus. In Figure 2.8, the solid line is the result of Case 1; the dotted line is the result of Case 2; the dashed line is the result of Case 3; and the dotted dashed line is the result of Case 4.

The simulation results of the four cases show that with increasing difference in Young's modulus of two materials (decreasing β_E), the initial frequency of the first stop band becomes lower and the transmission coefficient in the pass band drops, especially for high contrast.

2.3.2 Influence of density on the stop band

The second group of tests focused on the influence of materials densities on the stop band phenomenon. Similar to the simulations conducted in Section 2.3.1, four cases (Cases 5-8) were studied by varying the density ratio β_ρ while keeping the other parameters of M_1 and M_2 equal (see Table 2.5).

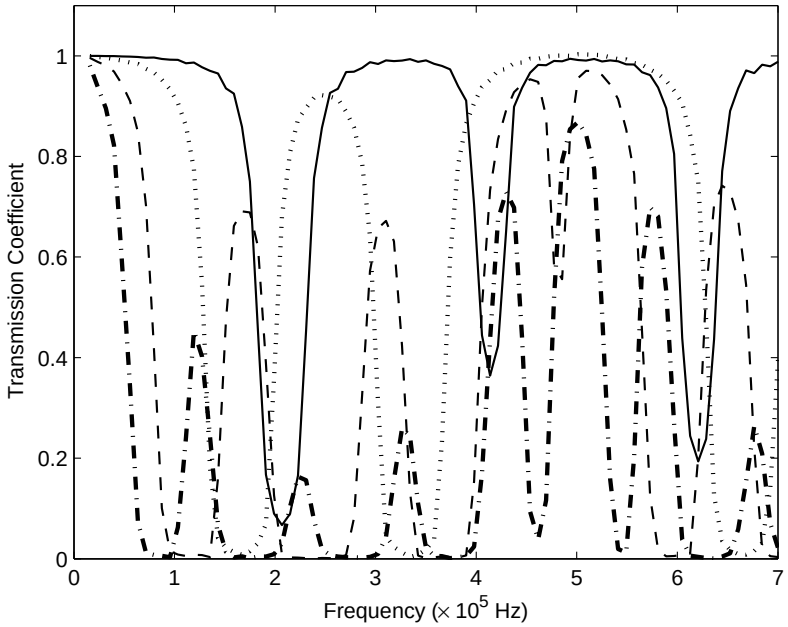

Figure 2.8: Simulation results of Young's modulus influence test (Solid line: $\beta_E = 0.5$, Dotted line: $\beta_E = 0.25$, Dashed line: $\beta_E = 0.1$, Dotted dashed line: $\beta_E = 0.05$)

Table 2.5: Values of material parameters for density influence test

Case	β_E	β_ρ	L_{unit}
5	1	0.5	10 mm
6	1	0.25	10 mm
7	1	0.1	10 mm
8	1	0.05	10 mm

The simulation results of Cases 5-8 are presented in Figure 2.9 (here the solid line indicates Case 5; the dotted line illustrates Case 6; the dashed line represents Case 7; and the dotted dashed line shows Case 8).

As shown in Figure 2.9, when the ratio of density in two materials is increased the width of the first stop band increases at the same time that the transmission coefficient of the second pass band drops.

2.3.3 Influence of length of unit cell on the stop band

The third group of tests focused on the material's geometrical features, i.e. on the influence of the unit cell length. Similar to the simulations performed in Section 2.3.1, four cases (Cases 9-12) have been studied using $L_{unit} = 2$ mm, $L_{unit} = 4$ mm, $L_{unit} = 10$ mm and $L_{unit} = 20$ mm while other parameters of M_1 and M_2 are the same in all cases (as shown in Table 2.6).

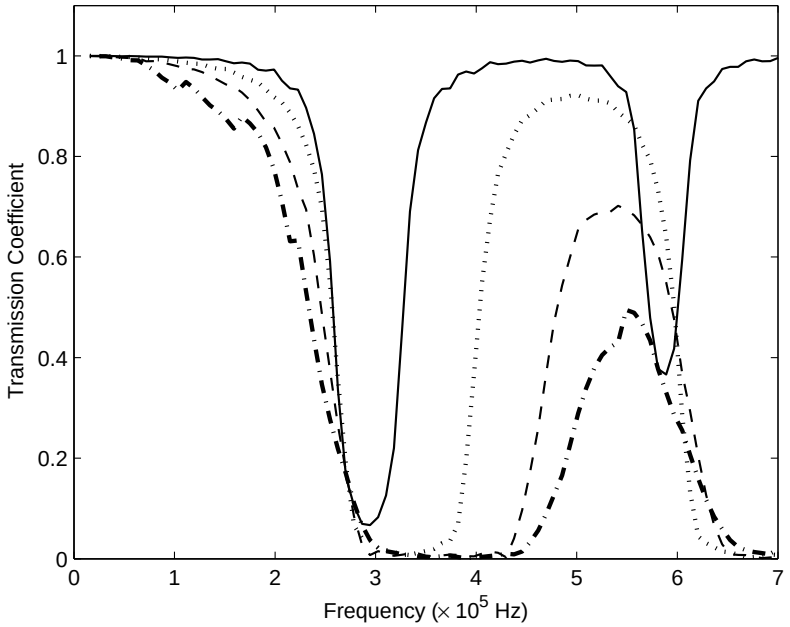

Figure 2.9: Simulation results of density influence test (Solid line: $\beta_\rho = 0.5$, Dotted line: $\beta_\rho = 0.25$, Dashed line: $\beta_\rho = 0.1$, Dotted dashed line: $\beta_\rho = 0.05$)

Table 2.6: Values of material parameters for geometry influence test

Case	β_E	β_ρ	L_{unit}
9	0.25	0.1	2 mm
10	0.25	0.1	4 mm
11	0.25	0.1	10 mm
12	0.25	0.1	20 mm

The simulation results are shown in Figure 2.10. Here, the solid line indicates the case with $L_{unit} = 2$ mm; the dotted line illustrates the case with $L_{unit} = 4$ mm; the dashed line represents the case with $L_{unit} = 10$ mm; and the dotted dashed line shows the case with $L_{unit} = 20$ mm.

Results in Figure 2.10 indicate that, by increasing the length of the unit cell in the heterogeneous material, the frequency of the starting point of the stop band decreases significantly.

2.3.4 Analysis and interpretation of influence of material's mechanical and geometrical properties on stop band

Simulation results of Cases 1-8 show that, when the difference of Young's modulus between *inclusion* material and *matrix* material is increased, the initial frequency of the stop band decreases. Conversely, when the difference in density between the inclusion

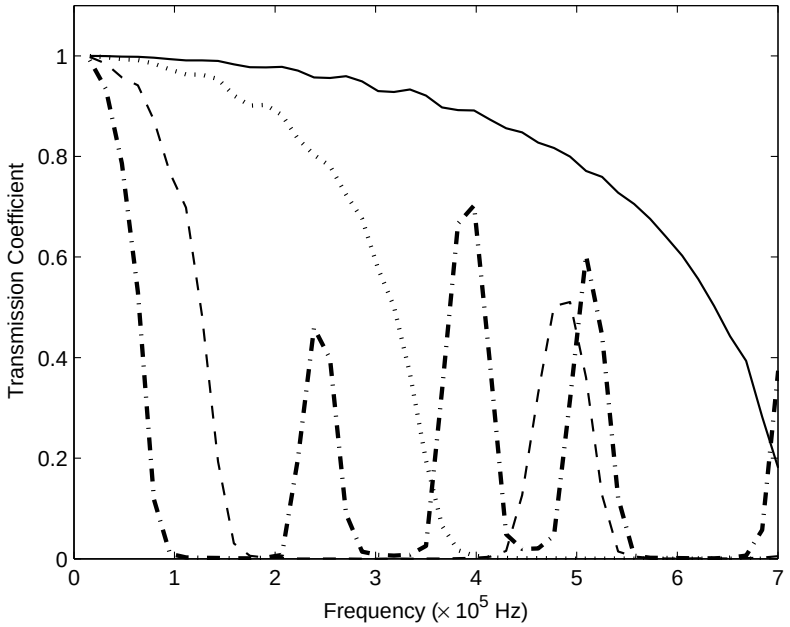

Figure 2.10: Simulation results of geometry influence test (Solid line: $L_{unit} = 2$ mm, Dotted line: $L_{unit} = 4$ mm, Dashed line: $L_{unit} = 10$ mm, Dotted dashed line: $L_{unit} = 20$ mm)

material and matrix material is increased, the initial frequency of the stop band increases slightly. To understand this, we focus on the wave speed (V) of the material, which is given by Eq. (2.8). Here, the average wave speed ($\bar{V}$) of the heterogeneous material is defined by Eq. (2.9).

$$\bar{V} = \sqrt{\frac{\bar{E}}{\bar{\rho}}} \tag{2.9}$$

in which the average Young's modulus $\bar{E}$ of the heterogeneous material is found by the arithmetic mean (where α is the volume fraction which is equals to 0.5), i.e.

$$\bar{E} = \frac{E_1 E_2}{(1-\alpha)E_1 + \alpha E_2} \tag{2.10}$$

and the average density of the heterogeneous material $\bar{\rho}$ is obtained by Eq. (2.11) [82].

$$\bar{\rho} = \alpha\rho_1 + (1-\alpha)\rho_2 \tag{2.11}$$

Note that these results come from low-frequency homogenization theory. For each frequency the average wavelength $\bar{\lambda}$ is calculated as

$$\bar{\lambda} = \frac{\bar{V}}{f} \tag{2.12}$$

We compared $\bar{\lambda}$ obtained using Eq. (2.12) at each frequency with the length of the unit cell L. Results indicate that $\bar{\lambda}$ and $2L$ are equal for the first frequency within the first stop band. Hence the first frequency within the stop-band, say f_{s1} can be predicted as

$$f_{s1} = \frac{\bar{V}}{\bar{\lambda}} = \frac{1}{2L}\sqrt{\frac{\bar{E}}{\bar{\rho}}} \tag{2.13}$$

Note here that Eq. (2.13) contains information about the mechanical properties (Young's modulus and density) of the material as well as the geometrical properties (volume fraction and length of unit cell), and can thus be used to predict the frequency at which the first stop band arises. Here, the frequency at the first stop band is calculated by applying Eq. (2.13) for each case, as shown in Table 2.7. Here the starting frequency of the first stop band, calculated by Eq. (2.13), in each case is similar to the simulation results.

Table 2.7: Frequency at the first stop band

Case number	Starting frequency by calculation	Starting frequency by simulation
1	2.05×10^5	2.07×10^5
2	1.58×10^5	1.43×10^5
3	1.07×10^5	9.55×10^4
4	7.72×10^4	7.16×10^4
5	2.89×10^5	2.94×10^5
6	3.16×10^5	2.86×10^5
7	3.37×10^5	2.86×10^5
8	3.45×10^5	2.94×10^5
9	1.07×10^6	Extended the testing frequency range
10	5.33×10^5	3.82×10^5
11	2.13×10^5	1.59×10^5
12	1.07×10^5	9.55×10^4

2.4 Stop band phenomenon in material with random properties

So far, the discussion has been based around material with heterogeneous but strictly periodic structure. In this section, the influence of the randomness of the material's mechanical properties (Young's modulus and density) and geometrical property (length of the unit cell) will be addressed. Unless mentioned otherwise, the same test parameters and 1D bar employed in Section 2.2 are used (the frequency interval is changed to be 1×10^5 rad/s).

In this section, to begin with, randomness has been added to the material's Young's modulus to test its influence on the stop band. After this, randomness has been added to the material's density to test the influence on the stop band. Next, randomness has been added to the length of the unit cell of the material to test the influence on the stop band. Randomness has been added to the length of the unit cell in two different ways: first by directly adding randomness to each unit cell following normal distribution; and second by constructing a "Fibonacci bar" to realise the "semi-random" aspect of the geometry. Finally, randomness has been added to both the mechanical properties (Young's modulus and density) and geometrical properties (length of the unit cell) of the material to test the influence on the stop band.

2.4.1 Influence of randomness on Young's modulus in the stop band

The first set of simulations tested the influence of randomness only in the Young's moduli of the heterogeneous material. To do this, Young's moduli followed a normal distribution with constant mean μ and increasing standard deviation σ, as indicated in Table 2.8. The randomness was added to each layer in the heterogeneous material separately which means that each layer had different mechanical properties but followed the same type of randomness rule.

Table 2.8: Variations of material parameters for Young's modulus influence test

Case	E_{M_1}		ρ_{M_1}		E_{M_2}		ρ_{M_2}		L_{unit}
	μ	σ	μ	σ	μ	σ	μ	σ	
13	E_{M_1}	0	ρ_{M_1}	0	E_{M_2}	0	ρ_{M_2}	0	10 mm
14	E_{M_1}	$0.05E_{M_1}$	ρ_{M_1}	0	E_{M_2}	$0.05E_{M_2}$	ρ_{M_2}	0	10 mm
15	E_{M_1}	$0.1E_{M_1}$	ρ_{M_1}	0	E_{M_2}	$0.1E_{M_2}$	ρ_{M_2}	0	10 mm
16	E_{M_1}	$0.2E_{M_1}$	ρ_{M_1}	0	E_{M_2}	$0.2E_{M_2}$	ρ_{M_2}	0	10 mm

The reference (deterministic) case is Case 13, in which the standard deviation of Young's modulus and density of both materials 1 and 2 is 0. For this section i.e. case (13-16) and for further cases (17-22), $E_{M_1} = 2 \times 10^{11}$ Pa, $E_{M_2} = 0.25E_{M_1}$, $\rho_{M_1} = 8 \times 10^3$ kg/m^3, and $\rho_{M_2} = 0.1\rho_{M_1}$. Five realisations were carried out in each of Cases 14-22 to obtain average values of the results. The results of Cases 13-16 are shown in Figure 2.11, and it is clear that the influence of randomness of the Young's modulus on stop band frequency is minimal. The frequency corresponding to the first stop band and the width of the first stop band were unaffected by the small perturbations in Young's modulus. In this study, the small perturbation represented the randomness with standard deviation less than 0.2, which can be treated as a low level of randomness. Note here, that different levels of randomness, e.g. semi-random and fully random have been also looked at in Section 2.4.4 and Section 2.5. The slight change can only be noted in the value of transmission coefficient in the second pass band. Note that, although the number of realisations is 5, the randomness was added to each material component in each layer in the composite material in each realisation. The composite material was constructed of 10 layers; hence, the Young's modulus of the material component was randomly sampled 20 times in a

single simulation. This process ensured the composite material has randomly distributed Young's modulus. Hence, despite the small number of realisations, the simulation can still provide qualitative trends.

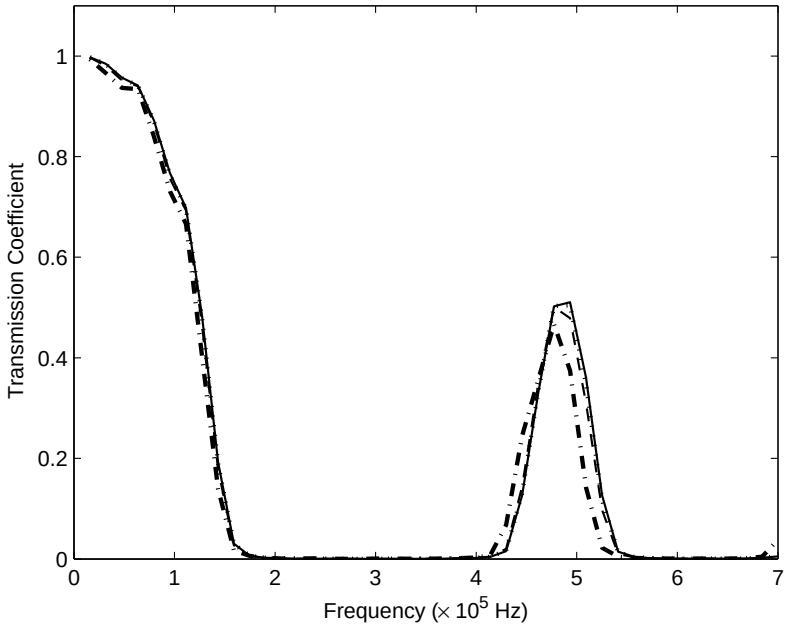

Figure 2.11: Simulation results of randomness in Young's modulus influence test (Solid line: $\sigma = 0$, Dotted line: $\sigma = 0.05$, Dashed line: $\sigma = 0.1$, Dotted dashed line: $\sigma = 0.2$)

2.4.2 Influence of randomness of mass density on the stop band

The second group of simulations tested the influence of randomness on the mass density. Similar to the tests in Section 2.4.1, three cases have been studied and the values of all the parameters of the heterogeneous material in these three cases are shown in Table 2.9. Randomness was added to each layer in the heterogeneous material in a similar way as in Section 2.4.1.

Table 2.9: Variations of material parameters of randomness in density influence test

Case	E_{M_1}		ρ_{M_1}		E_{M_2}		ρ_{M_2}		L_{unit}
	μ	σ	μ	σ	μ	σ	μ	σ	
17	E_{M_1}	0	ρ_{M_1}	$0.05\rho_{M_1}$	E_{M_2}	0	ρ_{M_2}	$0.05\rho_{M_2}$	10 mm
18	E_{M_1}	0	ρ_{M_1}	$0.1\rho_{M_1}$	E_{M_2}	0	ρ_{M_2}	$0.1\rho_{M_2}$	10 mm
19	E_{M_1}	0	ρ_{M_1}	$0.2\rho_{M_1}$	E_{M_2}	0	ρ_{M_2}	$0.2\rho_{M_2}$	10 mm

The results of Case 17-19 are shown in Figure 2.12 and compared with the deterministic Case 13.

As shown in Figure 2.12, the influence of randomness on the stop band frequency range

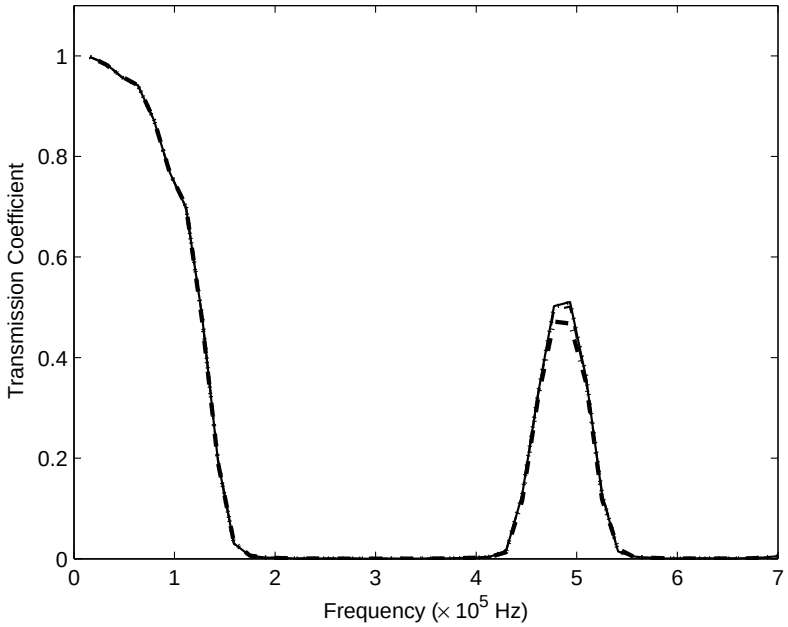

Figure 2.12: Simulation results of randomness in density influence test (Solid line: $\sigma = 0$, Dotted line: $\sigma = 0.05$, Dashed line: $\sigma = 0.1$, Dotted dashed line: $\sigma = 0.2$)

is similar to that noted in Section 2.4.1, and is minimal. All the conclusions regarding the frequency of the first stop band and the width of the first stop band are again unaffected by the small perturbation in the material's densities. In fact, even the second pass band virtually followed the deterministic case.

2.4.3 Influence of randomness of the unit cell length on the stop band or *"small perturbations"* in the geometrical properties

The third group of simulations tested the influence of adding randomness to the unit cell length, which means the third group of simulations was focused on geometry rather than the mechanical properties studied in Sections 2.4.1 and 2.4.2. We achieved this by taking random values of the unit cell length (L_{unit}), or rather the lengths of phases (L_{M_1} and L_{M_2}) within the cell length from a normal distribution, and keeping the total length of test material fixed. The latter can be viewed as a case of conditional probabilities. The microstructure of the heterogeneous material is as shown in Figure 2.2, but note that the volume fraction is no longer exactly 50%. Again, three cases (Cases 20-22) were studied and the parameter values are shown in Table 2.10. Note that so far randomness has been discussed in terms of the *"small perturbation"* of the analysed properties. The *"semi-random"* case and *"fully-random"* case will be studied in the following subsections.

Table 2.10: Variations of material parameters of unit cell length study

Case	E_{M_1}	ρ_{M_1}	E_{M_2}	ρ_{M_2}	L_{M_1}		L_{M_2}	
					μ	σ	μ	σ
20	E_{M_1}	ρ_{M_1}	E_{M_2}	ρ_{M_2}	5 mm	0.05×5 mm	5 mm	0.05×5 mm
21	E_{M_1}	ρ_{M_1}	E_{M_2}	ρ_{M_2}	5 mm	0.1×5 mm	5 mm	0.1×5 mm
22	E_{M_1}	ρ_{M_1}	E_{M_2}	ρ_{M_2}	5 mm	0.2×5 mm	5 mm	0.2×5 mm

The results of Cases 20-22 are shown in Figure 2.13 and compared with Case 13.

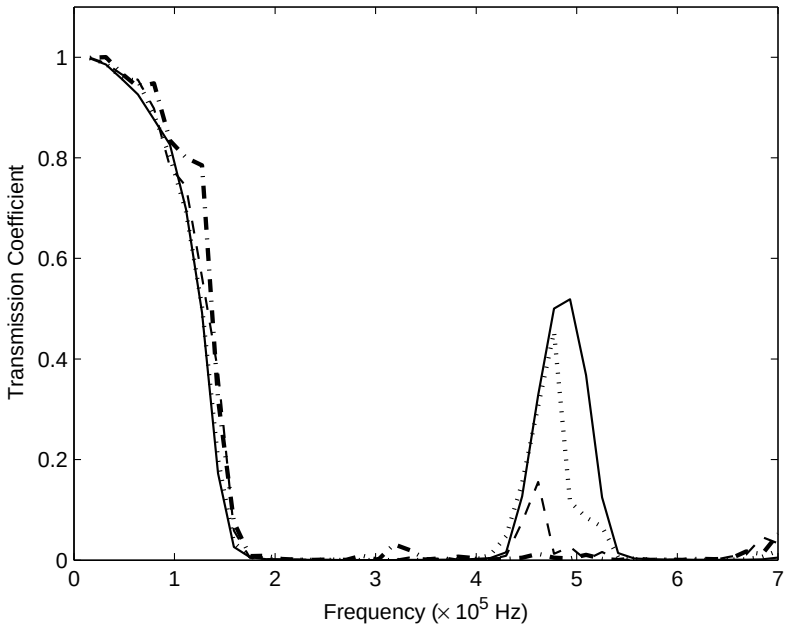

Figure 2.13: Simulation results of randomness in geometry influence test (Solid line: $\sigma = 0$, Dotted line: $\sigma = 0.05$, Dashed line: $\sigma = 0.1$, Dotted dashed line: $\sigma = 0.2$)

As shown in Figure 2.13, in contrast to adding randomness to mechanical properties, as discussed in Section 2.4.1 and 2.4.2, a significant effect is presented by adding randomness to the microstructural geometry. In the second pass band the transmission coefficient decreased rapidly with increasing standard deviation and even finally dropped to zero when the standard deviation approached 0.2. This result signifies that adding small perturbations to the geometry makes it possible to turn a pass band into a stop band.

2.4.4 Stop band prediction based on 1-D Fibonacci layout or material with *"semi-random"* geometry

In Section 2.4.3 the influence of randomness added to the material's geometry on stop band was discussed. Randomness was added in the form of small perturbations following normal distribution with μ and σ. By applying this method the length of every unit cell in the test material was random and had 99% possibility of being longer than

$\mu - 3\sigma$ and shorter than $\mu + 3\sigma$. When σ is small (*"small perturbation"* is generated in the material) this method can generate appropriate lengths for the unit cell and the computer is able to realize the simulation. However, when σ is large, some of the unit cells could be too long or too short and may lead the whole structure generated by the computer to have unrealistic parts (some layer to be extremely large or small) or to miss one or two layers, which changes the entire structure.

Hence, another method to realize *"semi-random"* material geometry is applied in this section: it is the generation of a random microstructure by fixing the length of the unit cell and arranging the cells in a Fibonacci sequence. The Fibonacci sequence is defined as $F_N = F_{N-1} + F_{N-2}$ with seeds values $F_1 = 1$ and $F_2 = 1$. Here, following similar logic, a *"Fibonacci bar"* (F^N_{bar}) can be constructed.

The *"Fibonacci bar"* is defined as a laminate material with two different materials and with the length of each layer fixed to be either *"long"* or *"short"*. The *"long"* layer is defined as L_L and the *"short"* is defined as L_S. These two parts become the seed parts of the *"Fibonacci bar"*:

1. for $N = 1$, the *"Fibonacci bar"* (F^1_{bar}) is constructed by one *"short"* layer: $F^1_{bar} = L_S$;
2. for $N = 2$, the *"Fibonacci bar"* is constructed by one *"long"* layer: $F^2_{bar} = L_L$.
3. for $N = 3$, the *"Fibonacci bar"* is constructed by two parts; the first part is F^2_{bar} (L_L) and the second part is F^1_{bar} (L_S) which is placed at the end of the first part: $F^3_{bar} = L_L L_S$.
4. for $N >= 3$, F^N_{bar} is generated by F^{N-2}_{bar} placed at the end of F^{N-1}_{bar}

The geometry of the *"Fibonacci bar"* generating process is shown in Figure 2.14.

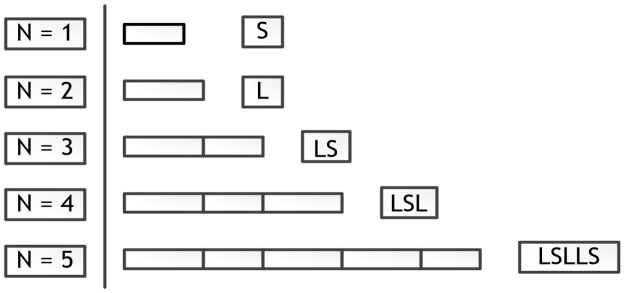

Figure 2.14: The geometry of the *"Fibonacci bar"* from $N = 1$ to $N = 5$

The constructed *"Fibonacci bar"* is a laminate material with two different material phases (Materials 1 and 2). The length of each layer is determined by the Fibonacci sequence. For example, for the $N = 5$ case shown in Figure 2.15, the length of each layer is $L_L L_S L_L L_L L_S$ but the material is $M_1 M_2 M_1 M_2 M_1$.

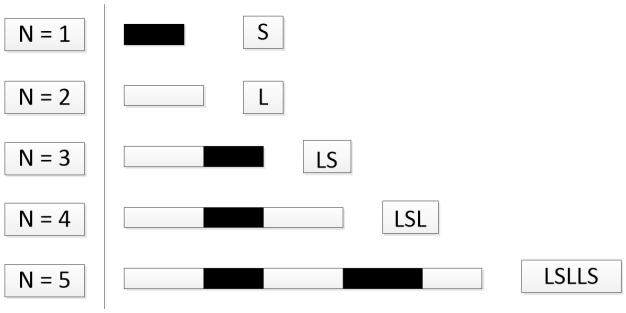

Figure 2.15: *"Fibonacci bar"* from $N = 1$ to $N = 5$

When N is large enough, the distribution of the *"long"* layer and the *"short"* layer will become as *"semi-random"* and distributed in F_{bar}^{N}. Under this condition, the length of the unit cell is fixed at two different lengths but randomly located. Hence, when running simulations, the randomness can be realized by the computer without creating extremely large or small unit cells. Here, the *"short"* layer is set to be 4.5 mm ($L_S = 4.5$mm) and the *"long"* layer is set to be 5.5 mm ($L_S = 5.5$mm). With the chosen length of different fixed layer lengths and the random position of the *"long"* and *"short"* layers, the generated microstructure is then comparable to randomness added to the length of the unit following normal distribution, with $\mu = 5$mm and $\sigma = 0.5$mm. To compare the results to the previous cases in Section 2.4.3, the tested heterogeneous material for one case had 20 layers and the total length of the testing material was around 100 mm. In this section, 10 simulations were run. To generate the structure for 10 cases, a *"Fibonacci bar"* with $N = 20$ was generated first. F_{bar}^{13} had 233 layers and the position of *"long"* and *"short"* layers in the bar was treated as randomly placed. For each simulation case, 20 layers were picked from F_{bar}^{13} in sequence (for example, layer 1 to 20 of F_{bar}^{13} becomes the testing heterogeneous material of Case 23(1) and layer 21 to 40 of F_{bar}^{13} becomes the testing heterogeneous material of Case 23(2)). The detail of the microstructure of each case is shown in Table 2.11.

Table 2.11: Microstructure of cases of *"semi-random"* material

Case	Microstructure (L for L_L and S for L_S)	Total length of testing part(mm)
23(1)	*LSLLSLSLLSLLSLSLLSLS*	102
23(2)	*LLSLLSLSLLSLLSLSLLSL*	103
23(3)	*SLLSLLSLSLLSLSLLSLLS*	102
23(4)	*LSLLSLLSLSLLSLSLLSLL*	103
23(5)	*SLSLLSLLSLSLLSLSLLSL*	102
23(6)	*LSLSLLSLSLLSLLSLSLLS*	102
23(7)	*LLSLSLLSLSLLSLLSLSLL*	103
23(8)	*SLSLLSLLSLSLLSLLSLSL*	102
23(9)	*LSLSLLSLLSLSLLSLLSLS*	102
23(10)	*LLSLSLLSLLSLSLLSLSLL*	103

The simulation process for each case followed the procedure introduced in Section 2.2.4. However, because the length of the testing heterogeneous material changed in every

case, the total length of the simulation model was no longer fixed but altered with the length of the testing material. The difference ratio of material 1 and 2 of the testing heterogeneous material followed the previous section $\beta_E = 0.25$ and $\beta_\rho = 0.1$, and other parameters were kept the same as the simulation example in Section 2.2.4. The simulation frequency was from 1×10^5 rad/s to 4.5×10^6 rad/s with interval of 1×10^5 rad/s. After running the simulation for 10 cases, the transmission coefficient was calculated for each testing frequency for each case. The average transmission coefficient of 10 cases was then calculated and compared to the transmission coefficient results of the wave propagated though the periodic laminate material (Case 13 in Section 2.4.1, in which the mechanical properties of the two material components are the same as material components simulated in this case). The comparison is shown in Figure 2.16.

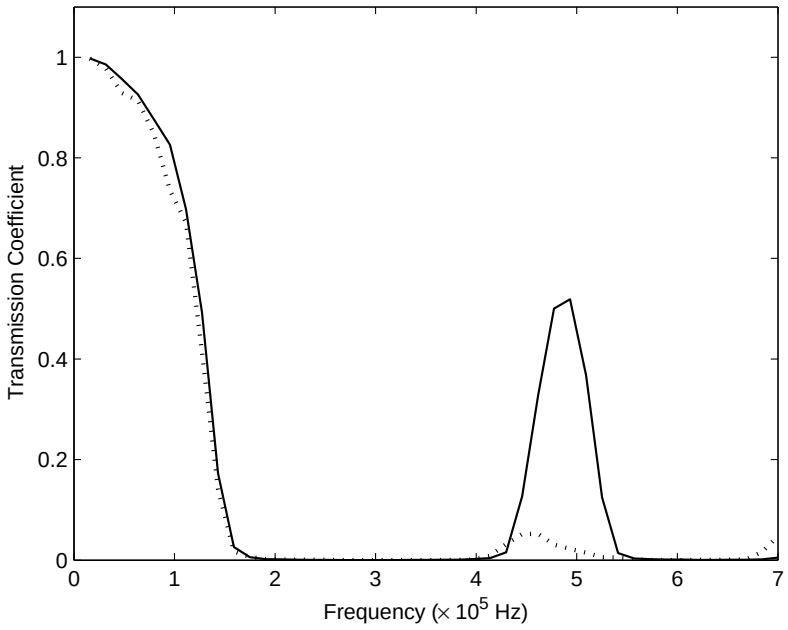

Figure 2.16: Simulation results of *"semi-random"* compare with periodic case (Solid line: periodic case, Dotted: *"semi-random"* case)

The results shown in Figure 2.16 indicate that the *"semi-random"* material can reduce the value of the transmission coefficient in the second pass band significantly (the maximum value of transmission coefficient dropped from 0.52 to 0.052), compared to periodic laminate material without any randomness. Meanwhile, material with a *"semi-random"* microstructure will not influence the first stop band properties, compared to periodic material.

This research was carried out with Roth Voisey and Ellis Branwell from the University of Manchester. They implemented wave propagation research through a mass spring system, and when constructing the system they applied the Fibonacci random method.

2.5 Stop band prediction based on *"fully-random"* material

In Sections 2.4.1, 2.4.3 and 2.4.4, the wave propagation in periodic material, material with small perturbations, and material with a *"semi-random"* microstructure (laminate material following Fibonacci sequence layout) has been simulated. In this section, the wave propagation in material with a higher degree of randomness (known as *"fully-random"*) will be tested, to understand the influence of randomness in microstructures in terms of identifying the stop band position for different randomness levels.

The *"fully-random"* material presented in this section was constructed with randomness added not only to the length of each unit cell but also the position of each unit cell. The testing material was still constructed by two material phases, called Material 1 and Material 2 and the difference between these two materials can still be described by β_E and β_ρ, which in this simulation will be $\beta_E = 0.25$ and $\beta_\rho = 0.1$. To realize the *"fully-random"* aspect, the length of unit cells was again related to added randomness following a normal distribution with mean value (μ) of 5 mm and standard deviation (σ) of 0.2 mm. Then all unit cells became a testing bar with a total length of 100 mm (the last one or two unit cells may need to modify the length to avoid extreme situations). At the same time, the type of each unit cell was randomly decided, following uniform distribution with 50% possibility, which means that each unit cell could either be Material 1 or Material 2. Three typical examples of the microstructure with *"fully-random"* material are shown in Figure 2.17.

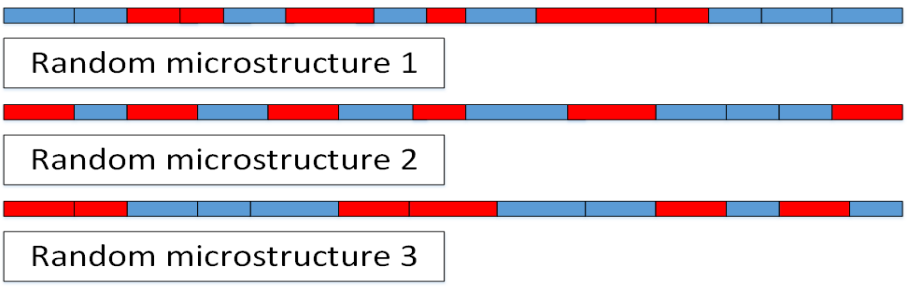

Figure 2.17: Microstructure of *"fully-random"* material

As shown in Figure 2.17, with randomness added into the length of the unit cell, the length of each unit cell becomes different. At the same time, with randomness added into the material decision progress, the testing material becomes *"fully-random"*.

In this section, 10 cases were constructed to test the influence of the *"fully-random"* microstructure on wave propagation in the material. The simulation process for each case followed the procedure introduced in Section 2.2.4. The difference ratio of two material components of the tested heterogeneous material was $\beta_E = 0.25$ and $\beta_\rho = 0.1$, and other parameters were kept the same as the simulation example in Section 2.2.4. The simulation frequency was from 1×10^5 rad/s to 4.5×10^6 rad/s with interval of

1×10^5 rad/s. After 10 cases were simulated, the transmission coefficient was calculated for each testing frequency for each case. The average transmission coefficient of 10 cases was then calculated and compared to the transmission coefficient results of waves propagating though the periodic laminate material (Case 13 in Section 2.4.1). The results are compared in Figure 2.18.

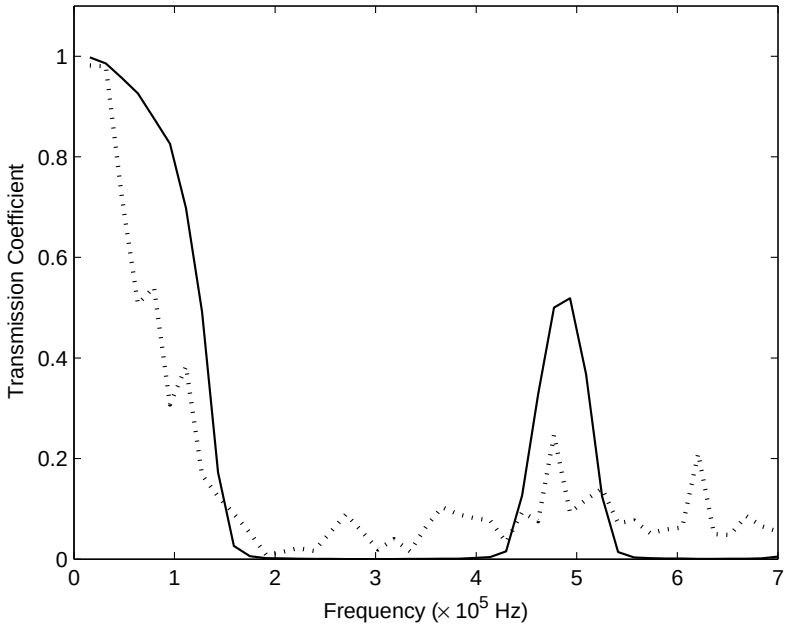

Figure 2.18: Simulation results of *"fully-random"* compare to periodic case (Solid line: periodic case; Dotted line: *"fully-random"* case)

As shown in Figure 2.18, when a harmonic wave was propagated through material with a *"fully-random"* microstructure there was no clear stop band. However, the transmission coefficient was kept around 10% from 2×10^5 Hz (the frequency of the first stop band started in the periodic laminate material case) to the largest testing frequency and at several frequencies the transmission coefficient was below 5% (for example, at 1.91×10^5 Hz). Hence, material with *"fully-random"* microstructure can reduce the wave propagation to a certain level (around 10%) when frequency is high enough but cannot create "strict" stop bands.

2.6 Results and discussion

In this chapter, the influence of both heterogeneous material's mechanical and geometrical properties on wave propagation were tested from the perspective of the stop band phenomenon for the 1D case. Finite element simulations of wave propagation through a homogeneous or heterogeneous material were performed. Whilst performing the simulation, the longitudinal harmonic wave was actuated at the source point, and after the wave had propagated though the testing material, it was recorded at the record point on the testing model (see Figure 2.1). Here, the displacements caused by the wave

propagation were recorded and then run through the Fourier transform to obtain amplitudes of the propagated waves. By comparing amplitudes calculated by the wave propagating through testing heterogeneous material to amplitudes calculated by the wave propagating through homogeneous material, the transmission coefficient of the wave propagating through the testing heterogeneous material could then be calculated by Eq. (2.4). The value of the transmission coefficient determined the frequency ranges, that either fell into the stop band range or the pass band range. As this study concentrated on a wave propagating through finite length material, the stop band was then defined by the transmission coefficient when lower than 5%, which, for each frequency, was calculated. Then, all transmission coefficients were plotted against frequency to gain the stop band and pass band picture for the tested frequency range.

In this thesis, a wave propagated through two types of material was tested; one being *periodic* laminate material with varied mechanical and geometrical properties; the other one being material with *randomness* added into either mechanical or geometrical properties. Note, that the stop band phenomenon will only occur when a wave is propagated through heterogeneous materials; hence, in both cases, heterogeneous material was constructed in two different material phases: Material phase 1 (M_1) and Material phase 2 (M_2). Note also, that a convergence study was undertaken to ensure the accuracy of the finite element simulation.

Periodic laminate material
For periodic laminate material three different tests have been conducted:

- Changing the difference ratio of Young's modulus (β_E) of M_1 and M_2 to test the influence of Young's modulus contrast on the stop band.
- Varying the difference ratio of density (β_ρ) of M_1 and M_2 to test the influence of density contrast on the stop band.
- Changing the length of the unit cell (L_{unit}) to analyse the influence of geometry difference on the stop band.

The difference ratio of Young's modulus with four values (β_E equals to 0.5, 0.25, 0.1 and 0.05) have been tested in Section 2.3.1. The results shown in Figure 2.8 indicate:

- With an increase in β_E, the value of the transmission coefficient decays in both the stop band and the pass band.
- With an increase in β_E, the frequency of the starting point of the first stop band becomes lower.
- All four cases also indicate that, at low frequency (less than 1.5×10^5 Hz), increasing β_E does not have a significant influence on wave propagation.

To test the influence of the density contrast of the material on the stop band, four tests were also completed (see Section 2.3.2). In these four cases, β_ρ was set at 0.5, 0.25, 0.1 and 0.05 and the simulation results are shown in Figure 2.9, revealing the following:

- An increase in β_ρ leads to the transmission coefficient dropping in both the stop band and the pass band, which is similar to the influence of an increase in β_E.
- The band width (frequency range) of the first stop band increase with an increase in β_ρ.
- The frequency of the starting point barely changes with an increase in β_ρ, which is quite different from the change situation for β_E.

Similar to simulations with changing values for β_ρ and β_E, four simulations were run with the length of unit cell equal to 2 mm, 4 mm, 10 mm and 20 mm, to study the influence of microstructure difference on the stop band (see Section 2.3.3).

The simulation results for these four cases, shown in Figure 2.10, indicate the following:

- with increased L_{unit} in the heterogeneous material the frequency of the starting point decreases, which means that a short L_{unit} compared to a long L_{unit} creates greater difficultly in sensing the wave at low frequencies.

After the results of three different tests (β_E changing test, β_ρ changing test, and L_{unit} changing test) were analysed with periodic laminate material, the relations among the average wavelength ($\bar{\lambda}$) of the heterogeneous material, the length of the unit cell, and the frequency of the starting point of the first stop band (f_{s1}) were studied. The process of $\bar{\lambda}$ calculation for the heterogeneous material at a certain frequency was introduced in Section 2.3.4. The calculation process determined that the average wavelength contains information related to the mechanical properties of M_1 and M_2 and the volume fraction of each material in the heterogeneous material. Through analysis, it was found that when the average wavelength is equal to two times the length of the unit cell ($2 \times L_{unit}$) the corresponding frequency then becomes the frequency of the starting point of the first stop band. This relation is expressed by Eq. 2.13.

In Young's modulus contrast test, with an increase in β_E, the average Young's modulus of the heterogeneous material [calculated by Eq. 2.10] decreases significantly, leading to $\bar{\lambda}$ decreasing significantly, as well. Hence, with an increase in β_E, the $\bar{\lambda}$ will equal $2L_{unit}$ at the lower frequency, which means the f_{s1} has decreased.

In the density contrast test, with an increase in β_ρ, the average density of the heterogeneous material [calculated by Eq. 2.11] increased slightly, which causes $\bar{\lambda}$ to decrease slightly. Hence, with an increase in β_ρ, the $\bar{\lambda}$ will equal $2L_{unit}$ roughly at the same frequency, which means the f_{s1} will not change much in the four cases examined in this test.

In the difference of length of unit cell test, the average wavelength of the heterogeneous material was the same for all cases, with an increase in L_{unit} in different cases, the frequency of the $\bar{\lambda}$ equal to $2L_{unit}$ becomes lower, which means the f_{s1} is decreased. All analyses therefore agreed with the relations [Eq. (2.13)] among $\bar{\lambda}$, L_{unit}, and f_{s1} found in this study.

Random laminate material

The simulations based on periodic laminate material presented the influence of the material's mechanical properties and geometrical properties on the stop band in an ideal situation. However, in real life, errors can be introduced in various situations, such as during the material manufacturing process. These errors can be treated as the randomness of the material; thus, the study of the influence of randomness, added into the material's mechanical and geometrical properties on the stop band, then becomes necessary. To accomplish the study, first, two tests were performed with randomness added into material's mechanical properties; second, two tests were performed with randomness added into material's geometrical properties; and finally, one test was performed with randomness added into both the material's mechanical properties and geometrical properties. One simulation with a periodic laminate material (Case 13 in Section 2.4.1) was treated as the reference case to identify the effect of randomness added into the material. In this case, $\beta_E = 0.25$ and $\beta_\rho = 0.1$ were applied to determine the mean value of the mechanical properties of the material with randomness.

Different cases of randomness added into material's mechanical properties have been introduced in Section 2.4.1 and 2.4.2. In Section 2.4.1, the randomness in the form of small perturbations, following normal distribution, is added into Young's modulus of each unit cell of the heterogeneous material. Three cases with the same mean value and different standard deviation parameter values (shown in Table 2.8) have been simulated and compared to the reference case of periodic laminate. The comparison of the results is shown in Figure 2.11; it indicates that, compared to the reference case, the influence of randomness added into Young's modulus of the heterogeneous material on wave propagation is minimal. With an increase in the standard deviation of the Young's modulus, the transmission coefficient at the second pass band dropped very slightly and the transmission coefficient at other frequencies was almost the same in the testing frequency range. Similarly, in Section 2.4.2, the randomness in the form of small perturbations, following normal distribution, was added into the density of each unit cell of the heterogeneous material. Three cases with the same mean value and different standard deviation (parameter values shown in Table 2.9) were simulated and compared to the reference case of the periodic laminate. The comparison is shown in Figure 2.12, which indicates that the influence of randomness added into the density of the heterogeneous material on the wave propagation was almost negligible for small standard deviation cases (Cases 17 and 18), and the influence was rather limited for a slightly larger standard deviation case (Case 19, in which the transmission coefficient at the second pass band dropped a little, compared to the reference case).

Tests of randomness added into the material's geometrical properties were introduced in Section 2.4.3, 2.4.4 and 2.5. In Section 2.4.3 the randomness in the form of small perturbation, following the normal distribution, was added into the length of each unit cell of the heterogeneous material. Three cases with the same mean value and different standard deviation (parameter values shown in Table 2.9) were simulated. The mean value was 5 mm and standard deviation was 0.05, 0.1 and 0.2. The simulation results were compared to the reference case of the periodic laminate and presented in Figure 2.13. The results indicate that, with an increase in the standard deviation the transmission coefficient at the second pass dropped significantly. When the standard deviation was 0.2, the influence of randomness almost removed the second pass band.

To study the influence of a higher degree of randomness (compared to small perturbation cases) added into the material's geometrical property on the stop band, wave propagation in *"semi-random"* material was tested in Section 2.4.4. While generating the microstructure, the computer program may create extremely large or small unit cells. Hence, limited by the program's realisations and with the conscious aim of avoiding extreme situations, a new method of randomness realization was introduced, as the material's microstructure layout, following the Fibonacci sequence. Ten realisations with different random microstructures were simulated to obtain the average transmission coefficient at each tested frequency. For each case, the microstructure was constructed from 20 unit cells picked from the *"Fibonacci bar"* (the method of *"Fibonacci bar"* creation is introduced in Section 2.4.4) with a Fibonacci number equal to 20 in sequence. The average transmission coefficient was then compared to the reference case of the periodic laminate, shown in Figure 2.16. The results reveal that the heterogeneous material with *"semi-random"* microstructure can reduce the transmission coefficient at the second pass band significantly and the transmission coefficient retains almost the same degree of success in the other frequency range as in the reference case.

By comparing the influence of randomness, added into the material's mechanical properties (Section 2.4.1 and 2.4.2) and the material's geometrical properties (Section 2.4.3 and 2.16) on the stop band phenomenon, it is fair to say that, with the same randomness level added into the material's mechanical and geometrical properties, geometry is more likely to influence the wave procreation at certain frequencies.

Generally speaking:

- The randomness added to the mechanical properties does not influence either the starting frequencies of the first stop band, the width of the first stop band or the second pass band.
- However, adding randomness of the same order (small perturbation) to the geometrical characteristics changes the picture significantly. Although the properties (the starting frequency and the width) of the first stop band remain unaffected, the second pass band is significantly reduced: thus, the transmission coefficient can be lowered by introducing small perturbations into material geometry.

The final test with randomness added into both the material's mechanical properties and geometrical properties was illustrated in Section 2.5, which referred to a *"fully-random"* case. The randomness added into the material's mechanical properties was realised by adding randomness into the material type-choosing process of each unit cell (whether it was to be Material 1 or 2); while uniform distribution and randomness added into the material's geometrical properties was realised by adding randomness into the length of each unit cell following normal distribution. The example microstructure with both types of randomness is shown in Figure 2.17. Ten realisations were simulated and the averaged transmission coefficient then compared to the reference case of the periodic laminate. The results are shown in Figure 2.18, which highlights the fact that no clear stop band occurred but the transmission coefficient remained at a low level (around 10%) after the initial drop. The *"fully-random"* case was also compared with the *"semi-random"* case and small perturbation case, along with the reference case, together (see Figure 2.19).

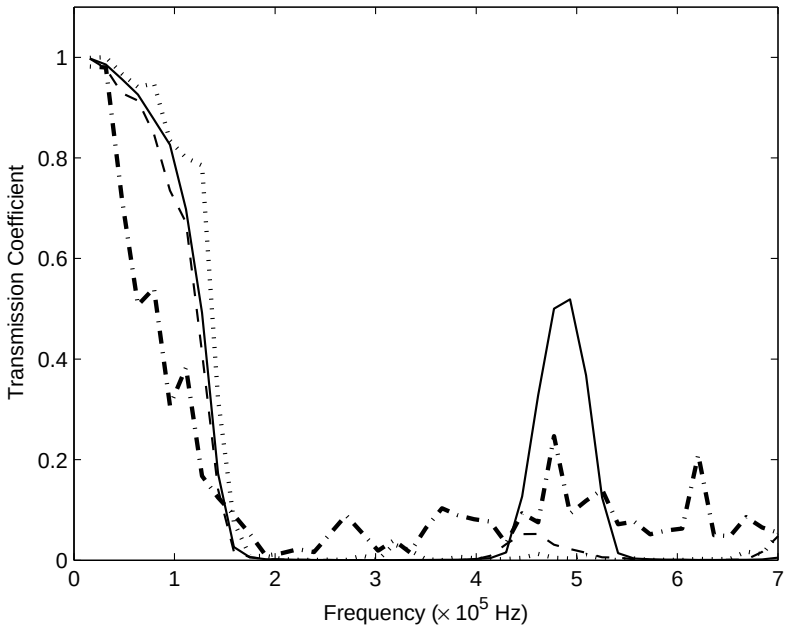

Figure 2.19: Simulation results of periodic case, small perturbation case, *"semi-random"* case and *"fully random"* case compared (Solid line: periodic case, Dotted line: small perturbation case, Dashed line: *"semi-random"* case, Dotted dashed line: *"fully-random"* case)

As shown in Figure 2.19, once randomness was added into the material's geometrical properties, the transmission coefficient at the second pass band was reduced significantly. When comparing the *"semi-random"* to the small perturbation case, in the first stop band the transmission coefficient was always less than 0.01 for the *"semi-random"* case but at some frequencies the transmission coefficient was slightly over 0.01 (still not over 0.05) for a small perturbation case. This means the *"semi-random"* nature of the material can create a smoother stop band compared to the small perturbation case. For the second pass band, at several frequencies the

transmission coefficient became slightly over 0.05 for the *"semi-random"* case, but the transmission coefficient was always lower than 0.02 for the small perturbation case. This signifies that a small perturbation of the material can nearly remove the second pass band but with a *"semi-random"* material, the wave can still pass into the second pass band. Randomness in both cases had a slight influence on wave propagation in the stop band compared to periodic material, but could reduce the transmission coefficient significantly in the second pass band. However, the *"fully-random"* case changed the stop band into a pass band (although it maintained the transmission coefficient at a low level) and reduced the transmission coefficient at the second pass band.

Chapter 3

Stop band prediction based on gradient elasticity

As an alternative way of describing the material without explicitly defining it, but still including all the information of the material's microstructure, a gradient-enriched formulation can be used. Thus, it is of interest to analyse the emergence of stop bands following gradient elasticity methodology. The gradient theory explored below is used because it is simple to implement; alternative micro-structure theories based on nonlocal (integral) assumptions [86] or micro-polar formulations [87, 88] have not been considered here.

3.1 Introduction of gradient theory

Classical elasticity has been widely used in engineering after Robert Hooke discovered the relation between stress and strain in materials in 1660. For a very simple case, the relation is shown as follows:

$$\sigma = E\varepsilon \tag{3.1}$$

where σ, E and ε are stress, Young's modulus and strain, respectively. These relations are limited to small displacements and one-dimensional situations. To describe the behaviour of a continuum material, the constitutive equation is expanded as follows:

$$\sigma_{ij} = D_{ijkl}\varepsilon_{kl} \tag{3.2}$$

where σ_{ij}, D_{ijkl} and ε_{kl} are stress tensors, stiffness tensors and strain tensors, respectively. Eq. (3.2) can be used to describe the behaviour of continuum material in three dimensions.

However, classical elasticity is only valid when the material is homogeneous. When the material is heterogeneous, results calculated by applying classical elasticity may become unrealistic on the microscopic level. Hence, to overcome these anomalies, gradient theory is developed by enriching the field equations with appropriate higher-order spatial gradients of state variables. In the 1960s, gradient extensions of elasticity were formulated by Toupin [87] and Mindlin [89]. After this, many formats of gradient

elasticity were suggested with additional gradients of strain. In this section, different ways to obtain gradient elasticity formats will be discussed and compared. The first was introduced by Aifantis and co-workers [90–92] for the static case. The second was developed by Eringen [93] for the dynamic case. The third was proposed by Metrikine and Askes [94] for the response of a discrete material model.

In the previous chapter, while running different simulations, the heterogeneous material has been modeled and meshed explicitly. However, by applying gradient theory, the heterogeneous material has to be homogenised first to create an *equivalent continuum material*. The modelling and meshing process will then be based on this homogenised material. In this case the meshing process will be more efficient. Additionally, the simulation time based on gradient theory is lower. This signifies that, the gradient theory provides a more efficient tool.

3.1.1 Gradient elasticity formulation suggested by Aifantis

The gradient elasticity formulation suggested by Aifantis [81] is based on the static point of view. This format was derived by extending the strain energy density with an additional term, and the constitutive relation is modified to

$$\sigma_{ij} = D_{ijkl}\left(\varepsilon_{kl} - \ell^2 \varepsilon_{kl,mm}\right) \tag{3.3}$$

Kinematically, the strains are the same as in classical elasticity, namely

$$\varepsilon_{kl} = \frac{1}{2}\left(\frac{\partial u_k}{\partial x_l} + \frac{\partial u_l}{\partial x_k}\right) \tag{3.4}$$

where u_i are the displacement components. Stresses (σ_{ij}) and stiffness (D_{ijkl}) have the same meaning, as in Eq. (3.2). The difference between Eq. (3.3) and Eq. (3.2) is that Eq. (3.3) includes higher-order spatial gradients of strain and an additional internal length scale parameter ℓ, which represents the microstructure of the material [95].

For statics, the equilibrium equation of gradient theory is the same as classical elasticity:

$$\sigma_{ij,j} + b_i = 0 \tag{3.5}$$

where b_i are the body force components. Combining Eq. (3.3) to (3.5) leads to a system of partial differential equations:

$$D_{ijkl}\left(u_{k,jl} - \ell^2 u_{k,jlmm}\right) + b_i = 0 \tag{3.6}$$

3.1.2 Gradient theory formulation suggested by Eringen

The gradient theory formulation suggested by Eringen is obtained based on the dynamic viewpoint. Eringen considered nonlocal elasticity with integral formulation, in which volume averages of relevant state variables are computed [93]. In particular, nonlocal and local stresses are linked together and can be computed from local stresses via:

$$\sigma^g_{ij} - \ell^2 \sigma^g_{ij,kk} = \sigma^c_{ij} \tag{3.7}$$

where σ^g_{ij} and σ^c_{ij} represent gradient stress and classical stress, respectively. The equation of motion is written as

$$\sigma^g_{ij,j} + b_i = \rho \ddot{u}_i \tag{3.8}$$

where ρ is the mass density.

The constitutive relation here is the same as in Eq. (3.2), but the reader should recall the difference between gradient stresses and classical stresses. Combining Eqns. (3.2), (3.4), (3.7) and (3.8) the irreducible form is derived:

$$D_{ijkl} u_{k,jl} + b_i = \rho \left(\ddot{u}_i - \ell^2 \ddot{u}_{i,mm} \right) \tag{3.9}$$

3.1.3 Gradient theory formulation based on response of discrete material model

This formulation of gradient theory can be obtained from the response of continualising a discrete material model to capture the dynamic behaviour of heterogeneous materials. The constitutive relation is derived as [88, 94]:

$$D_{ijkl} \left(u_{k,jl} + \ell^2 u_{k,jlmm} \right) + b_i = 0 \tag{3.10}$$

The only difference between Eq.(3.10) and Eq.(3.6) is the sign of the higher-order term. Because this relation is obtained via the continualisation of a discrete material model (for example a mass-spring system), the length scale ℓ is related to the geometry straightforwardly. However, this formulation of gradient theory is unstable [96].

Metrikine and Askes [97] modified this relation by combining it with the advantages of Eq. (3.6) in the static part. The constitutive relation, now stable, becomes:

$$\sigma_{ij} = D_{ijkl} \left(\varepsilon_{kl} - \ell_s^2 \varepsilon_{kl,mm} \right) + \rho \ell_m^2 u_{i,jtt} \tag{3.11}$$

where ℓ_s^2 is the length scale with higher-order stiffness term and ℓ_m^2 is the length scale with higher-order inertia term.

3.1.4 Length scale in gradient theory

In the gradient theory discussed above, two different length scales are proposed: the length scale in statics, ℓ_s, and the length scale in dynamics, ℓ_m. Length scale in gradient theory is a parameter used to quantify the influence of material near the sample point. Based on the homogenisation of a Representative Volume Element (RVE) of a material [95], Gitman and co-workers derived a relation between the length scale ℓ_s, and the size of the RVE in statics [98]. For the length scale ℓ_m, a similar relation could be identified with the linking of ℓ_m and the size of the RVE in dynamics [98]. These two relations are shown below:

$$\ell_s^2 = \frac{1}{12} \ell_{RVE_s}^2 \tag{3.12}$$

$$\ell_m^2 = \frac{1}{12} \ell_{RVE_m}^2 \tag{3.13}$$

The question of identifying the size of an RVE in the static case has been addressed by Gitman [95]. However the dynamic RVE size requires further investigation.

3.2 1D Dispersion analysis

Dispersion analysis in this section is based on harmonic wave propagation. The displacement is assumed to be the general harmonic solution:

$$u = Ae^{i(kx-\omega t)} \tag{3.14}$$

where A, k and ω are amplitude, wave number and angular frequency.

For the homogeneous material with consideration of classical elasticity, substituting the displacement with the general harmonic solution Eq. (3.14) and changing body force to the standard inertia term in the equilibrium equation of classical elasticity Eq. (3.5), yields:

$$-\rho\omega^2 Ae^{i(kx-\omega t)} = -Ek^2 Ae^{i(kx-\omega t)} \tag{3.15}$$

From Eq. (3.15), the dispersion relation based on classical elasticity can be found:

$$\frac{\omega^2}{k^2} = \frac{E}{\rho} \tag{3.16}$$

The left side of Eq. (3.16) is the phase velocity ($c = \omega/k$), and on the right side of Eq. (3.16) is a constant value (where the elastic bar velocity c_e is defined by $c_e^2 = E/\rho$) depending on the material. As the phase velocity c does not depend on the wave number k, this result means that there is no dispersion effect in a homogeneous material, without considering the influence of the material's microstructure. However, with consideration of the material's microstructure, the wave dispersion effect can be predicted, based on gradient theories. Following a similar procedure, the dispersion relations based on different gradient theories have been obtained, as reported below [99]:

Dispersion relation based on Aifantis' theory:

$$\frac{c^2}{c_e^2} = 1 + k^2\ell^2 \tag{3.17}$$

Dispersion relation based on Eringen's theory:

$$\frac{c^2}{c_e^2} = \frac{1}{1 + k^2\ell^2} \tag{3.18}$$

Dispersion relation based on the model modified by Metrikine and Askes:

$$\frac{c^2}{c_e^2} = \frac{1 + k^2\ell_s^2}{1 + k^2\ell_m^2} \tag{3.19}$$

From Eqs. (3.17-3.19), it is obvious that phase velocity c depends on the wave number k, which means that all models can predict the dispersion of wave propagation in the

material. Additionally, the length scale can influence phase velocity. Although, all gradient theory models mentioned in this report can predict dispersion in material, the results are different, based on different models. The dispersion analysis results based on Aifantis's gradient model, Eringen's gradient model, and classical elasticity, are shown in Figure 3.1.

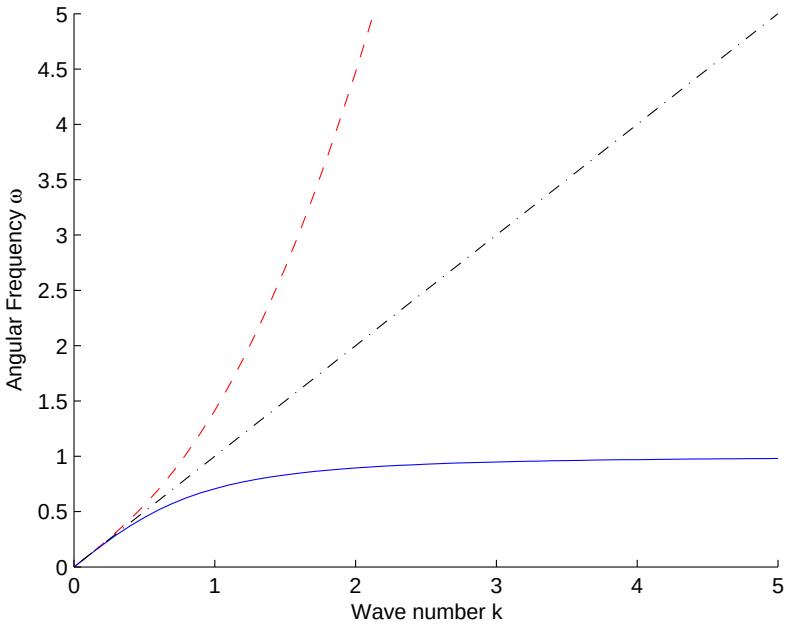

Figure 3.1: Angular frequency ω versus wave number k for Aifantis' model(dashed), Eringen's model(solid) and Classical elasticity model(dot-dashed)

Figure 3.1 shows that dispersion relation based on Aifantis's gradient model is unrealistic (angular frequency becomes ultimate when wave number keeps increasing, shown in Figure 3.1 by dashed line). Dispersion relation based on Eringen's gradient model (solid line in Figure 3.1) shows that angular frequency will approach one certain value when the wave number keeps increasing, which means that a wave cannot propagate through material where the wave number increases to a significantly large number. Hence, it is possible to apply gradient theory to predict stop band phenomenon analytically [see Section (3.3)].

As for Metrikine and Askes' model, with two length scale parameters, ℓ_s and ℓ_m, it is a more complex model than the two discussed above. Figure 3.2 shows the results predicted by applying Metrikine and Askes' gradient model for dispersion analysis (normalized phase velocity versus normalised wave number). Here, normalised phase velocity not only depends on wave number but also relies on the ratio between static length scale ℓ_s and dynamic length scale ℓ_m. As shown in Figure 3.2, if the wave number k is large enough, the normalised phase velocity will lead to a constant number which is the ratio of ℓ_s and ℓ_m. This relation can also be derived analytically by assuming wave number k to be infinitely large in Eq. (3.19) and it will be:

$$\frac{c}{c_e} = \lim_{k\to\infty} \sqrt{\frac{1+k^2\ell_s^2}{1+k^2\ell_m^2}} = \frac{\ell_s}{\ell_m} \tag{3.20}$$

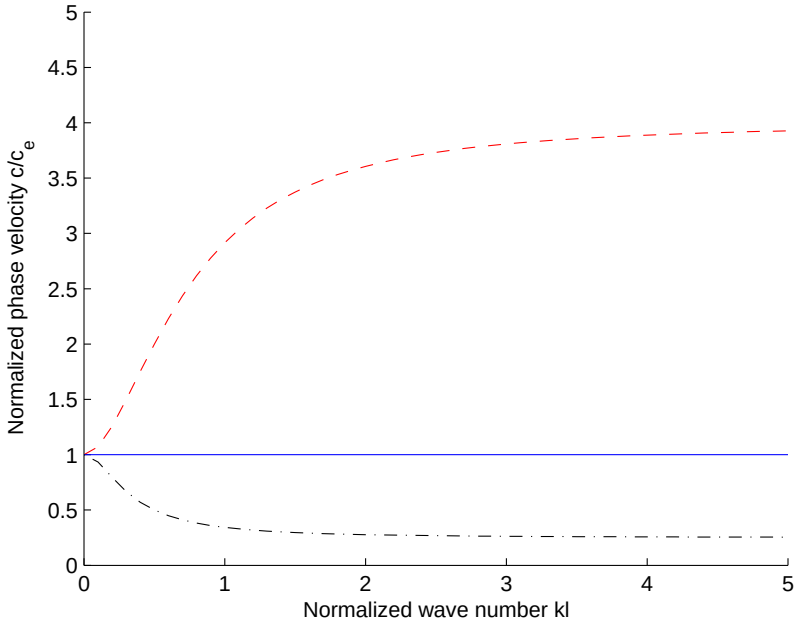

Figure 3.2: Normalized phase velocity c/c_e versus normalized wave number $k\ell$ for Metrikine and Askes' model with $\ell_s/\ell_m = 4$ (dashed), $\ell_s/\ell_m = 1$ (solid) and $\ell_s/\ell_m = 0.25$ (dotted dashed)

3.3 Periodic laminate material stop band prediction based on gradient elasticity

Since this study is focused on dynamic behaviour of the material, the gradient elasticity format with inertia gradient will be applied to predict the stop band for a one-dimensional, two-phase laminate material with periodic structure under dynamic loading. By considering the influence of material microstructure, which is represented by a length scale (an additional parameter preceding the extra gradient term), it is possible to use gradient theory to predict the stop band [as introduced in Section (3.2)]. The gradient theory applied in the calculation can be expressed by Eq. (3.21) (which is similar to Eringen's gradient model; see, for example, [82]), where ρ and E are the averaged mass density and Young's moduli, respectively, ℓ is the size of the periodic unit cell in the laminate material (see Figure 2.2). They can be found by Eq. (3.22) and Eq. (3.23), where α is the volume fraction with value of 0.5 for periodic microstructure; ρ_1^p and ρ_2^p are mass densities of material phases 1 and 2 for periodic microstructure, respectively; E_1^p and E_2^p are Young's moduli of materials 1 and 2 for periodic

microstructure, respectively; coefficient γ is obtained by Eq. (3.24) [82]. Note that, the coefficient γ is created by Terry [82] that is only applied to the one-dimensional laminate material [100] to ensure the accuracy of the length scale parameter.

$$\rho u_{,tt} - \gamma \ell^2 \rho u_{,ttxx} = E u_{,xx} \tag{3.21}$$

$$\rho = \alpha \rho_1^p + (1-\alpha)\rho_2^p \tag{3.22}$$

$$E = \frac{E_1^p E_2^p}{(1-\alpha)E_1^p + \alpha E_2^p} \tag{3.23}$$

$$\gamma = \frac{1}{12}\left[\frac{\alpha(1-\alpha)(E_1^p\rho_1^p - E_2^p\rho_2^p)}{(1-\alpha)\rho E_1^p + \alpha\rho E_2^p}\right]^2 \tag{3.24}$$

In this section, Young's moduli of material phase 1 and 2 are suggested to be related: $E_2^p = \beta_E E_1^p$ and mass densities of materials 1 and 2 are suggested to be $\rho_2^p = \beta_\rho \rho_1^p$ where $\beta_E = \beta_\rho = \beta$ for simplicity is a constant proportionality coefficient. Based on Eq. (3.21), and replacing displacement by a harmonic solution [see Eq. (3.14)], the dispersion relation can be obtained:

$$-\rho\omega^2 A e^{i(kx-\omega t)} - \gamma\rho\ell^2\omega^2 k^2 A e^{i(kx-\omega t)} = -Ek^2 A e^{i(kx-\omega t)} \tag{3.25}$$

$$\omega = \frac{Ek^2}{\rho(1+\gamma k^2\ell^2)} \tag{3.26}$$

After substituting E_1^p, E_2^p, ρ_1^p, ρ_2^p, and β into Eq. (3.26), the first stop band starting frequency ω can be found from Eq. (3.27) (assume k to be infinite).

$$\omega = \lim_{k\to\infty}\sqrt{\frac{\bar{E}k^2}{\bar{\rho}(1+\gamma k^2\ell^2)}} = \sqrt{\frac{24\beta E_1^p}{(1-\beta)^2\ell^2\rho_1^p}} \tag{3.27}$$

3.4 Finite element implementation

In this section the discussion on the finite element implementation will be presented for the case of homogenised material based on gradient theory.

3.4.1 Implementation of gradient theory in finite element simulation

In this section, the discussion of the finite element implementation will be presented for the case of homogenised material based on gradient theory. To apply gradient theory in finite element simulation, discretisation of the gradient elasticity equations is necessary. Based on different forms of the gradient elasticity, discretisation can vary. In this section, the discretisation process is introduced in detail in relation to the 2D situation, but a similar process can be applied to 1D and 3D.

By applying the finite element method, the continuous displacement u^c is approximated by $\mathbf{u}$ in terms of the finite element's nodal values $\mathbf{d} = \left[d_{1x}, d_{1y}, d_{2x}, d_{2y}, \cdots\right]^T$ (depending

on the shape of the finite element). The relation between **d** and **u** is linked by a shape function **N** [shown in Eq. 3.28] as $\mathbf{u} = \mathbf{Nd}$.

$$\mathbf{N} = \begin{bmatrix} N_1 & 0 & N_2 & 0 & \cdots \\ 0 & N_1 & 0 & N_2 & \cdots \end{bmatrix} \tag{3.28}$$

For example, a bar element (the bar element has only one degree of freedom, hence it is capable of simulations in 1D cases in this study) is shown in Figure 3.3.

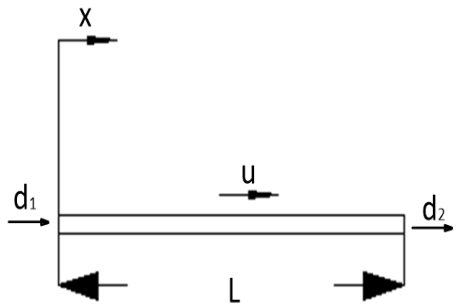

Figure 3.3: The bar element

As shown in the figure, the displacement can be expressed as:

$$\mathbf{u} = [N_1 N_2] \begin{Bmatrix} \mathbf{d_1} \\ \mathbf{d_2} \end{Bmatrix} \tag{3.29}$$

where $\mathbf{d_1}$ and $\mathbf{d_2}$ are nodal displacement of two ends of the finite element and L is the length of the finite element. Assuming the displacement is a linear variable, the shape function N_1 and N_2 become:

$$N_1 = (1 - \frac{x}{L}), N_2 = \frac{x}{L} \tag{3.30}$$

In the 2D situation, the relation of **u** and **d** is the same as in 1D, but the shape function is different. For example, a square element is shown in Figure 3.4.

Assuming that the displacement is a linear variable in the square element, the shape function (assume the shape function in the horizontal direction and vertical direction is the same) is calculated:

$$N_1 = (1 - \frac{x}{a})(1 - \frac{x}{a}) \tag{3.31}$$

$$N_2 = (1 - \frac{x}{a})\frac{y}{a} \tag{3.32}$$

$$N_3 = \frac{x}{a}\frac{y}{a} \tag{3.33}$$

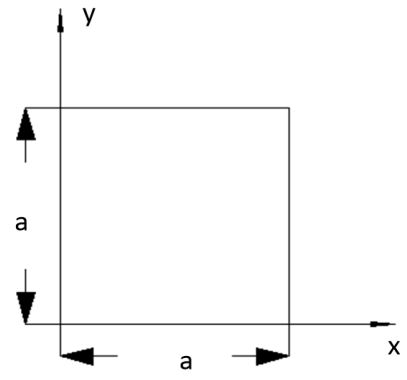

Figure 3.4: The square element

$$N_4 = \frac{x}{a}(1-\frac{y}{a}) \tag{3.34}$$

Meanwhile, the usual derivative operators ∇ and $\mathbf{L}$ are defined:

$$\nabla = \begin{bmatrix} \frac{\partial}{\partial x} \\ \frac{\partial}{\partial y} \end{bmatrix} \tag{3.35}$$

$$\mathbf{L} = \begin{bmatrix} \frac{\partial}{\partial x} & 0 \\ 0 & \frac{\partial}{\partial y} \\ \frac{\partial}{\partial y} & \frac{\partial}{\partial x} \end{bmatrix} \tag{3.36}$$

At the same time, $\nabla^2 \equiv \nabla^T \nabla$

Applying the above process to the constitutive relation of normal classical elasticity, the equation then changes from tensor notation to matrix-vector notation:

$$\mathbf{L}^T \mathbf{D}\mathbf{L}\mathbf{u} + \mathbf{b} = 0 \tag{3.37}$$

where $\mathbf{D}$ is the matrix form of the constitutive tensor D_{ijkl}, and $\mathbf{b} = [b_x, b_y]^T$ is the body force.

Similarly, applying the above process to the constitutive relation of gradient elasticity with inertia gradient [Eq. (3.9)], the matrix-vector notation of the equation becomes

$$\mathbf{L}^T \mathbf{D}\mathbf{L}\mathbf{u} + \mathbf{b} = \rho\left(\ddot{\mathbf{u}} - \ell^2 \nabla^2 \ddot{\mathbf{u}}\right) \tag{3.38}$$

Taking the weak form of Eq.(3.37) with domain Ω and boundary Γ, and then integrating by parts, gives

$$\int_\Omega (\mathbf{L}\mathbf{w})^T \mathbf{D}\mathbf{L}\mathbf{u} d\Omega = \int_\Omega \mathbf{w}^T \mathbf{b} d\Omega + \int_{\Gamma_n} \mathbf{w}^T \mathbf{t} d\Gamma \tag{3.39}$$

where $\mathbf{w} = [w_x, w_y]^T$ is a vector with test functions and $\mathbf{t} = [t_x, t_y]^T$ are the user-prescribed tractions on the Neumann part Γ_n of the boundary. The discretised equation of Eq. (3.37) is then obtained as

$$\int_{\Omega} \mathbf{B}^T \mathbf{D}\mathbf{B} \mathrm{d}\Omega \mathbf{d} \equiv \mathbf{K}\mathbf{d} = \mathbf{f} \tag{3.40}$$

in which the stiffness matrix $\mathbf{K}$ and the strain-displacement matrix $\mathbf{B} = \mathbf{L}\mathbf{N}$ have been defined. The force vector $\mathbf{f}$ includes the body force and the externally applied tractions.

Similarly, taking the weak form of Eq. (3.38) with domain Ω and boundary Γ, then integrating by parts, the equation becomes

$$\int_{\Omega} (\mathbf{L}\mathbf{w})^T \mathbf{D}\mathbf{L}\mathbf{u} \mathrm{d}\Omega + \int_{\Omega} \rho \left[\mathbf{w}^T \ddot{\mathbf{u}} + \ell^2 \left(\frac{\partial \mathbf{w}^T}{\partial x} \frac{\partial \ddot{\mathbf{u}}}{\partial x} + \frac{\partial \mathbf{w}^T}{\partial y} \frac{\partial \ddot{\mathbf{u}}}{\partial y} \right) \right] \mathrm{d}\Omega = \int_{\Omega} \mathbf{w}^T \mathbf{b} \mathrm{d}\Omega + \int_{\Gamma_n} \mathbf{w}^T \mathbf{t} \mathrm{d}\Gamma \tag{3.41}$$

where $\mathbf{w}$ is the same as in Eq. (3.39) and $\mathbf{t}$ now also includes the inertia effects. After discretisation, Eq. (3.38) leads to

$$\mathbf{K}\mathbf{d} + \left[\mathbf{M} + \ell^2 \mathbf{H} \right] \ddot{\mathbf{d}} = \mathbf{f} \tag{3.42}$$

in which $\mathbf{K}$ and $\mathbf{f}$ are the same as in Eq. (3.40). The two parts of mass matrix are defined by the following equations:

$$\mathbf{M} = \int_{\Omega} \rho \mathbf{N}^T \mathbf{N} \mathrm{d}\Omega \tag{3.43}$$

$$\mathbf{H} = \int_{\Omega} \rho \left(\frac{\partial \mathbf{N}^T}{\partial x} \frac{\partial \mathbf{N}}{\partial x} + \frac{\partial \mathbf{N}^T}{\partial y} \frac{\partial \mathbf{N}}{\partial y} \right) \mathrm{d}\Omega \tag{3.44}$$

The above process introduced the discretisation algorithm in the space domain; a time integration algorithm in the time domain was also needed. In the next section, this finite element methodology illustrated when it was used to simulate a 1D stop band behaviour, while 2D numerical analysis will be covered in Chapter 4.

3.5 1D Numerical analysis based on gradient theory

The finite element simulation procedure based on gradient theory, followed the same process introduced in Section 2.2. For each testing frequency as in Section 2.2, a homogeneous reference case was used to calculate the amplitude (A_h) of the wave propagation. Then the homogeneous material was replaced and simulated with the same loading and boundary conditions to obtain the amplitude of the wave propagating through the heterogeneous material (A_c). In Section 2.2, the amplitude A_c was found while considering the wave propagating through the explicitly constructed heterogeneous material. In this section, information about the heterogeneous structure of the material enters via effective properties, obtained through averaging, and the length scale of the newly defined homogenised material. Then the wave propagating through this homogenised material is simulated, and the amplitude of wave propagating through the homogenised material can be calculated (defined as A_g). For each testing frequency the transmission coefficient of the wave propagating through the homogenised material can then be calculated as $T = A_g/A_h$, similarly to Section 2.2.

The initial heterogeneous material used here was similar to the one used in Section 2.2.4, with two different components: M_1 with $E = 2 \times 10^{11}$ Pa and $\rho = 8 \times 10^3$ kg/m^3. The contrast ratio for Young's modulus was $\beta_E = 0.25$ and for the density was $\beta_\rho = 0.1$. The average mechanical properties were obtained via Eq.(3.23) and Eq.(3.22), and resulted in $E = 8 \times 10^{10}$ Pa and $\rho = 4.4 \times 10^3$ kg/m^3. The information about the geometrical properties enters via a "length scale" and is linked to the RVE of the heterogeneous material (see Gitman [95] for reference). Here, the length scale was first chosen to be the same length ($\ell = 10$mm) as the length of the unit cell (which can be treated as the RVE size in the 1D case for a periodic material). The length scale was then chosen to be twice ($\ell = 20$mm) the length of the unit cell, based on the prediction that the first stop band should exist when the average wavelength is twice the length of the unit cell (see Section 2.3.4). Simulations were carried out with both length scales and are discussed later in this section.

In the first simulation a continuous longitudinal harmonic wave was set to propagate through the homogeneous material at a frequency of 2×10^6 rad/s. The displacements at the receiving point were recorded and are shown in Figure 3.5, which match identically with the homogeneous material test undertaken in Section 2.2.4. After applying the Fourier transform of the displacements the amplitude was calculated as $A_h = 2.47 \times 10^{-6}$. The second simulation was for a continuous longitudinal harmonic wave propagating through the homogenised material at the same frequency. The displacements at the recording point were recorded and are shown in Figure 3.6. Comparing the displacements with the wave propagating through heterogeneous material (recorded displacements are shown in Figure 2.5), it can be seen that the displacement changes, based on the homogenised material, are similar to the displacement changes based on heterogeneous material in terms of the overall trend, but smoother. Following the Fourier transform of the displacements, the amplitude was found to be $A_g = 1.22 \times 10^{-9}$. Hence, the transmission coefficient was:

$$T = \frac{A_g}{A_h} = \frac{1.22 \times 10^{-9}}{2.47 \times 10^{-6}} = 1.08 \times 10^{-3} \tag{3.45}$$

At the next step, the testing frequency range from 1×10^5rad/s to 4.5×10^6rad/s is considered with an interval of 1×10^5rad/s, similar to those discussed in Section 2.2. The simulation results are presented in Figure 3.7. The numerical result for homogenised and heterogeneous materials are compared here with analytical prediction, calculated by Eq.(3.27).

Two different numerical predictions for homogenised material with two different length scales are presented in Figure 3.7, and compared with corresponding analytical predictions. It illustrates that, when the length scale equals 20 mm (twice the length of the unit cell) the simulation result, based on gradient elasticity and classical elasticity, agreed well with the frequency of the starting point of the first stop band, and coincided with the analytical prediction. Note here; that, together with the advantages described at the beginning of this chapter, gradient elasticity, due to its nature, can only predict the first stop band, which is a limitation of this type of gradient theory.

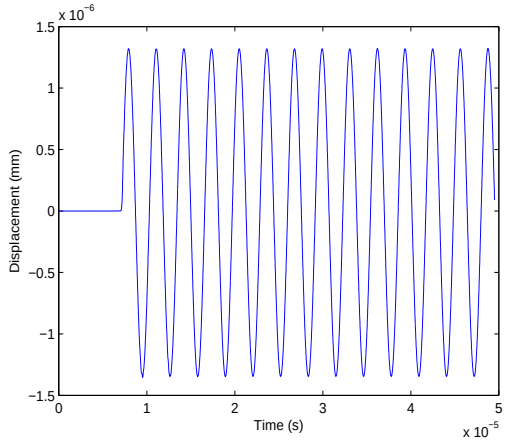

Figure 3.5: Displacements at the receiving point for wave propagation simulation for homogeneous material (classical elasticity)

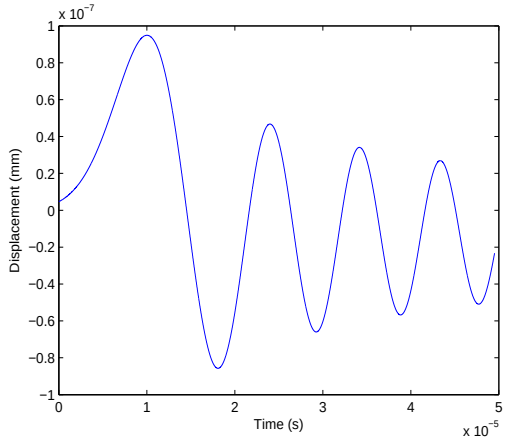

Figure 3.6: Displacements at the receiving point of wave propagation simulation for homogenised material (gradient elasticity)

3.6 Influence of randomness on stop band phenomenon using gradient elasticity theory

In this section, following the procedure introduced in Chapter 2, a discussion on the influence of randomness in mechanical and geometrical material properties on the stop band will be presented. Note: as the gradient elasticity is used to model the material's behaviour, the randomness could be added not only to the effective mechanical properties, but also into the length scale.

The analysis starts with randomness added into the length scale (ℓ). The homogenised material is a 100 mm bar with effective Young's modulus $E = 8 \times 10^{10}$ Pa and effective density $\rho = 4.4 \times 10^3$ kg/m^3. The deterministic length scale is taken as $\ell = 20$ mm in this case,after adding randomness into the length scale, in the form of a small perturbation, following the normal distribution, with a mean value $\mu = 20$ mm and standard deviation $\sigma = 0.2 \times 20$ mm. Because the randomness is added into the

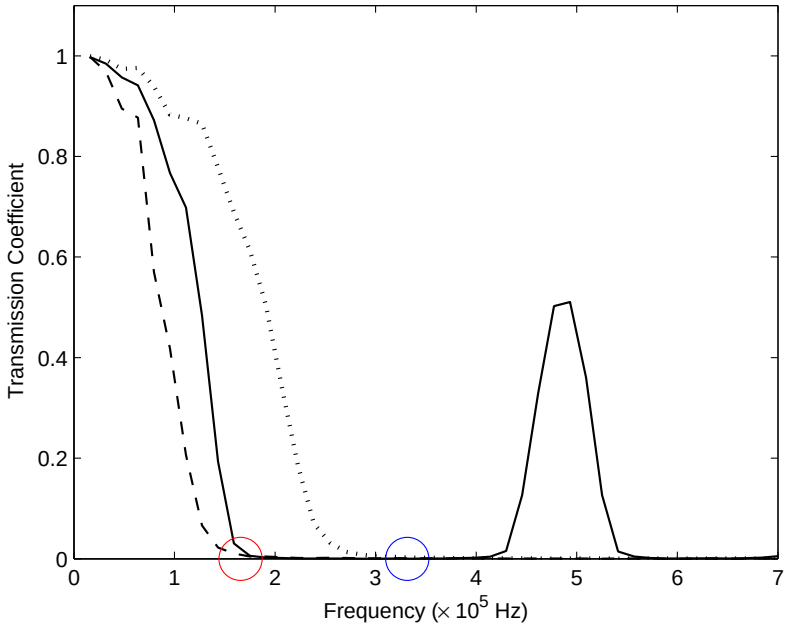

Figure 3.7: Results of wave propagation simulation. Solid line – classical elasticity; dotted line – gradient elasticity with $\ell = 10mm$; dashed line – gradient elasticity with $\ell = 20mm$; red circle – analytical prediction with $\ell = 20mm$; and blue circle – analytical prediction with $\ell = 10mm$

homogenised material, the value of the length scale will not change for a single realisation but will vary for different realizations. In this test, 10 realisations have been generated. The simulation process is the same for every realisation as introduced in Section 3.5; frequency ranges from 1×10^5 rad/s to 4.5×10^6 rad/s. At each frequency, one average transmission coefficient was calculated by averaging ten different transmission coefficients gained from 10 realisations with different length scales. All averaged transmission coefficients were then analysed for the stop band and pass band ranges.

Randomness was also added into the effective mechanical properties of the homogenised material. The material used in this simulation is the same as that used above with effective Young's modulus $E = 8 \times 10^{10}$ Pa and effective density $\rho = 4.4 \times 10^3$ kg/m^3 and $\ell = 20$ mm. The randomness is added, similar to that described above, in the form of a small perturbation, following the normal distribution: $N(E, 0.2E)$ and $N(\rho, 0.2\rho)$, i.e. with mean values for effective properties $\mu_E = E$ and $\mu_\rho = \rho$ and standard deviations of $\sigma_E = 0.2E$, $\sigma_\rho = 0.2\rho$. The mechanical properties were kept the same for each frequency in one realisation but varied in different realisations. Ten realisations with frequencies ranging from 1×10^5 rad/s to 4.5×10^6 rad/s were implemented as well. The average transmission coefficients for all frequencies for material with random effective mechanical properties were compared to the average transmission coefficients gained from the randomness added into the length scale and the transmission coefficients gained from the simulation, based on gradient elasticity without any randomness added

(simulation in Section 3.5). The results are compared in Figure 3.8.

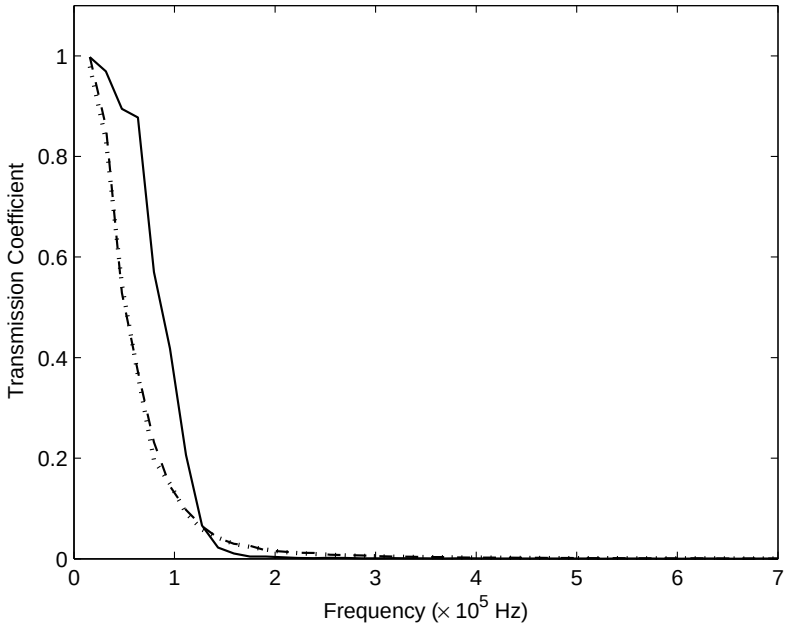

Figure 3.8: Results of wave propagating through material without randomness (Solid line) and with randomness added into the length scale (Dotted line) or mechanical properties (Dashed line)

As shown in Figure 3.8, the influence of randomness added to the material's effective mechanical properties and randomness added to the length scale produced nearly identical results. An explanation of this phenomenon can be given as follows:

- As introduced in Section 3.1.4, the length scale quantities influence material near to the infinitesimal point, i.e. the material's actual micro-structure.
- Hence, the length scale can be expressed as a function of the Young's modulus, density and the geometry of the underlying heterogeneous material: $\ell = f_\ell(E_1, E_2, \rho_1, \rho_2, geometry)$; here E_1, E_2, ρ_1 and ρ_2 are Young's modulus and the density of the two material phase in the underlying heterogeneous material.
- Additionally, the Young's modulus of the homogenised material can be expressed as a function of Young's modulus and the geometry of the underlying heterogeneous material. $E = f_E(E_1, E_2, geometry)$
- As such, it can be concluded that the length scale is coupled with effective E and ρ.
- Hence, adding similar types of randomness into the length scale and the effective E and ρ leads to a similar effect on the stop and pass band curves.

When randomness is added directly into the heterogeneous material's microstructure (see Sections 2.4.1-2.4.3), the results show that randomness added into the length of the unit cell will reduce the second pass band significantly; and randomness added to the mechanical properties will hardly influence the second pass band. Alternatively, randomness added to both the material's geometrical property and mechanical properties will hardly change the first pass band and first stop band. In this section, randomness added to effective material's mechanical properties and geometrical properties separately have almost the same influence on the first pass band and the first stop band. These two results showed good consistency on the influence of randomness added to the material on the first stop band. Although randomness added to homogenised material will reduce the transmission coefficient slightly in the first pass-band, nevertheless the trend remains consistent. More importantly, the randomness added to homogenised material will barely change the lower bound of the first stop band. Hence, simulation with randomness added to homogenised material can qualitatively replace simulation with randomness added into heterogeneous material's microstructure, to predict the first stop band. This technique can reduce the computational resource and time required and still result in acceptable accuracy.

3.7 Results, analysis, and discussion

The gradient elasticity theory was introduced to predict the stop band both analytically and numerically. Both analytical and numerical results indicate that applying gradient theory can predict the lower bound of the stop band with acceptable accuracy. Furthermore, material with randomness added can also be simulated, based on gradient theory.

To remind the reader, a very short overview of gradient theories is presented below. The gradient extensions of elasticity were first formulated by Toupin [87] and Mindlin [89] in the 1960s. The gradient theory was introduced to solve the problem encountered when the scale is close to the microstructure of the material. The gradient theory considers not only the local point but also the field surrounding it. In addition to this, the gradient theory can be applied to analyse the dispersion effect during wave propagation [101]. Many formats of gradient elasticity have been developed and three were introduced in this section: a) by Aifantis and co-workers [90–92] for the static case; b) by Eringen [93] for the dynamic case; c) by Metrikine and Askes [94] for the response of a discrete material model.

The gradient format introduced by Aifantis and co-workers [90–92] was derived by extending the strain energy density with an additional term [shown in Eq. (3.3)]. This format is based on the static point of view and the gradient term was only added to the stiffness part [shown in Eq. (3.6)]. The gradient format developed by Eringen [93] considered nonlocal elasticity with integral formulation [shown in Eq. (3.7)]. This format is based on the dynamic point of view and the gradient term was only added into the inertial part [shown in Eq. (3.9)]. The gradient format introduced by Metrikine and Askes [94] was obtained from the response of continualising a discrete material model. This format included the gradient term in both stiffness and inertial parts, as shown in

Eq. (3.11).

In all formats of gradient elasticity, a parameter referred to as length scale exists. This is a parameter that quantifies the influence of material surrounding the infinitesimal point. The length scale is dependent on material, and can be a single scale [see Eq. (3.6) and Eq. (3.9)] or multiple, different length scales [see Eq. (3.11)], depending on the format of the gradient elasticity model chosen. One way to derive the length scale is to link it with a Representative Volume Element. By applying this method, Gitman and co-workers derived the relation between the length scale in statics and the size of the RVE in statics [98].

Based on harmonic wave propagation, the dispersion analysis was conducted in this section by applying different formats of gradient elasticity. The dispersion relation was calculated based on different formats of gradient theory. Based on Aifantis' format, it indicates that the wave speed will become infinite with an increase in wave number. This result is unrealistic for wave propagation because wave speed can not be faster than the speed of light. The calculated dispersion relation, based on Eringen's format shows that the wave speed will decrease to zero with an increases in wave number. The calculated dispersion relation, based on Metrikine and Askes' format, shows that the wave speed will equal the ratio of two different length scales [introduced in Eq. (3.11)], with the increase in wave number. Dispersion analysis based on these gradient formats indicates the possibility of predicting the stop band analytically.

In this chapter, a gradient theory has been applied to predict the stop band for the harmonic wave propagating through homogenised material with an underlying microstructure of periodic laminate material. The process was introduced in Section 3.3 in detail. The analytical prediction of the stop band, based on gradient elasticity, can indicate the lower bound of the first stop band with acceptable accuracy [see Eq. (3.27)] but is unable to predict further stop bands because the gradient theory applied here only considered second-order derivatives.

Following the analytical prediction of stop band based on gradient theory, numerical simulations were performed to analyse the stop band. The simulation results were then compared with the simulation results, based on classical elasticity, and analytical prediction based on gradient theory (shown in Figure 3.7). The result shows that the analytical prediction based on gradient elasticity can predict the lower point of the first stop band, the value of which is similar to the numerical simulation results based on both classical elasticity and gradient elasticity. The simulation results based on gradient elasticity gave a similar first pass band as the results from the simulation based on classical elasticity. This proves that simulation based on gradient elasticity can predict the first stop band. However, both analytical prediction and numerical prediction based on gradient theory failed to predict the second pass band due to its limitation. Although the two results were consistent in terms of the first stop band prediction, the failure of the second pass band prediction indicates the limitation of applying gradient theory in stop band prediction.

Furthermore, simulation of the influence of randomness added to homogenised material, based on gradient theory, on the stop band had been implemented. Randomness was added to the length scale and mechanical properties of the homogenised material separately; and was added to both cases following the normal distribution with similar parameters. With randomness added into the material, multiple realisations were required. To perform a statistical analysis to study the randomness phenomenon several (in our case, 10) realisations have been considered. The results were then averaged and compared to the simulation results, based on gradient elasticity without randomness (shown in Figure 3.8). The results indicate that, with the same randomness level, the influence of randomness added to the length scale and to the mechanical properties on the stop band is almost identical. Both lowered the transmission coefficient slightly but retained the same trend as the simulation, based on gradient elasticity without any randomness added. Comparing the simulation results with randomness added directly to the microstructure of the heterogeneous material based on classical elasticity, the lower bound of the first stop band was found to be similar in both cases, and randomness added to material (either heterogeneous or homogenised material) barely changed the first pass band.

Hence, the gradient theory can be applied to predict the stop band both analytically and numerically. In higher-order situations, with a given materials' mechanical and geometrical properties, applying gradient theory to predict the stop band can save a huge amount of time and resources compared to simulations with heterogeneous material.

Chapter 4

Influence of material properties on the stop band phenomenon based on classical and gradient elasticity in 2D

Wave propagation in 2D material is much more complex than it is in 1D material because the wave can propagate in multiple directions. In this chapter, wave propagation through heterogeneous material with a deterministic periodic microstructure will be studied first, and then randomness will be introduced into the microstructure in different ways, to study the influence of randomness on the stop band in the 2D case. After this, the influence of the shape difference brought about by the inclusion of the testing material on the stop band will be studied. Finally, FE simulation of 2D material based on gradient elasticity will be undertaken, to research the possibility of applying gradient elasticity in a 2D case to predict the stop band.

4.1 FE simulation process

To study the wave propagation in 2D material, a finite element simulation was applied. The simulation procedure is similar to the 1D case, which was introduced in Section 2.2.3. However, because simulation in this section is applied to 2D material, the input signal is not a point source anymore, but a source distributed along a straight line. Thus, the recordings will also be obtained along this straight line. The illustration for the new 2D test set-up is shown in Figure 4.1.

As shown in Figure 4.1, the simulation model is constructed in three parts: test material (Part C); signal input and output parts (Part B on the left for the input and Part B on the right for the output); and perfect match layers (both Part A1 and Part A2). The length of Part C was 20 mm; the length of Parts A1 and A2 on both sides was 19 mm; and the length of Part B on both sides was 2 mm. The width is the same along the entire model, being set at 20 mm so that the test material becomes a square. In this chapter, all simulations are based on the same geometry set-up but with different test materials (Part C).

As mentioned above, unlike a point source in 1D, the input source in 2D is distributed

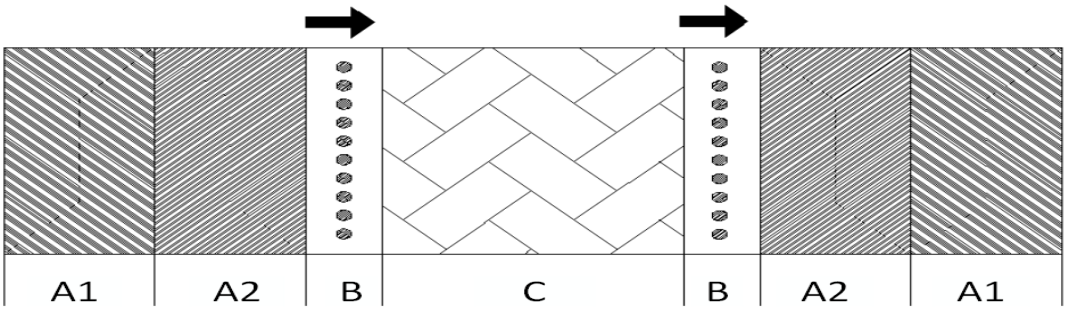

Figure 4.1: Simulation model of wave propagation in 2D

along the vertical line at the horizontal center of the left Part B. Numerically speaking, in this line, a continuous harmonic longitudinal wave was applied at each finite element node to create the input source. The force at each node was set to be:

$$F_g = A_g \sin(\omega t)$$

where A_g is amplitude, ω is forcing frequency and t is time, except for the two nodes on the top and bottom of the line. The amplitude of the force applied at the top and bottom edge is half of the force applied in other points on the source line ($A_e = 0.5 \times A_g$, where A_e is the amplitude of the force applied on the edge of the source line). The reason for this is that each node in the middle of the source line will provide force to four finite elements. However, the node on the edge can only provide force to two finite elements. Hence, to create a source line with the same reaction along the line, the amplitude set at the points on the edge should be half the amplitude set at the point in the middle of the line.

Although the input signal was applied as a line, to simplify the analysis process, only ten points on the line were picked as testing input points (or reference input points), as shown in Figure 4.1. The output displacements were recorded at the horizontal center of the right Part B with a line as recording line. Similarly, only ten points on this line were picked as reference recording points with the same vertical coordinates corresponding to the reference input points. Both reference input points and recording points were averaged and located at the corresponding source and recording line.

Similarly, as with the 1D case, at each testing frequency, the transmission coefficient was calculated as an amplitude obtained from a simulation with heterogeneous material (Part C) divided by an amplitude obtained from simulation with homogeneous material (Part C). The transmission coefficient was calculated at each reference recording point. The influence of heterogeneous material on wave propagation was then denoted by transmission coefficient at each recording point.

4.2 Stop band analysis for the material with *deterministic* structure

Simulation of wave propagation in 2D material is first carried out based on periodic *chess board* layout material. The whole material (20 mm $\times$ 20 mm) is constructed of 400 squares (1 mm $\times$ 1 mm) with two different materials, laid-out as a chess board. A part of the microstructure is shown in Figure 4.2 (one fourth of the entire testing material). Numerically, four nodes square finite elements have been used with the element size 0.1 mm $\times$ 0.1 mm, which brought the total elements number to 1.2×10^5 elements. As a regular rectangular structure has been analysed, it has been assumed that square elements offer smooth and accurate description. In this section, the attention is focused on **deterministic** material; randomness will be discussed in later sections.

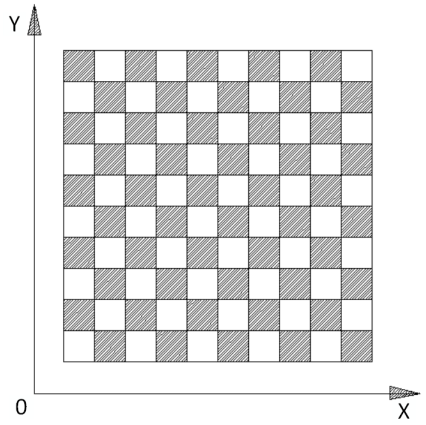

Figure 4.2: Part of microstructure of *deterministic* heterogeneous material

The two different materials are labeled material A (M_A) and material B (M_B). The Young's modulus of M_A is $E_A = 1.6 \times 10^6$ kg/ms^2, and the density of M_A is $\rho_A = 10^9$ kg/m^3. The Young's modulus of M_B is $E_B = 0.25E_A$, and the density of M_B is $\rho_B = 0.1\rho_A$. Throughout this Chapter, the Poisson's ratio of all material components in analysed geometries was set to be zero. This simplification has been done in order to numerically reinforce the roller boundary conditions, so that the deformation of the material in the horizontal direction would not influence the deformation in the vertical direction. The wave speed calculated by Eq. (2.8) in M_A was 40 mm/s and in M_B was 63.2 mm/s. When the testing frequency is 50 Hz the wavelength in any material (M_A or M_B) will be less than the length of the unit square. Hence, if the testing frequency is set between 1 Hz and 50 Hz, in this frequency range the stop band phenomenon should occur. Note that the frequency range is different from the 1D case, due to numerical restrictions. Following the process introduced in Section 4.1, the tests were performed in the discussed frequency range, with results as shown in Figure 4.3.

As shown in Figure 4.3, at each testing frequency, 10 transmission coefficients were calculated for 10 reference recording points. At certain frequencies the values of these transmission coefficients were similar to each other (such as 12 Hz to 19 Hz) while at

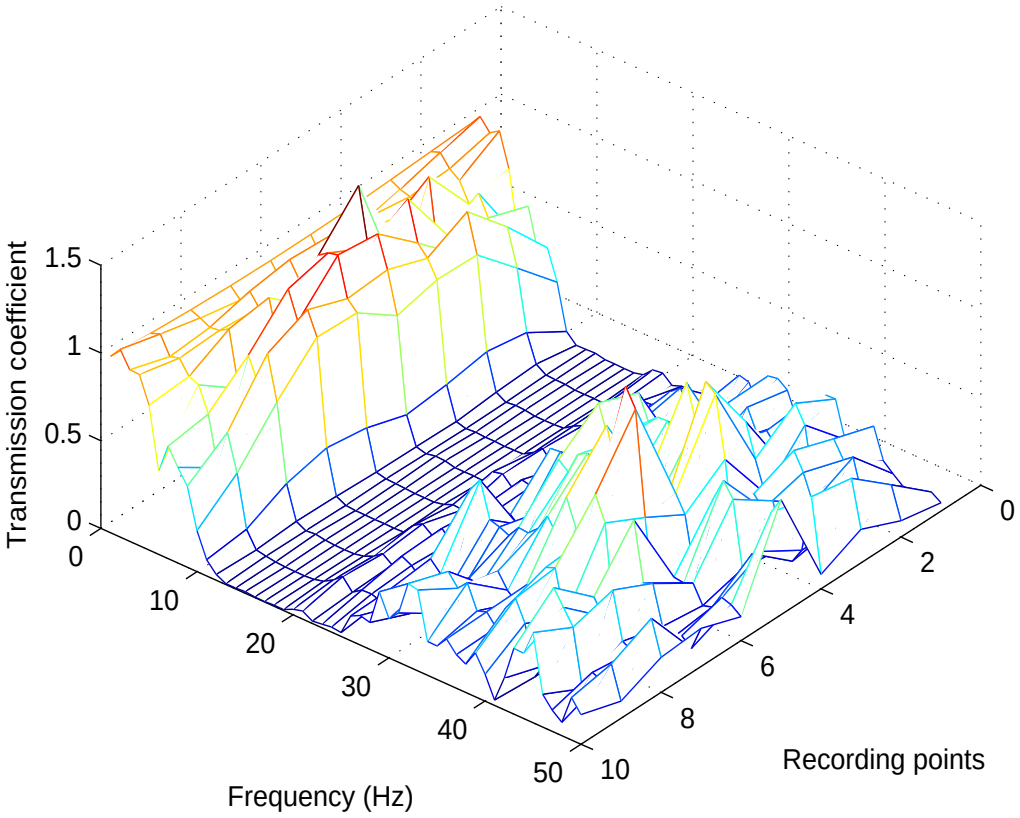

Figure 4.3: Simulation results of wave propagating through the *deterministic* heterogeneous material

some frequencies the transmission coefficient was quite varied at different recording points (such as 30 Hz to 40 Hz). In this case, the frequency range of the transmission coefficient, which was similar at different reference recording points, could be divided into two ranges: one at low frequencies (1 Hz to 3 Hz), where all transmission coefficients are roughly equal to 1; another at mid frequencies (12 Hz to 19 Hz), where all transmission coefficients are lower than 5%. A possible explanation for this phenomenon is that at low frequencies, the wavelength is long (compared to the length of the constructed square) and the influence of heterogeneous material on wave propagation is minor; at mid frequencies, the wave propagation is blocked by the heterogeneous material, and hence the values of the transmission coefficients at all reference recording points decrease to below 5%. At other frequencies, the transmission coefficients are different from each other at varying reference recording points because the wave propagation inside the heterogeneous material is in both horizontal and vertical directions. The vertically propagating waves may interact with each other, and with horizontally propagating waves can create focus fields in which the transmission coefficients could be significantly larger than other reference recording points (such as the transmission coefficient calculated at point 6, compared to transmission coefficients calculated at other points at 34 Hz). Hence, the definition of the stop band is given as a certain frequency range where the transmission coefficients calculated at all reference

recording points are below 5%.

To simplify the results and make them comparable with results obtained from other simulations, the transmission coefficients calculated at 10 reference recording points were averaged and denoted as average transmission coefficient (T_f). Then, the average transmission coefficient for the entire testing frequency range was calculated, and is shown in Figure 4.4. The reader should note that the averaged transmission coefficient was only applied to indicate the trend of the transmission coefficient change along frequencies but can not be treated as the only value to describe the wave propagating through the testing material at a certain frequency. However, at the stop band, the transmission coefficients of 10 reference recording points were roughly the same (as shown in Figure 4.3). Hence, the value of the averaged transmission coefficient at the stop band can represent the transmission coefficient distribution on the recording line. In this case, with a periodic *chess board* lay-out, the microstructure of a testing material, the stop band frequency range was from 12 Hz to 19 Hz, as shown in Figure 4.4.

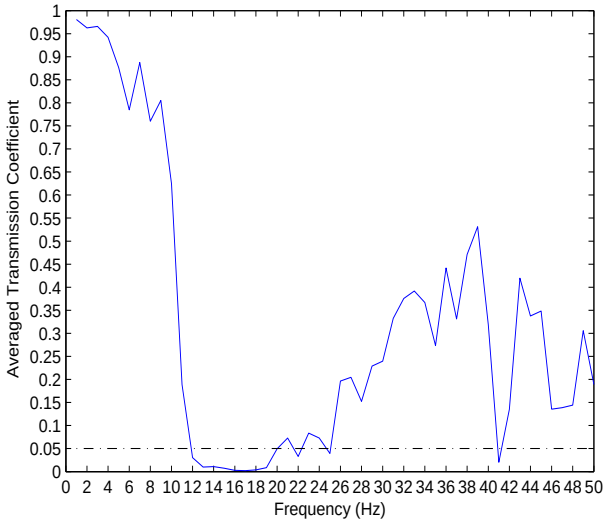

Figure 4.4: Averaged results of wave propagating through the *deterministic* heterogeneous material

Scaling effect

In this simulation, the Young's modulus of M_A is $E_A = 1.6 \times 10^6$ kg/ms^2, and the density of M_A is $\rho_A = 10^9$ kg/m^3. The Young's modulus of M_B is $E_B = 0.25E_A$, and the density of M_B is $\rho_B = 0.1\rho_A$, which means that the testing material was artificial. In the simulation frequency range (from 1 Hz to 50 Hz), the properties of the artificial material led the wavelength of material A to change from 40 mm to 0.8 mm and the wavelength of material B to change from 63.2 mm to 1.26 mm. These two wavelength ranges are at the same level as the length of the unit cells (2 mm), which led the stop band to appear.

Since the simulation is a linear analysis, the frequency range can be scaled with the wave

speed without changing the transmission coefficient of the wave. The transmission coefficient is related to the mechanical property difference of the material components in the testing material, the shape of the unit cells, the size of the unit cells, the position of the unit cells, the testing frequency, and the wave speed and the wavelength. Without changing the mechanical property difference of the material components in the testing material, the shape of the unit cells, the size of the unit cells, and the position of the unit cells, but by instead changing the testing frequency and the wave speed at the same time with the same ratio, the wavelength will remain the same as the case without any changes added. The transmission coefficient of the new material at the new frequency will be the same as the unchanged material at the unchanged frequency.

For example, assume that a test material M_o has two components, M_{o1} and M_{o2}. The Young's moduli of M_{o1} and M_{o2} are E_{o1} and E_{o2}. The densities of M_{o1} and M_{o2} are ρ_{o1} and ρ_{o2}. The wave speeds of M_{o1} and M_{o2} are V_{o1} and V_{o2}. The length of the unit cells is L_uo. Assume that a wave at frequency f_o propagates through the material and the transmission coefficient is T_o. The wavelength of M_{o1} and M_{o2} are λ_{o1} and λ_{o2}.

Assume that another test material M_n has two components M_{n1} and M_{n2}. The Young's moduli of M_{n1} and M_{n2} are $E_{n1} = \theta E_{o1}$ and $E_{n2} = \theta E_{o1}$. The densities of M_{n1} and M_{n2} are $\rho_{n1} = \rho_{o1}/\theta$ and $\rho_{n2} = \rho_{o2}/\theta$. The wave speeds of M_{n1} and M_{n2} then become $V_{n1} = \theta V_{o1}$ and $V_{n2} = \theta V_{o2}$. Assume that a wave at frequency f_n propagates through the material and the transmission coefficient is T_n. Now, assuming that $f_n = \theta f_o$, the wavelength of M_{n1} and M_{n2} then become $\lambda_{n1} = \lambda_{o1}$ and $\lambda_{n2} = \lambda_{o2}$. While the length of the unit cells remains the same ($L_un = L_uo$), the transmission coefficient T_n is then the same as T_o. The materials' properties of M_o and M_n are listed in Table 4.1.

Table 4.1: Materials' properties comparison of M_o and M_n

	M_o		M_n	
Material	M_{o1}	M_{o2}	M_{n1}	M_{n2}
Properties	E_{o1}	E_{o2}	$E_{n1} = \theta E_{o1}$	$E_{n2} = \theta E_{o1}$
	ρ_{o1}	ρ_{o2}	$\rho_{n1} = \rho_{o1}/\theta$	$\rho_{n2} = \rho_{o2}/\theta$
	L_uo		$L_un = L_uo$	
Wave	f_o		$f_n = \theta f_o$	
Properties	V_{o1}	V_{o2}	$V_{n1} = \theta V_{o1}$	$V_{n2} = \theta V_{o2}$
	λ_{o1}	λ_{o2}	$\lambda_{n1} = \lambda_{o1}$	$\lambda_{n2} = \lambda_{o2}$
	T_o		$T_n = T_o$	

Now, assume that the artificial testing material applied in the *deterministic* case is M_o, $\theta = 1.25 \times 10^5$, the Young's modulus of M_{n1} is $E_{n1} = \theta E_{o1} = 2 \times 10^{11}\ Pa$, and the density of M_{n1} is $\rho_{n1} = \rho_{o1}/\theta = 8 \times 10^3\ kg/m^3$, which makes the material M_{n1} become steel. This is the scaling process; after scaling, the simulation frequency range is between 1.25×10^5 Hz and 6.25×10^6 Hz with interval of 1.25×10^5 Hz, but the transmission coefficient remains the same as the *deterministic* case. The scaled transmission coefficient against frequency is shown in Figure 4.5. In this chapter, limited by the computation resources, all

simulations were undertaken with artificial materials. However, with the scaling process, the simulation results could represent real materials.

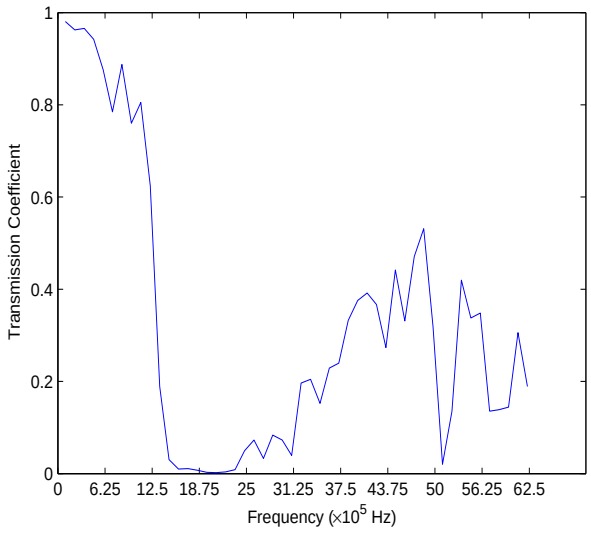

Figure 4.5: Scaled results of wave propagating through the *deterministic* heterogeneous material

4.3 Influence of *randomness* in material properties on stop band

As introduced in Chapter 2, adding randomness into the material will influence wave propagation significantly. Hence, the influence of randomness added into the 2D material on wave propagation will be studied in this section. As discussed in Section 2.6, adding randomness into the material's mechanical properties does not have a significant influence on the wave propagation but adding randomness into a material's geometrical properties (even with a small perturbation) can influence the wave propagation significantly. Based on the above mentioned conclusions, in this section, the randomness will only be added into the material's geometrical properties. Similarly to the previous chapter, different types of randomness will be added into the material: *small perturbation* and *Fibonacci* type. Note that both types of randomness only affect the length of the unit square but will not affect the mechanical properties of each unit square. Hence, the mechanical properties of each unit square remain the same as in the *deterministic* material, as with the position of each unit square (on *chess board* layout).

To compare the simulation results of *small perturbation* and *Fibonacci* type of randomness with the results obtained from *deterministic* material, the input signal, testing frequency range (1 Hz to 50 Hz), and the mechanical properties of the material (the mechanical properties of the constructed components, M_3 and M_4) are set at the same level as with the *deterministic* material.

4.3.1 Influence of *small perturbation* on geometrical properties on stop band

As discussed above, the first type of randomness added into the 2D material is in the form of a *small perturbation* following, similar to Section 2.4.3, normal distribution. The length of a unit square can then be described as $L_{us} = (\mu, \sigma)$, where μ is the average length and σ is the standard deviation. In this section, three different cases will be covered: randomness only added in the horizontal direction, randomness added in the vertical direction and randomness added into both horizontal and vertical directions.

Material geometry with *small perturbation* randomness in horizontal direction

The first simulation of material is with *small perturbation* added only in the horizontal direction in the microstructure. This means that the horizontal length of each unit square in the microstructure will follow normal distribution, but the vertical length of each unit square must be kept at 1 mm, as with the *deterministic* material introduced in Section 4.2. When realising randomness, the *chess board* layout was treated as layered material. The microstructure with 20 by 20 squares was seen as 20 by 1 layers, with each layer including 10 squares. Randomness was added into the horizontal length of the bottom square in each layer following normal distribution with $\mu = 1$ mm and $\sigma = 0.2$ mm. In this way, the horizontal length of the bottom square decides the horizontal length of other squares in the same column-layer. To avoid extreme situations, the lengths of the two bottom squares were adjusted based on the total horizontal length (20 mm) of the testing material. The microstructure of one realisation of the testing material is shown in Figure 4.6.

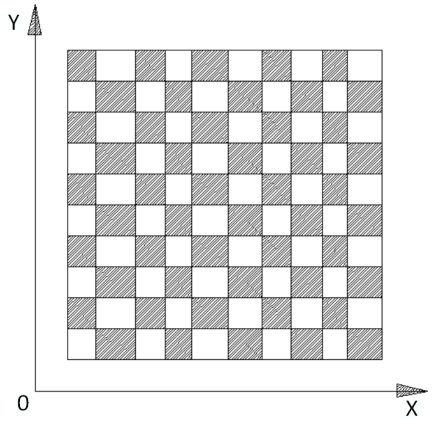

Figure 4.6: A part of the microstructure of the *small perturbation* randomness in horizontal direction

In the testing frequency range at each testing frequency, five realisations were made. At each reference recording point, five transmission coefficients are then calculated based on these realisations. Then at each testing frequency at each recording point, the average transmission coefficient (T_p) was calculated from five transmission coefficients gained from different realisations. The simulation results of the entire frequency range is shown

in Figure 4.7.

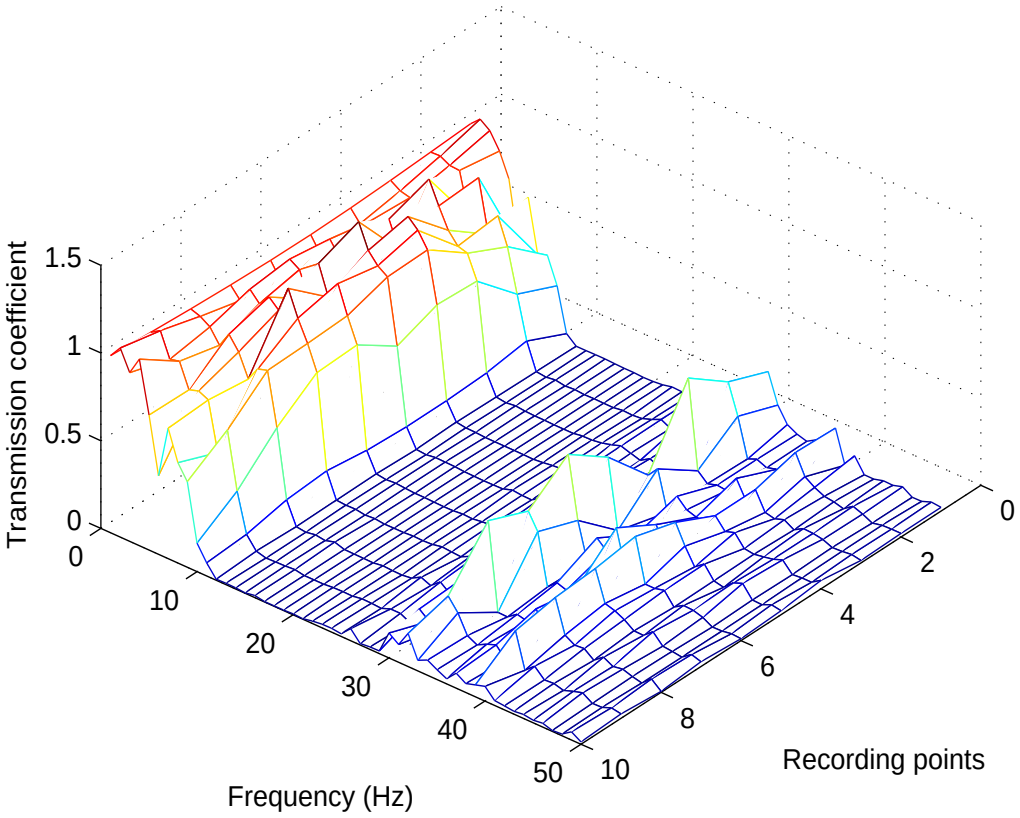

Figure 4.7: Simulation results of wave propagating through the *small perturbation* randomness in horizontal direction

As shown in Figure 4.7, the stop band occurs for frequencies ranging from 12 Hz to 24 Hz. The averaged transmission coefficient (T_f) has been calculated at each frequency and compared with the T_f gain from the simulation based on *deterministic* material. Comparison results are shown in Figure 4.8. The results indicate that after adding a *small perturbation* into the horizontal direction of the heterogeneous material, the width of the stop band increases. At the same time, the average transmission coefficient drops significantly to the second pass band. However, *small perturbation* randomness only has a minor influence on wave propagation at low frequencies and would hardly influence the lower bound of the stop band.

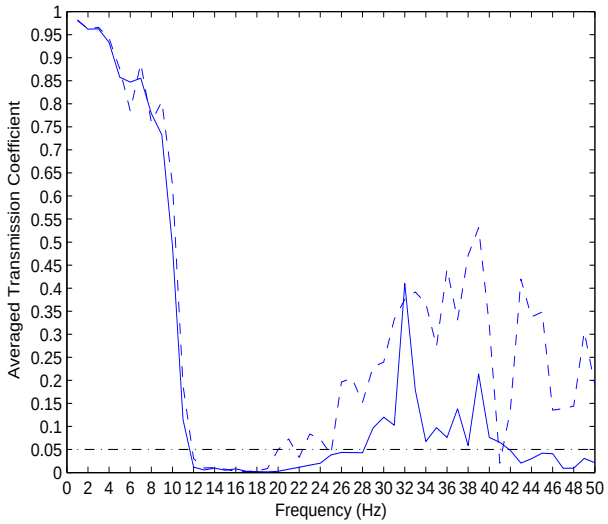

Figure 4.8: Averaged results of wave propagating through the *small perturbation* randomness in horizontal direction

(Solid line: *small perturbation* randomness in horizontal direction; Dashed line: *deterministic* material; Point dashed line: indicates the position of 5% along frequency)

Material geometry includes randomness in vertical direction

The second group of simulations is the analysis of *small perturbations* added only in the vertical direction in the microstructure. The vertical length of each unit square in the microstructure again follows normal distribution, but the horizontal lengths of all unit squares were the same and equal to 1 mm. While realising randomness, the microstructure was again treated as layered material, so the vertical length of the first unit square in each horizontal row will decide the vertical length of the corresponding horizontal row. The vertical length of the first unit square in each horizontal layer followed normal distribution, with $\mu = 1$ mm and $\sigma = 0.2$ mm. To avoid extreme cases, the vertical length of the last two horizontal layers was adjusted under the condition that the width of the testing material was kept at 20 mm. The microstructure of one realisation of the randomness added into vertical length is shown in Figure 4.9.

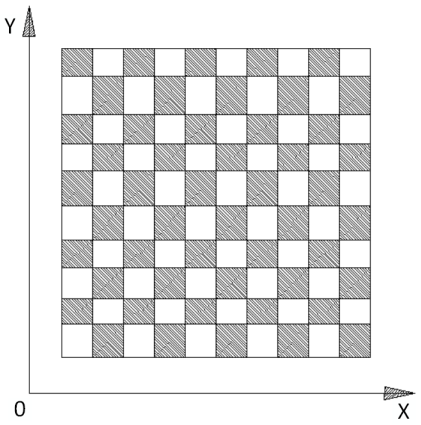

Figure 4.9: A part of the microstructure of the *small perturbation* randomness in vertical direction

In the testing frequency range at each testing frequency 5 realisations were made. After 5 simulations, the averaged transmission coefficient at each point at each frequency (T_p) was calculated and is plotted in Figure 4.10.

As shown in Figure 4.10, the stop band is now from 13 Hz to 20 Hz. The averaged transmission coefficient was calculated as well and compared to the *deterministic* case. The results are compared in Figure 4.11, and indicate that, with a *small perturbation* randomness added into the vertical length of each unit square, the first stop band remained the same as material without any randomness added to it. However, with randomness added in the vertical direction, the transmission coefficient dropped significantly in the second pass band.

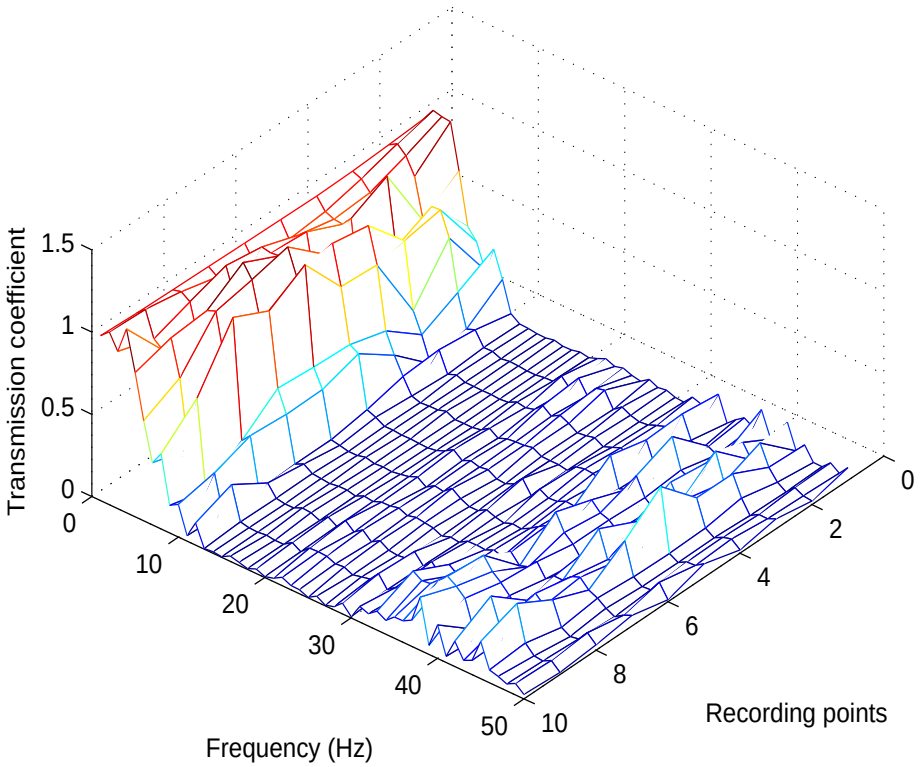

Figure 4.10: Simulation results of wave propagating through the *small perturbation* randomness in vertical direction

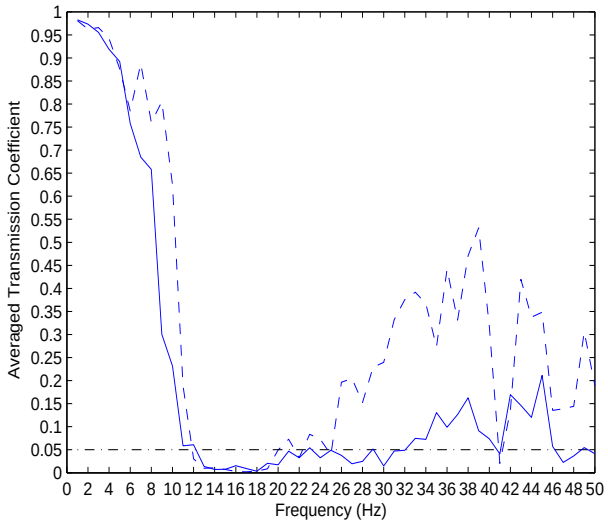

Figure 4.11: Averaged results of wave propagating through the *small perturbation* randomness in vertical direction

(Solid line: *small perturbation* randomness in vertical direction; Dashed line: *deterministic* material; Point dashed line: indicate the position of 5% along frequency)

Material geometry includes randomness in both horizontal and vertical directions

The third group of simulations was performed for the material with *small perturbation* added to both horizontal and vertical directions. Hence, both the horizontal and vertical length of each unit square will follow normal distribution with average value $\mu = 1$ mm and standard deviation $\sigma = 0.2$ mm. A similar randomness realisation technique has been applied which treats the microstructure as layered material and the randomness in the horizontal length of unit squares in the bottom layer and the vertical length of unit squares in the first vertical layer, and then decides the geometrical parameter of the entire microstructure. Still, adjustment had to be made (if necessary) to ensure that both the horizontal and vertical length of the entire testing material was 20 mm. One realisation of the microstructure is shown in Figure 4.12. Note, that the vertical and horizontal layers were constructed independently from each other.

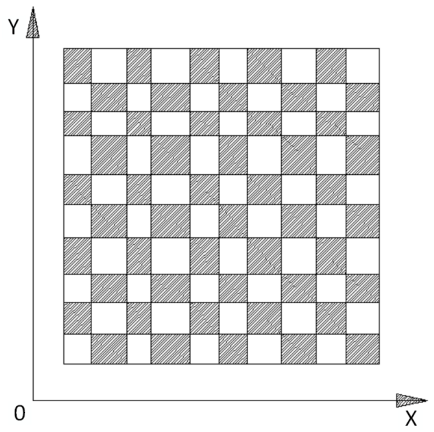

Figure 4.12: A part of the microstructure of the *small perturbation* randomness in both horizontal and vertical directions

In the testing frequency range at each testing frequency, five realisations have been undertaken. After five simulations, the average transmission coefficient at each point at each frequency (T_p) was calculated and is plotted in Figure 4.13.

As shown in Figure 4.13, the stop band ranged from 13 Hz to 25 Hz. The averaged transmission coefficient was calculated and compared to the *deterministic* case; the results are shown in Figure 4.14. The comparison indicates that, with a *small perturbation* added into both horizontal and vertical length of each unit square, the upper bound of the first stop band extended from 19 Hz to 25 Hz, but the lower bound remained the same as that for the material without any randomness added in. In addition, the average transmission coefficient reduced significantly in the second pass band, from 26 Hz to 50 Hz, while the average transmission coefficient remained consistently at around 5%, which means that with randomness in both horizontal and vertical directions the second pass band was nearly changed to a stop band.

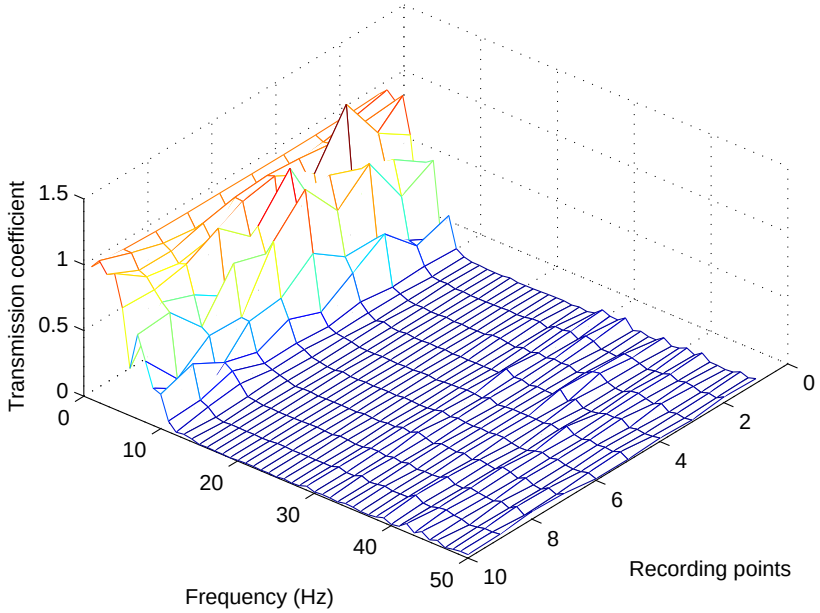

Figure 4.13: Simulation results of wave propagating through the *small perturbation* randomness in both horizontal and vertical directions

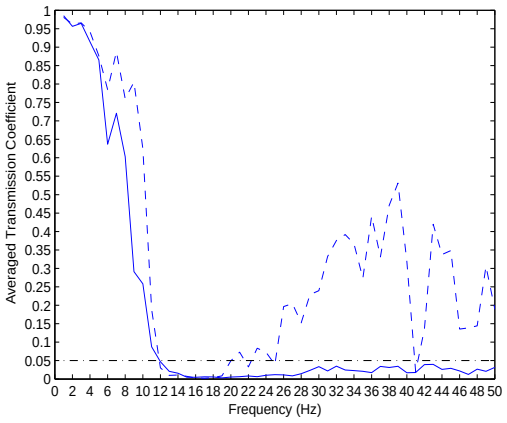

Figure 4.14: Averaged results of wave propagating through the *small perturbation* randomness in both horizontal and vertical directions

(Solid line: *small perturbation* randomness in both horizontal and vertical directions; Dashed line: *deterministic* material; Point dashed line: indicates the position of 5% along frequency)

4.3.2 Stop band prediction based on 2D Fibonacci layout material

As introduced in Section 2.4.4, to realise *"semi-random"* material the *Fibonacci* randomness can be used. The technique of generating a 1D Fibonacci bar was introduced in Section 2.4.4. In this section, the generation of the Fibonacci sequence and number follow this process. Thus, a Fibonacci bar with Fibonacci number equal to 20 has been generated (F_{bar}^{13}). On this bar, the *"short"* part is set to be L_S and *"long"* part is set to be L_L. This bar included 233 layers and was constructed from two materials (M_3 and M_4), for application in later cases simulated in this section.

In this section, two types of *Fibonacci* randomness will be studied, one is called *small Fibonacci*, with $L_S = 0.8$ mm and $L_L = 1.2$ mm which represents the same level of randomness as the *small perturbation* case. Another one is called *big Fibonacci*, with $L_S = 0.5$ mm and $L_L = 1.5$ mm which contains a higher level of randomness compared to the *small perturbation* case. The only difference between the two randomness types is the length of the unit cell in these two *Fibonacci* bars. The simulation process and other aspects of set-up follow the same procedure introduced in Section 4.3.1 for both types of randomness.

Material including *Fibonacci* randomness in horizontal direction

The first group of simulations is *Fibonacci* randomness added into the horizontal direction, which means that the length of unit squares in the microstructure followed the Fibonacci sequence in the horizontal direction. As with the *small perturbation* randomness material, the *Fibonacci* randomness realisation treated the microstructure as layered material (with vertical column-layers) so that the length of the bottom unit square decided the length of the corresponding layer.

The length of the bottom unit squares follows the Fibonacci sequence. To realise this, in each randomness realisation, layers were picked from the generated Fibonacci bar F_{bar}^{13}. The number of layers depends on the length of each layer, the total length of which is 20 mm. Hence, for both the *small Fibonacci* case and the *large Fibonacci* case, the number of layers is roughly 20. To keep the length of the tested material to 20 mm, the length of the last layer from the picked out bar was adjusted, where necessary. The length of the bottom unit squares was then set to be the same as the length of each layer in the picked out part of the Fibonacci bar. In different realisations, the picked out parts from the Fibonacci bar were varied, to ensure randomness. For example, in one realisation, the picked out part from the Fibonacci bar was laid out as *SLSSLSLSSLSSLSLSSLSL*, where *L* represents L_L and *S* represents L_S. A part of the microstructure generated based on this picked out part for one realisation is shown in Figure 4.15.

In the testing frequency range five realisations were done at each testing frequency for both types of randomness. After five simulations, the average transmission coefficient at each point at each frequency (T_p) was calculated. The simulation results of the *small Fibonacci* randomness in the horizontal direction is plotted in Figure 4.16, and the simulation results of the *large Fibonacci* randomness in the horizontal direction is plotted in Figure 4.17.

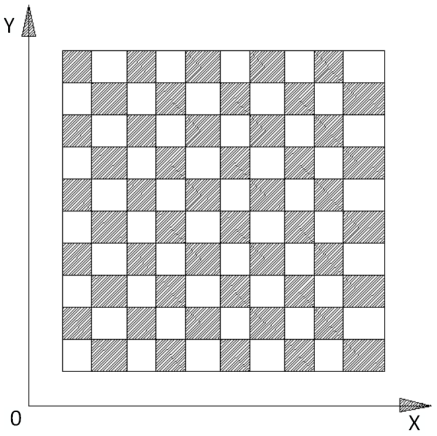

Figure 4.15: A part of the microstructure of the *small Fibonacci* randomness in horizontal direction

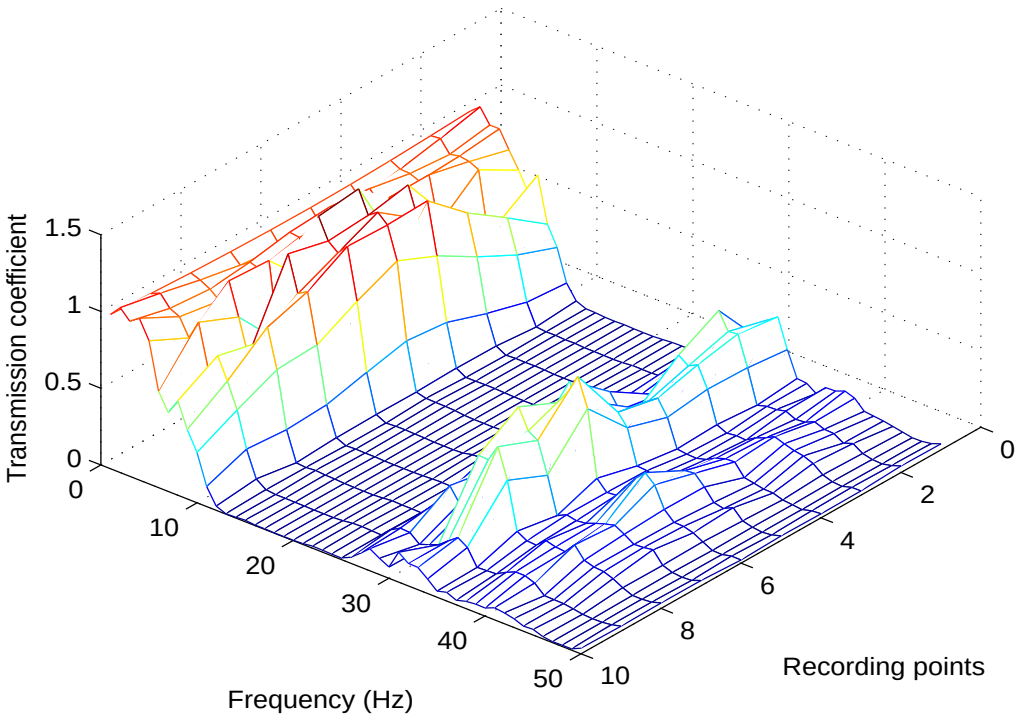

Figure 4.16: Simulation results of *small Fibonacci* randomness in horizontal direction

As shown in Figure 4.16, the frequencies, producing the stop band of the *small Fibonacci* in the horizontal direction case ranged from 13 Hz to 25 Hz. The average transmission coefficient was calculated as well and compared to the *deterministic* case; the results are shown in Figure 4.18. A comparison of the results indicates that with *small Fibonacci* randomness added to the horizontal direction, the first stop band increased and the average transmission coefficient dropped from 35 Hz to 40 Hz and

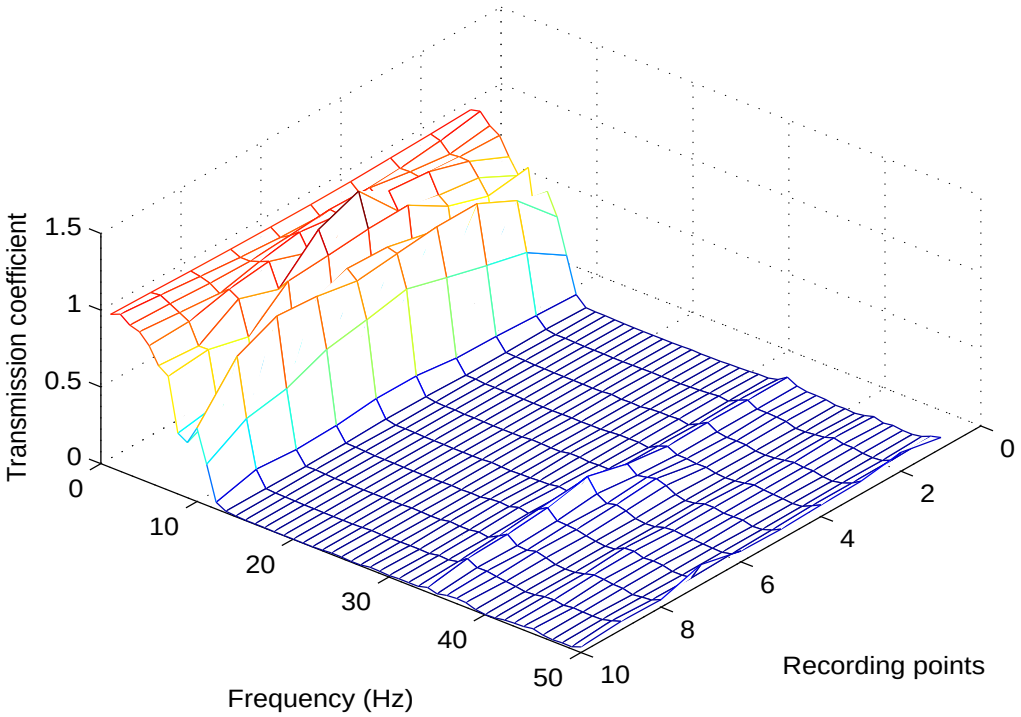

Figure 4.17: Simulation results of *large Fibonacci* randomness in horizontal direction

from 43 Hz to 50 Hz. The *Fibonacci* randomness in the horizontal direction barely influenced low frequency wave propagation or the lower bound of the stop band, compared to the *deterministic* case.

As shown in Figure 4.17, the stop band of *large Fibonacci* in the horizontal direction case ranged from 13 Hz to 32 Hz. The average transmission coefficient was calculated as well and compared to the *deterministic* case. The result is shown in Figure 4.19 and indicates that, with *large Fibonacci* randomness added to the horizontal direction, the upper bound of the first stop band increased from 19 Hz to 32 Hz, and the lower bound remained almost the same. The average transmission coefficient remained around 5% between 33 Hz and 50 Hz, which means with *large Fibonacci* randomness, the second pass band was almost removed, compared to the *deterministic* case.

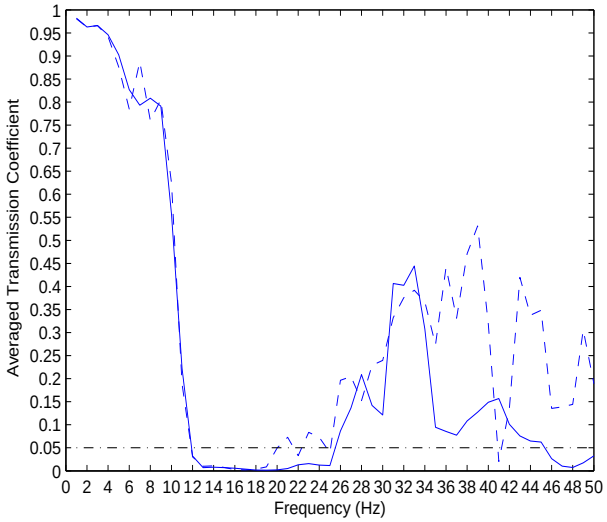

Figure 4.18: Averaged results of wave propagating through the *small Fibonacci* randomness in horizontal direction

(Solid line: *small Fibonacci* randomness in horizontal direction; Dashed line: *deterministic* material; Point dashed line: indicates the position of 5% along frequency)

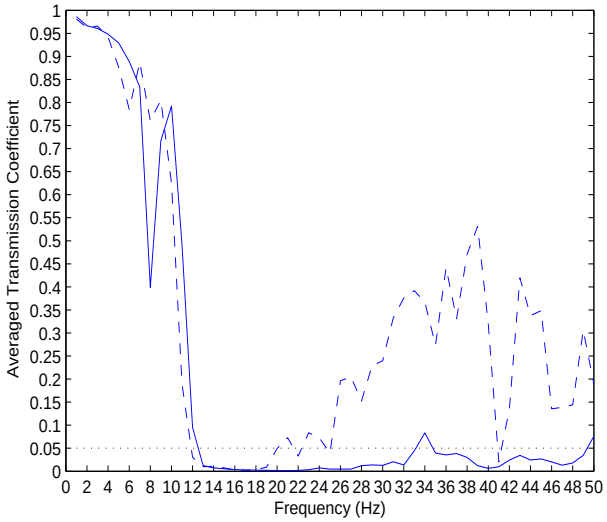

Figure 4.19: Averaged results of wave propagating through the *large Fibonacci* randomness in horizontal direction

(Solid line: *large Fibonacci* randomness in horizontal direction; Dashed line: *deterministic* material; Point dashed line: indicate the position of 5% along frequency)

Material geometry includes *Fibonacci* randomness in vertical direction

The second group of simulations of material with *Fibonacci* randomness consisted of the length of unit squares in the microstructure following the Fibonacci sequence in the vertical direction. The microstructure is treated as a horizontal layered material so that the width of the first unit square in each layer defines the width of the corresponding layer. In each realisation, a part with roughly 20 layers was picked from generated F_{bar}^{13}. The width of all first unit squares of all horizontal layers (from bottom to top) was set to be equal to the length of each layer of the picked part from F_{bar}^{13}. An example of a part of the microstructure is shown in Figure 4.20.

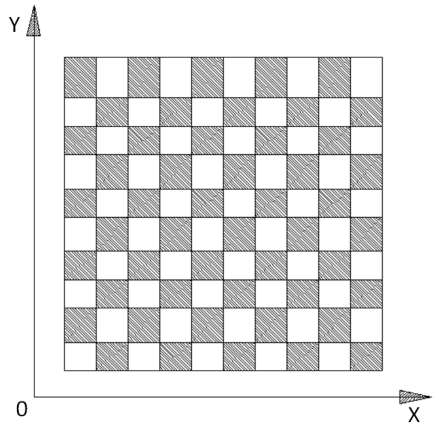

Figure 4.20: A part of the microstructure of the *small Fibonacci* randomness in vertical direction

In the testing frequency range, five realisations were carried out at each testing frequency for both types of randomness: *small Fibonacci* and *large Fibonacci* randomness. After five simulations, the average transmission coefficient at each point of each frequency (T_p) was calculated. The simulation results of *small Fibonacci* randomness in the vertical direction is plotted in Figure 4.21 and the simulation results of *large Fibonacci* randomness in the vertical direction is plotted in Figure 4.22.

As shown in Figure 4.21, the stop band of the *small Fibonacci* in vertical direction lies between 13 Hz and 19 Hz. The average transmission coefficient was calculated as well and compared to the *deterministic* case. The comparative results are shown in Figure 4.23, and the results indicate that, with *small Fibonacci* randomness added into the vertical direction, the first stop band can remain the same as the *deterministic* material, but the averaged transmission coefficient decreased significantly from 35 Hz to 40 Hz. The *Fibonacci* randomness in vertical direction reduced the average transmission coefficient from 6 Hz to 8 Hz at a low frequency range but did not change the lower bound of the stop band.

As shown in Figure 4.22, the stop band of *large Fibonacci* randomness in vertical direction lay between 16 Hz and 20 Hz. The average transmission coefficient was calculated again and was compared to the *deterministic* case. The results, shown in

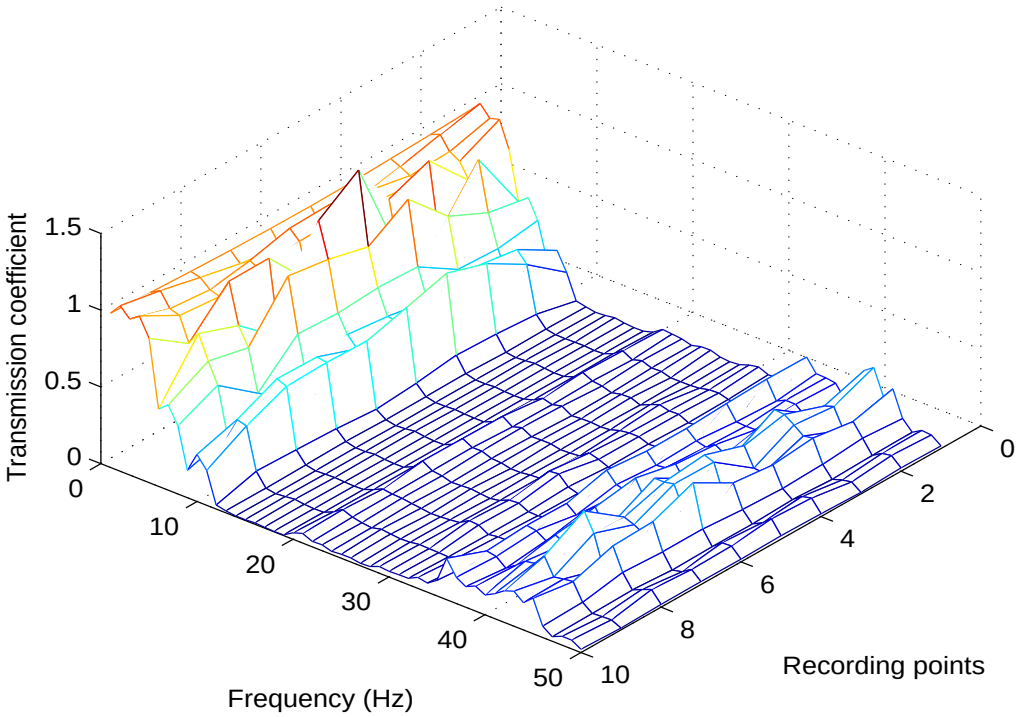

Figure 4.21: Simulation results of wave propagating through the *small Fibonacci* randomness in vertical direction

Figure 4.24, indicate that, with *large Fibonacci* randomness added to the vertical direction, the average transmission coefficient dropped to low frequency (from 3 Hz to 11 Hz); part of the stop band changed to pass band (13 Hz to 15 Hz); and the average transmission coefficient dropped significantly from 27 Hz to 40 Hz.

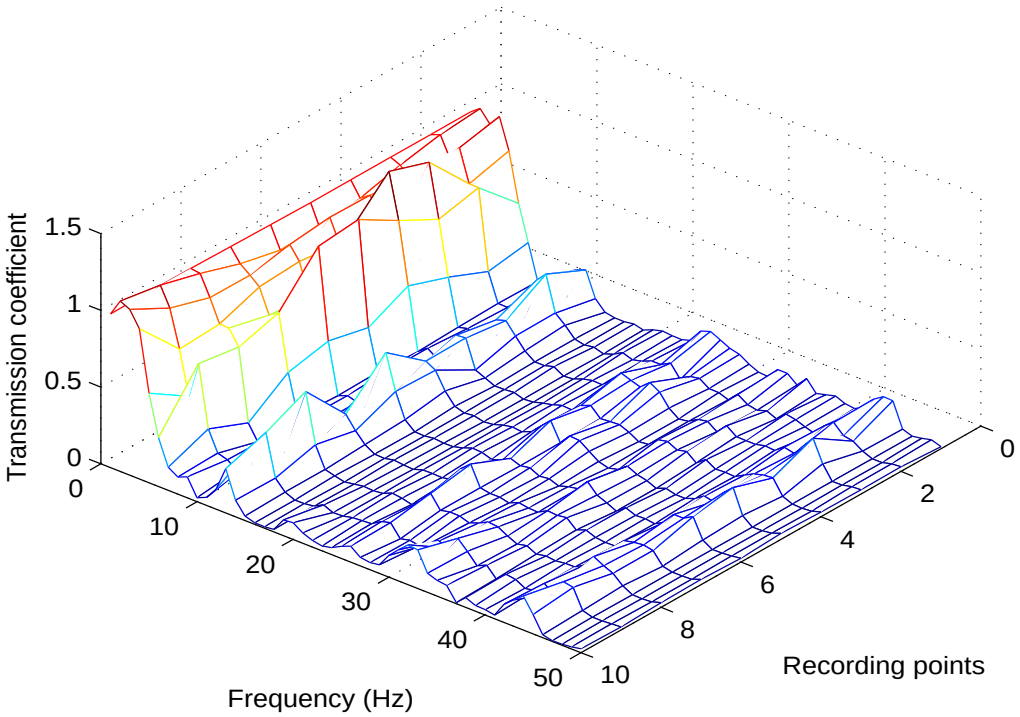

Figure 4.22: Simulation results of wave propagating through the *large Fibonacci* randomness in vertical direction

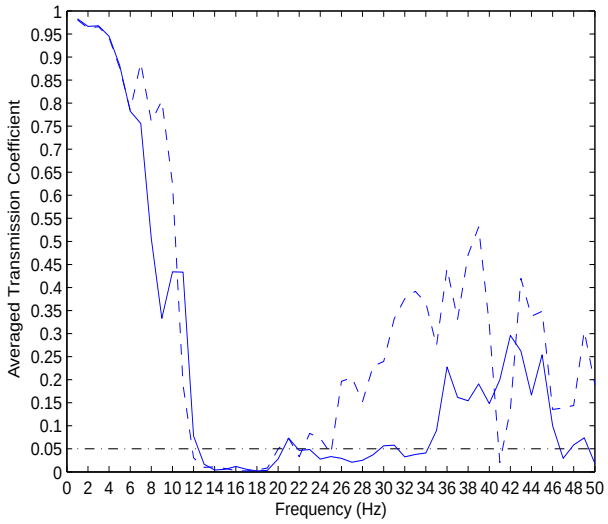

Figure 4.23: Averaged results of wave propagating through the *small Fibonacci* randomness in vertical direction
(Solid line: *small Fibonacci* randomness in vertical direction; Dashed line: *deterministic* material; Point dashed line: indicate the position of 5% along frequency)

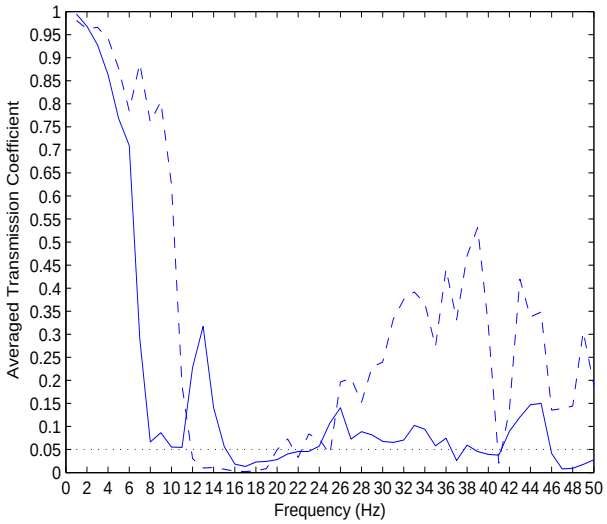

Figure 4.24: Averaged results of wave propagating through the *large Fibonacci* randomness in vertical direction
(Solid line: *large Fibonacci* randomness in vertical direction; Dashed line: *deterministic* material; Point dashed line: indicate the position of 5% along frequency)

Material geometry includes *Fibonacci* randomness in both horizontal and vertical directions

The third group of simulations of material with *Fibonacci* randomness consisted of the length of unit squares in the microstructure following the Fibonacci sequence in both horizontal and vertical directions. The randomness realisation in horizontal and vertical direction followed the process introduced earlier in this section. An example of a part of the microstructure is shown in Figure 4.25.

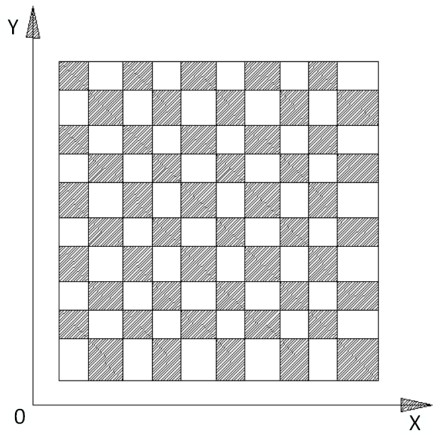

Figure 4.25: A part of the microstructure of the *Fibonacci* randomness in both horizontal and vertical directions

Following the procedure introduced previously, again in the testing frequency range, five realisations were implemented at each testing frequency for both types of randomness. After five simulations, the average transmission coefficient at each point at each frequency (T_p) was calculated. The simulation results of *small Fibonacci* randomness in both horizontal and vertical directions are plotted in Figure 4.26, and the simulation results of *large Fibonacci* randomness in both horizontal and vertical directions are plotted in Figure 4.27.

As shown in Figure 4.26, the stop band of *small Fibonacci* randomness in both horizontal and vertical direction cases was from 13 Hz to 26 Hz. The average transmission coefficient was calculated as well and compared to the *deterministic* case. The results are shown in Figure 4.28. They indicate that, with *Fibonacci* randomness added into both horizontal and vertical directions, the first stop band range increased from 7 Hz to 14 Hz, which roughly doubled the stop band range. From 26 Hz to 50 Hz, the average transmission coefficient was reduced by a significant amount, while the value of the average transmission coefficient remained roughly at 5% in this frequency range. This phenomenon signifies that *Fibonacci* randomness nearly removed the second pass band. However, *small Fibonacci* randomness in both directions had limited influence on wave propagation at low frequencies and did not change the lower bound of the first stop band.

As shown in Figure 4.27, the stop band of *large Fibonacci* randomness in both

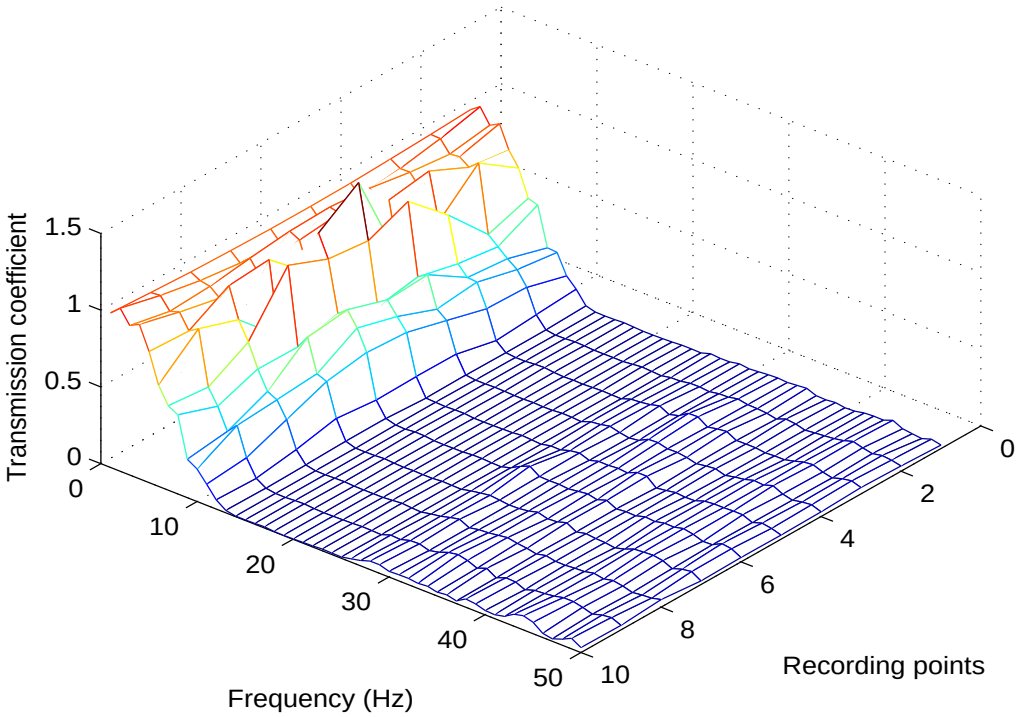

Figure 4.26: Simulation results of wave propagating through the *Fibonacci* randomness in both horizontal and vertical directions

horizontal and vertical direction cases ranges from 21 Hz to 48 Hz. The average transmission coefficient was calculated as well and compared to the *deterministic* case. The results, shown in Figure 4.29, illustrate how, when *large Fibonacci* randomness was added into both horizontal and vertical directions, the average transmission coefficient dropped to a low frequency range (from 2 Hz to 11 Hz); the stop band changed into a pass band (from 13 Hz to 19 Hz) but kept the average transmission coefficient at low value; and the second pass band changed into a stop band (between 21 Hz and 48 Hz).

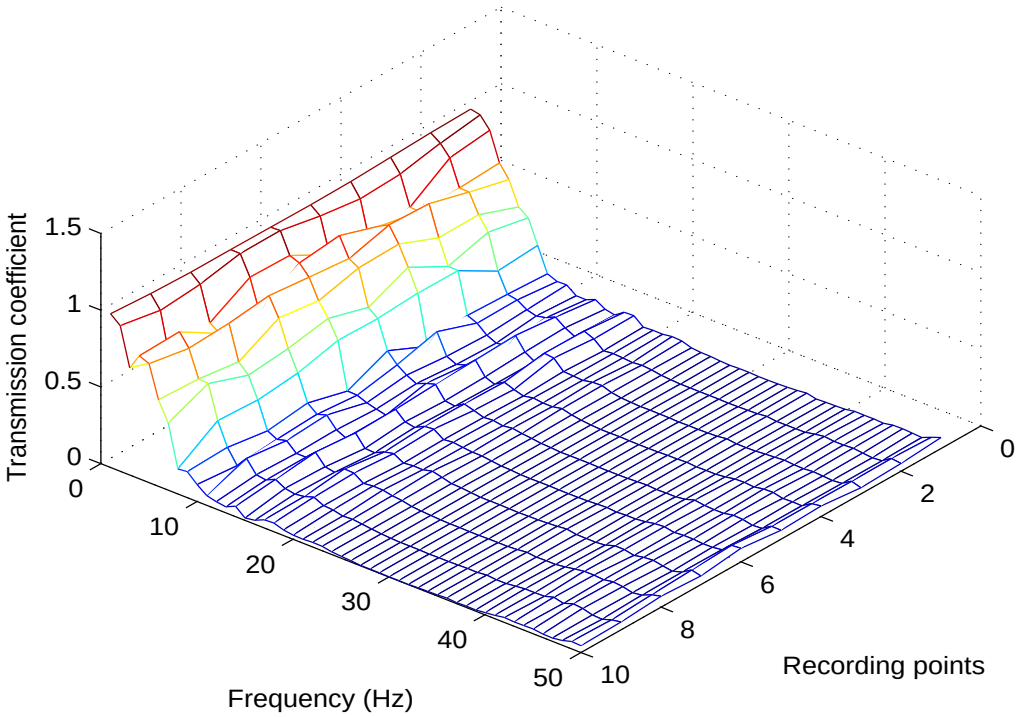

Figure 4.27: Simulation results of wave propagating through the *Fibonacci* randomness in both horizontal and vertical directions

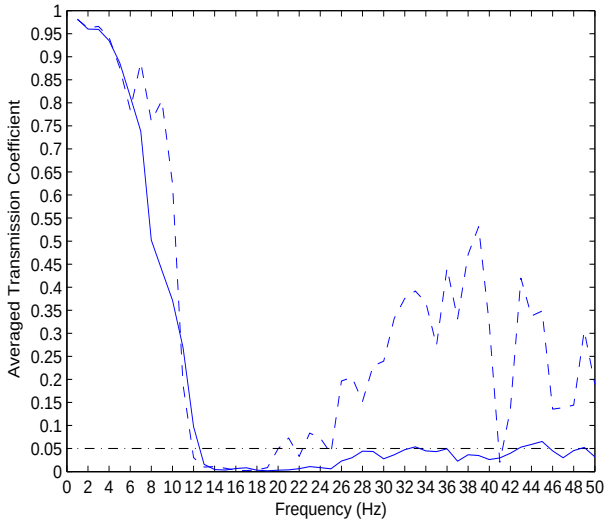

Figure 4.28: Averaged results of wave propagating through the *small Fibonacci* randomness in both horizontal and vertical directions

(Solid line: *small Fibonacci* randomness in both horizontal and vertical directions; Dashed line: *deterministic* material; Point dashed line: indicate the position of 5% along frequency)

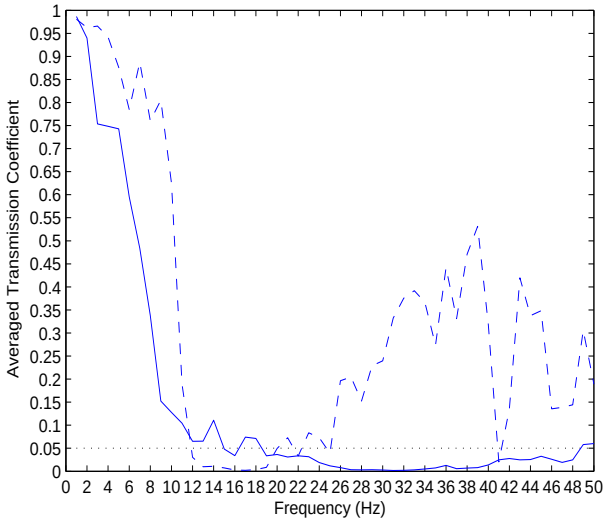

Figure 4.29: Averaged results of wave propagating through the *large Fibonacci* randomness in both horizontal and vertical directions

(Solid line: *large Fibonacci* randomness in both horizontal and vertical directions; Dashed line: *deterministic* material; Point dashed line: indicate the position of 5% along frequency)

4.4 Stop band analysis for material with circle inclusions

In previous sections (Section 4.2 and Section 4.3), the testing material were constructed by two components with square unit cells (deterministic material in Section 4.2) or rectangle unit cells (material with randomness in Section 4.3). In this section, the shape of one component was changed to a circular shape and this component was treated as the inclusion and another component as the matrix. In this way, the influence of the shape of the inclusion on the stop band can be analysed. Additionally, the influence of randomness added to the circular inclusion on the stop band can be studied as well.

4.4.1 Stop band analysis for material with circle inclusions with *deterministic* radius

In this section, the analysis will focus on the influence of a microstructure shape difference on the stop band. Hence, the simulation process and material parameters were set to be the same as in Section 4.2 except for the shape of the inclusions. In this section, the testing material was also constructed by two components, Material A and Material B. Material A was treated as an inclusion in a circular shape. A fragment of the testing material is shown in Figure 4.30.

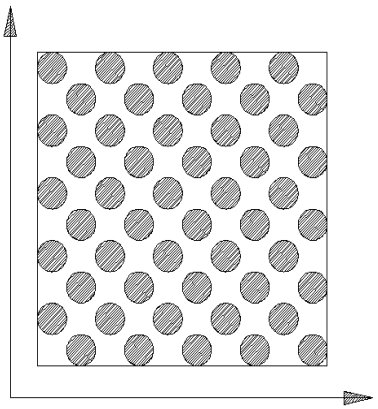

Figure 4.30: A part of the microstructure of the *deterministic* circle inclusion material

In Figure 4.31, the case of "the chess board" material was presented, together with the case of the material with circular inclusions. As can be seen, arrangements of these two materials were the same; however, the actual shapes of the inclusions were different. The diameters of all circular inclusions were similar (for this deterministic case) and equal to 1 mm, which was also the characteristic length of the unit squares on the "chess board" configuration. This logic, on a first look of geometric parameter choice had a further complication: the area, occupied by one circular inclusion was $A_c = 0.25d^2\pi \approx 0.79$ mm^2, but the area occupied by the square inclusion was $A_s = 1$mm^2, resulting in 10.5% difference in the volume fraction of inclusions overall in these two materials. This difference in volume fraction is explored further in Section 4.4.2.

Figure 4.31: Comparison of microstructure of "chess board" material and material with circular inclusions (P1: microstructure of "chess board" material; P2: microstructure of material with circular inclusions)

Numerically, again a mesh with square elements has been used. The size of finite elements has been chosen to be 0.01 mm^2, which signifies a circular inclusions having around 80 elements. The number of finite elements in one circular inclusion is large enough to ensure the accuracy of simulations.

The testing frequency range similarly to the previous simulations was set from 1Hz to 50Hz. Following the process introduced in Section 4.1, the tests were performed in the discussed frequency range; results are shown in Figure 4.32.

As can be seen in Figure 4.32, the first stop band range was from 8Hz to 13Hz. The average transmission coefficient (T_f) was calculated at each frequency and compared to the average transmission coefficient T_f of the "chess board" material discussed in Section 4.2. The results were compared in Figure 4.33. The results indicate that, with circle inclusions, the stop band occurs at lower frequencies compared to material with square units. From 14 Hz to 21 Hz, both types of materials showed a similar trend, but from 22 Hz to 50 Hz, the transmission coefficient of these two cases showed a significant variation. Hence, despite the same position arrangement, the change inclusions' shapes can significantly influence the stop band. Again, it should be noted here that the circular inclusions reduce the volume fraction of inclusion. Strictly speaking, following the conclusion of different volume fractions for the two analysed materials, the transmission coefficient-frequency curves should not be compared on the same graph. In this thesis they are presented together for the indicated reasons and to offer a starting point for further research (on randomness, as presented in the following Section).

4.4.2 Stop band analysis for the material with circle inclusions with *random* radius

After simulation of the wave propagation in deterministic material with circular inclusions, randomness was added to the test. To generate a comparison with the random "chess board" material (introduced in Section 4.3), randomness was only added to the radius of the circular inclusions. To have full circles, the radius of all circles on the edge was the same as with the deterministic circles, which was 0.5 mm. However, other radii followed a normal distribution: $R \sim N(\mu, \sigma)$, where μ was the average radius which

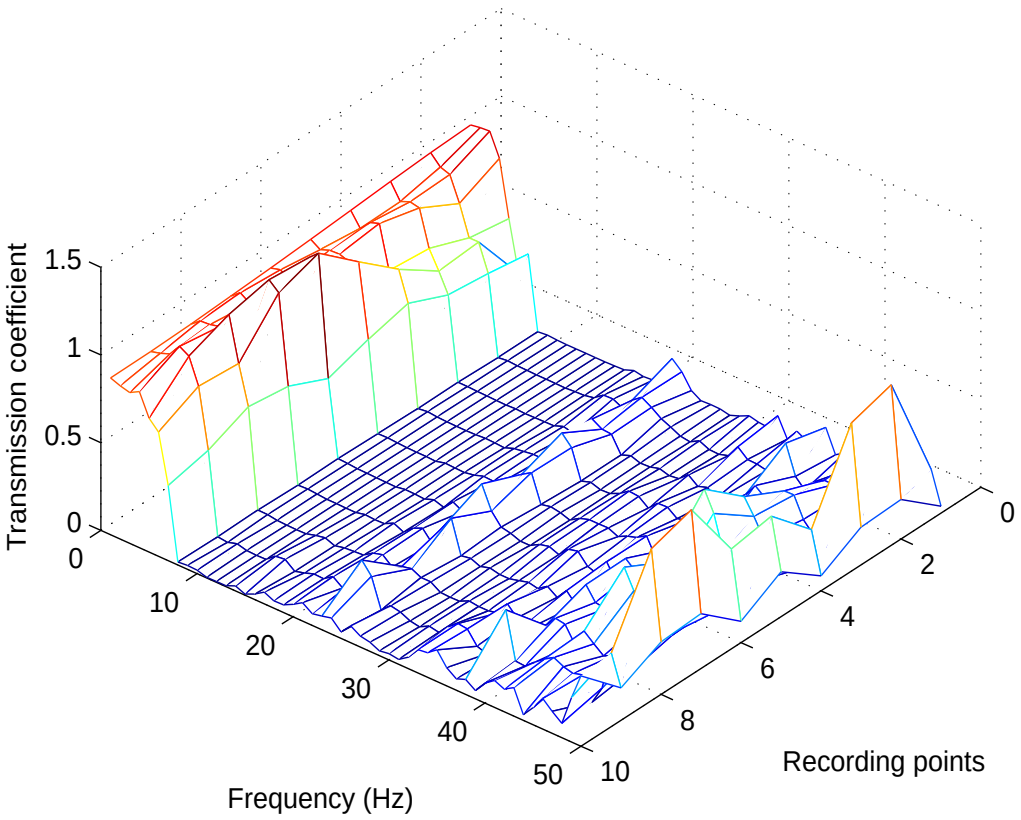

Figure 4.32: Simulation results of wave propagating through the *deterministic* circle inclusion material

equals 0.5 mm, and σ was the standard deviation, equal to 0.1 mm (to ensure that no overlap existed between circles). A part of the microstructure is shown in Figure 4.34.

In the testing frequency range, five realisations were undertaken at each testing frequency. After five simulations, the averaged transmission coefficient at each point at each frequency (T_p) was calculated. The simulation results of the entire frequency range is shown in Figure 4.35

As shown in Figure 4.35, the stop band occurred for frequencies ranging from 9 Hz to 14 Hz. The averaged transmission coefficient (T_f) was calculated at each frequency and compared to T_f gained from the simulation, based on the deterministic circle inclusion material. The comparison is shown in Figure 4.36. The results indicate that, after adding randomness to the radius of circle inclusions, the transmission coefficient can be reduced significantly at high frequency range but has limited influence at low and medium frequency levels.

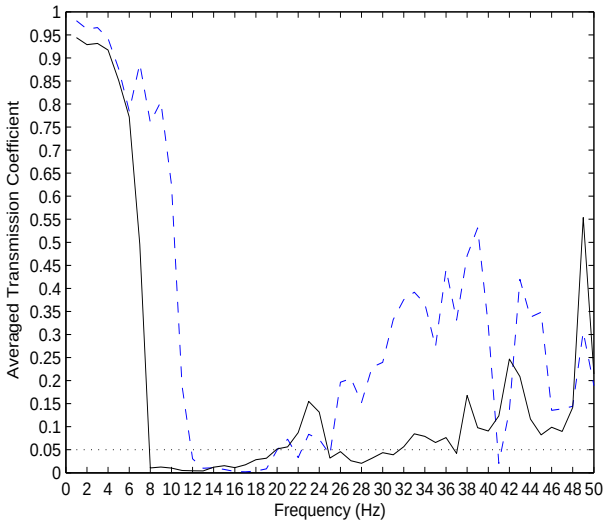

Figure 4.33: Averaged results of wave propagating through the *deterministic* circle inclusion material (Solid line: *deterministic* circle inclusion material; Dashed line: *deterministic* square unit material; Point dashed line: indicate the position of 5% along frequency)

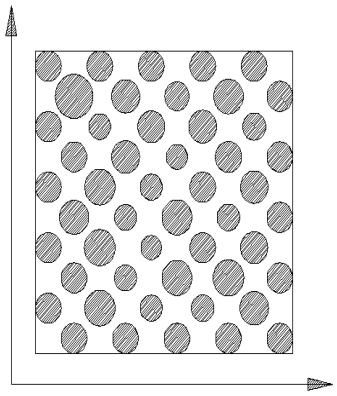

Figure 4.34: A part of the microstructure of the *randomness* circle inclusion material

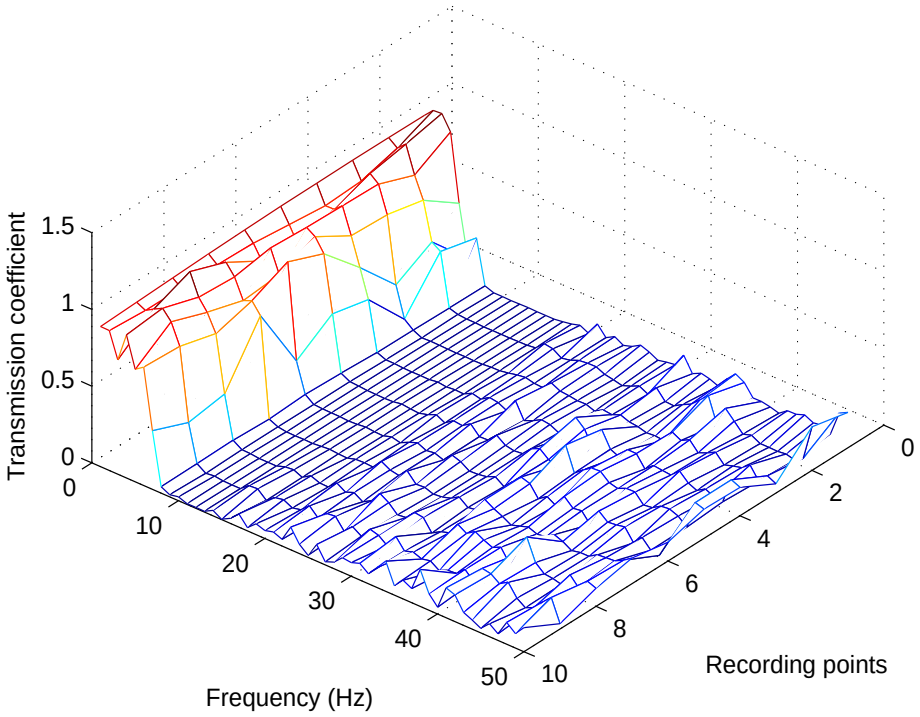

Figure 4.35: Simulation results of wave propagating through the *randomness* circle inclusion material

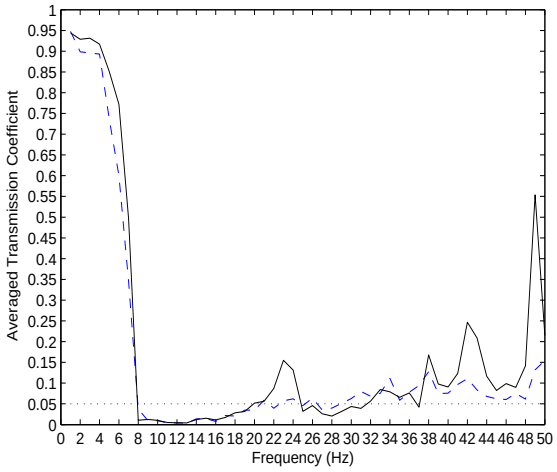

Figure 4.36: Averaged results of wave propagating through the *randomness* circle inclusion material (Solid line: *deterministic* circle inclusion material; Dashed line: *randomness* circle inclusion material; Point dashed line: indicates the position of 5% along frequency)

4.5 Stop band simulation based on gradient elasticity

The gradient elasticity theory can be applied to 2D material as well. The gradient theory has been discussed in detail in Chapter 3. As introduced in Chapter 3, gradient elasticity can be expressed in different forms, based on varying applications. Here, in this section, to simulate the wave propagation, the gradient theory formulation suggested by Eringen [93] was applied, as in Chapter 3.

Because the simulation was based on the gradient elasticity, the testing material had to be homogenised. The testing material is homogenised from the heterogeneous material used in Section 4.2, which was a periodic *chess board* microstructure. The Young's modulus of the homogenised material was the harmonic mean [see Eq. (3.23)] of the Young's modulus of the two components in the heterogeneous material used in Section 4.2 (*deterministic* material). The density of the homogenised material was the arithmetic mean [see Eq. (3.22)] of the density of the two components in the heterogeneous material used in Section 4.2 (*deterministic* material). The length scale was chosen to be 2 mm (the length of the unit cell), which, in the 2D sample, included 4 square units: 2 black square units and 2 white square units.

The simulation process is introduced in Section 4.1. The loading and the testing frequencies were the same as in the *deterministic* case (see Section 4.2). The simulation results are shown in Figure 4.37.

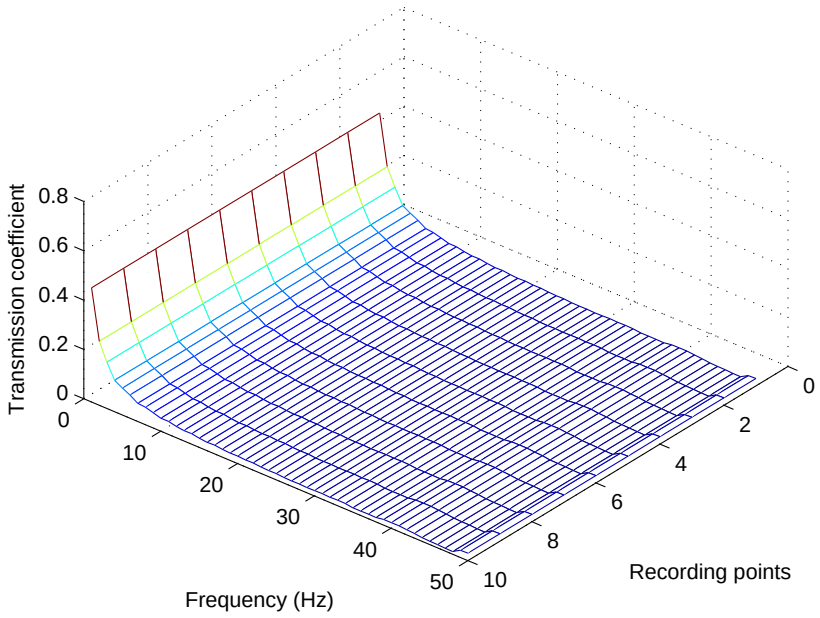

Figure 4.37: Simulation results of wave propagating through the homogenised material with gradient elasticity

The simulation results shown in Figure 4.37 indicate that, at each frequency at each

reference recording point, the transmission coefficient was the same, which is due to the testing material being homogenised. The transmission coefficient decreased with the increasing of frequency at low frequency range and stayed at a very low level (less than 5%) beyond 12 Hz. Note here, that, as discussed in Chapter 3, the artifacts of the gradient elasticity approach led to the possibility of only capturing the first stop band.

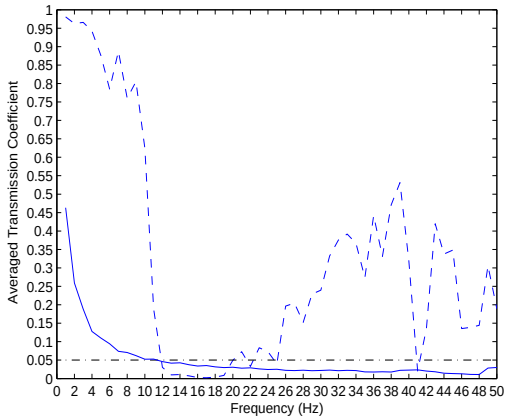

Figure 4.38: Averaged results of wave propagating through the homogenised material with gradient elasticity (Solid line: material with gradient elasticity; Dashed line: *deterministic* material with classical elasticity; Point dashed line: indicate the position of 5% along frequency)

The simulation results was compared with the *deterministic* case based on classical elasticity. The compared results are shown in Figure 4.38. The results indicate that simulations based on the gradient elasticity are capable of predicting the lower bound of the stop band (12 Hz in this case) but unable to simulate the wave propagation in the second pass band (from 19 Hz to 50 Hz). This compared result is consistent with the simulation results based on 1D material introduced in Section 3.5.

4.6 Results and discussion

In this chapter, the wave propagation was studied in 2D material from the position of the stop band phenomenon. The finite element method has been applied to study the influence of heterogeneous material on wave propagation. The study started with heterogeneous material with periodic *chess board* shape microstructure constructed with two different material phases. Then the influence of randomness added to the heterogeneous material on the stop band was studied. Because the randomness added into the material's mechanical property only had a limited influence on the stop band (see Section 2.6), in this chapter, randomness was added only into the material's geometrical properties. Two types of randomness were studied in this chapter, *small perturbation* and *Fibonacci* type randomness (or *semi-random* material). The influence of the shape difference of inclusion on the stop band has also been studied for the deterministic definition of inclusions and random (small perturbation) inclusions.

Additionally, the influence of randomness added into different shapes of inclusion was studied (see Section 4.4). Finally, the finite element method was applied to simulate a wave propagating through homogenised material with gradient elasticity.

All simulations were performed on a rectangular sample, as shown in Figure 4.1. The sample was divided into three parts and, for different tests, the material in Part C varied accordingly. A continuous longitudinal harmonic wave was initiated on the left Part B as input signal. In right Part B, ten reference recording points were chosen to represent the displacement distribution. The test frequency range was chosen to be the same for different materials, ranging from 1 Hz to 50 Hz. The input signal was similar for all tests. These set-ups ensured that the simulation results based on different materials were comparable to each other.

The simulation based on periodic *chess board* layout material, is denoted as the *deterministic* case, because no randomness was added into this material. Simulation results indicate that the stop band existed when wave propagated through such periodic *chess board* layout material (see Figure 4.3). At low frequencies, the transmission coefficients at all reference recording points were approximately 1, which signifies that the material had a limited influence on a wave with a long wavelength. At stop band frequencies, the transmission coefficient at all reference recording points was lower than 5% which means that the wave cannot propagate through the material. At other frequencies, the transmission coefficients at different recording points were different because of the counteracting or overlap effect of the waves. The transmission coefficient at all reference recording points can be averaged to gain a value denoted as average transmission coefficient at each frequency. This cannot strictly define the frequency as located at the stop band, but it can show the trend of transmission coefficient changes along the frequency range. Furthermore, this parameter can be used while comparing different cases.

The influence of randomness on wave propagation with 2D material was also studied in this chapter. Two types of randomness were introduced and since the material was analysed here in 2D, both types of randomness were added in three different ways: only in the horizontal direction (the same direction as the input signal), only in the vertical direction (perpendicular to the input signal) and in both horizontal and vertical directions. The first type of randomness is *small perturbation* randomness which adds randomness into the length of each unit square in the microstructure following normal distribution. The second type of randomness is *Fibonacci*-type randomness which contains two parts of different lengths, but with random positions. Two cases of *Fibonacci*-type randomness have been considered, based on different levels of randomness; they are denoted here as *large Fibonacci* and *small Fibonacci*.

The average transmission coefficients of *small perturbation* randomness in the horizontal direction case and the *small Fibonacci* randomness in the horizontal direction case were compared and this comparison is shown in Figure 4.39. The results indicate that the influence of both types of randomness was roughly the same on wave propagation. Comparing *small perturbation* randomness in the vertical direction case and *small*

Fibonacci randomness in the vertical direction case gives the same conclusion as comparing *small perturbation* randomness in both the horizontal and vertical directions case, and *small Fibonacci* randomness in both the horizontal and vertical directions case. All three comparisons indicate that, with a similar level of randomness, the *small Fibonacci* randomness can represent *small perturbation* randomness well in 2D material.

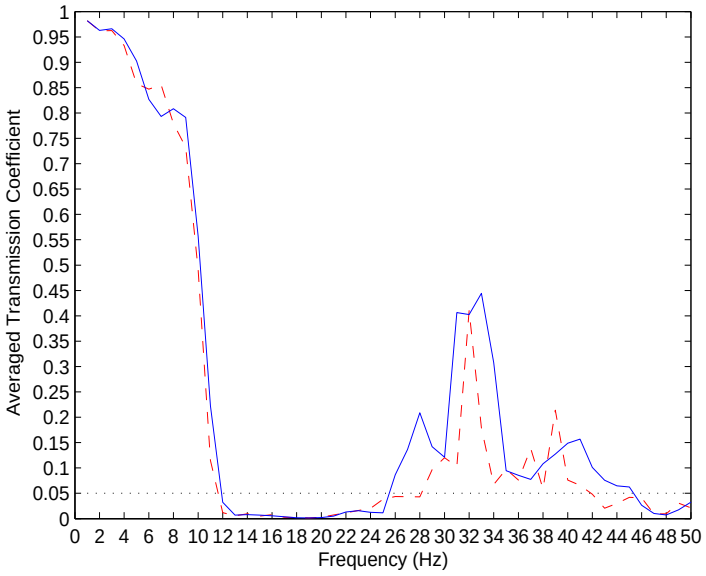

Figure 4.39: Influence of randomness in horizontal direction in 2D material on wave propagation with *small perturbation* randomness and *small Fibonacci* randomness (Solid line: *small Fibonacci* randomness case; Dashed line: *small perturbation* randomness case; Dotted line: indicate the position of 5% along frequency)

The average transmission coefficients of the *deterministic* case, *small perturbation* randomness in the horizontal direction case and *large Fibonacci* randomness in horizontal direction case were compared and are shown in Figure 4.40. The results indicate that compared to the *deterministic* case:
a) The randomness of both types added to the horizontal direction only have limited influence at the low frequency range and do not change the lower bound of the stop band.
b) The randomness of both types added into the horizontal direction extend the stop band.
c) The randomness of both types added into the horizontal direction reduced the averaged transmission coefficient significantly at high frequency (from 36 Hz to 50 Hz).

The average transmission coefficient was reduced by more in the *large Fibonacci* randomness case than the *small perturbation* case, from 26 Hz to 31 Hz. The complete trend showed that *large Fibonacci* randomness has a more significant influence on wave propagation compared to *small perturbation* randomness when they are added in a horizontal direction.

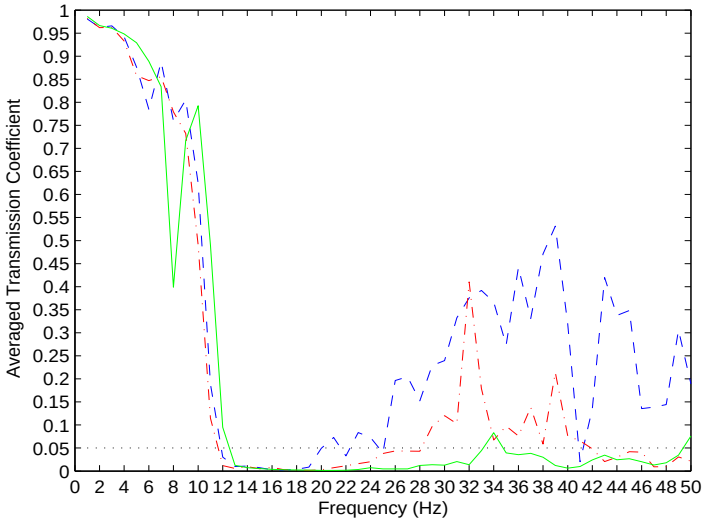

Figure 4.40: Influence of randomness in horizontal direction in 2D material on wave propagation (Solid line: *large Fibonacci* randomness case; Point dashed line: *small perturbation* randomness case; Dashed line: *deterministic* case; Dotted line: indicate the position of 5% along frequency)

The average transmission coefficients of the *deterministic* case, *small perturbation* randomness and *large Fibonacci* randomness in the vertical direction case were compared and are shown in Figure 4.41. The results indicate that compared to the *deterministic* case:
a) The randomness of both types added to the vertical direction reduced the average transmission coefficient at the mid and high frequency range (from 20 Hz to 50 Hz) to the same level.
b) The randomness of both types added into the vertical direction decreased the averaged transmission coefficient for the low frequency range from 6 Hz to 11 Hz.

The *large Fibonacci* randomness in the vertical direction case had more influence on wave propagation at the low frequency range (from 1Hz to 15Hz) compared to *small perturbation* randomness in the vertical direction case. The influence of both randomness types on wave propagation at mid and high frequency ranges was similar.

The average transmission coefficients of the *deterministic* case, *small perturbation* randomness, and *large Fibonacci* randomness in both horizontal and vertical directions cases are compared in Figure 4.42. The results indicate that compared to the *deterministic* case:
a) The randomness of both types added into both horizontal and vertical directions reduced the averaged transmission coefficient to around 5% from 20 Hz to 50 Hz, which means that both types of randomness roughly removed the second pass band.
b) The randomness of both types added into both horizontal and vertical directions reduced the averaged transmission coefficient slightly at the low frequency range (from 1 Hz to 11 Hz).

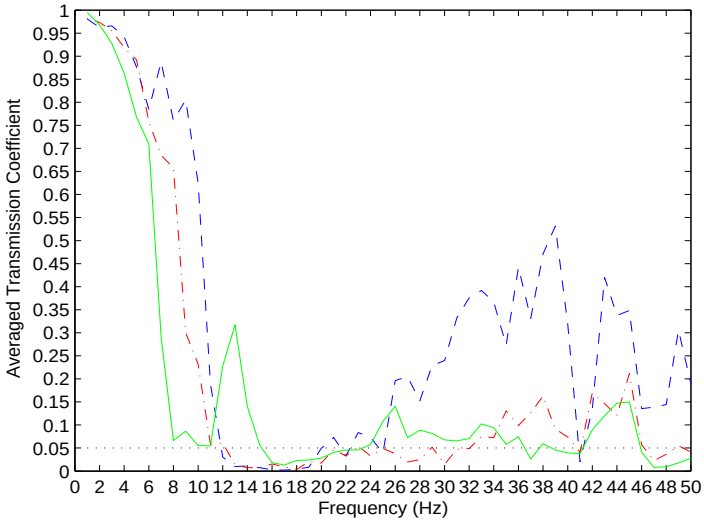

Figure 4.41: Influence of randomness in vertical direction in 2D material on wave propagation (Solid line: *large Fibonacci* randomness case; Point dashed line: *small perturbation* randomness case; Dashed line: *deterministic* case; Dotted line: indicate the position of 5% along frequency)

c) The *large Fibonacci* randomness in both the horizontal and vertical directions case changed the stop band to a pass band at a frequency range from 12 Hz to 15 Hz, but the *small perturbation* randomness in both the horizontal and vertical directions case extended the stop band.

Based on a comparison of the results of three different directions (horizontally, vertically and in both directions) of *small perturbation* randomness and *large Fibonacci* randomness added into material, it is fair to say that *large Fibonacci* randomness had a greater influence than *small perturbation* randomness on wave propagation.

The average transmission coefficients of the *deterministic* case and the three ways of *small perturbation* randomness added into 2D material were compared and are shown in Figure 4.43. Thus:

- The averaged transmission coefficient of randomness added into the vertical direction has the same trend as randomness added into both horizontal and vertical directions at low frequency (below 12 Hz).
- The influence of randomness added to the horizontal direction is larger compared to randomness added to the vertical direction in the mid frequency range (from 26 Hz to 33 Hz).
- The influence of randomness added to the vertical direction is larger compared to randomness added to the horizontal direction in the high frequency range (42 Hz to 50 Hz).
- Randomness added into both horizontal and vertical directions has the greatest

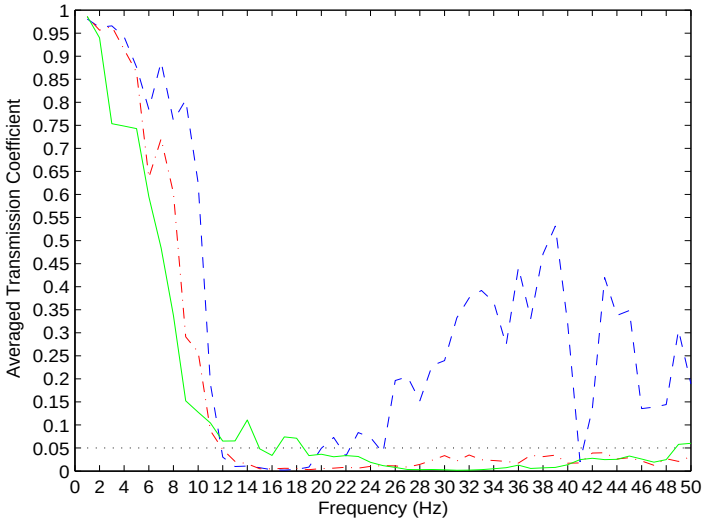

Figure 4.42: Influence of randomness in both horizontal and vertical directions in 2D material on wave propagation (Solid line: *large Fibonacci* randomness case; Point dashed line: *small perturbation* randomness case; Dashed line: *deterministic* case; Dotted line: indicates the position of 5% along frequency)

influence on wave propagation, because the second pass band was almost removed in this case.

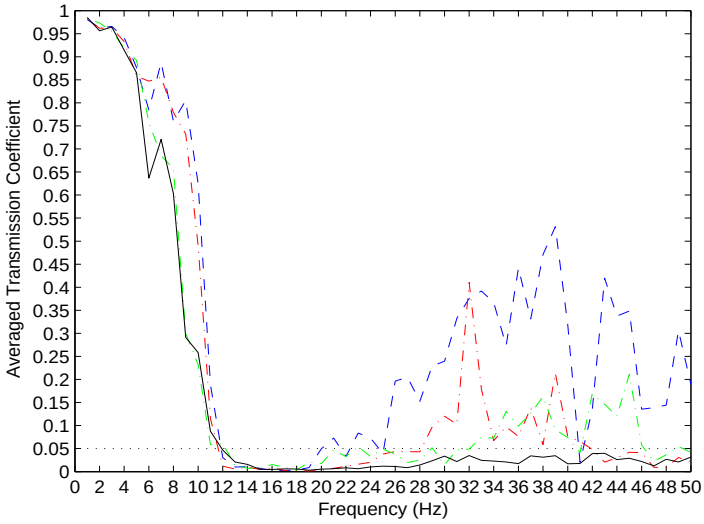

Figure 4.43: Influence of *small perturbation* randomness 2D material on wave propagation (Black solid line: randomness in both horizontal and vertical directions; Red point dashed line: randomness in horizontal direction; Green point dashed line: randomness in vertical direction; Dashed line: *deterministic* case; Dotted line: indicates the position of 5% along frequency)

The average transmission coefficients of the *deterministic* case and three ways of *large Fibonacci* randomness were compared and are shown in Figure 4.44. The results indicate that:

- Randomness added to the horizontal direction had more influence on wave propagation in the mid to high frequency range (from 19 Hz to 50 Hz).
- Randomness added to the vertical direction had more influence on wave propagation in the low frequency range (from 1 Hz to 18 Hz).

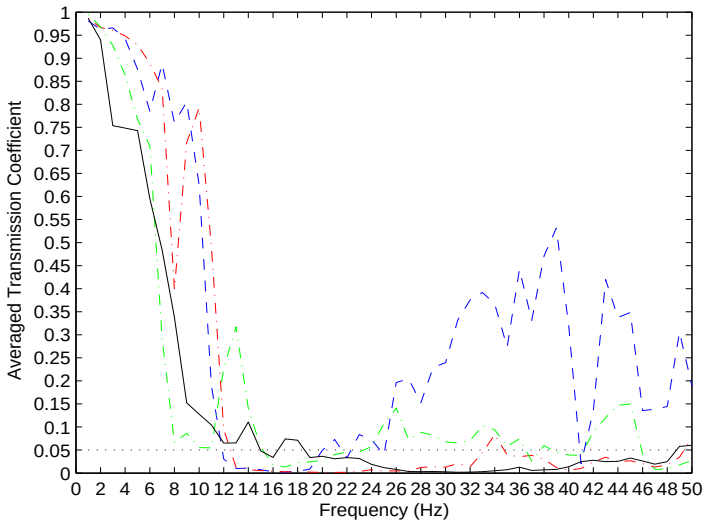

Figure 4.44: Influence of *large Fibonacci* randomness 2D material on wave propagation (Black solid line: randomness in both horizontal and vertical directions; Red point dashed line: randomness in horizontal direction; Green point dashed line: randomness in vertical direction; Dashed line: *deterministic* case; Dotted line: indicates the position of 5% along frequency)

The average transmission coefficients of *small perturbation* randomness in both the horizontal and vertical directions case and in the random circle inclusion case, were compared and are shown in Figure 4.45. The reason for comparing these two cases is that, when randomness is added to the radius, the volume fraction of Material A approaches the volume fraction of Material A in the "chess board" material, with randomness added in the form of a small perturbation in both directions. The randomness levels in these two cases are similar as well; i.e. the mean diameter of circular inclusions and mean length of the squares in the "chess board" are the same. Additionally, the standard deviation σ of the circular diameters matches the standard deviation of the squares. Hence, these two cases have a similar microstructure (mechanical properties and inclusion position arrangement) but with a different inclusion shape. The results indicate that:
a) The stop band occurs at different frequencies in these two cases, which means the shape of the inclusion can significantly influence the stop band.

b) The transmission coefficient remains at a low level (around 5%) since the stop band occurrence means that randomness can reduce the transmission coefficient to a certain level, despite the difference in the shape of the inclusion. Hence, it can be concluded that

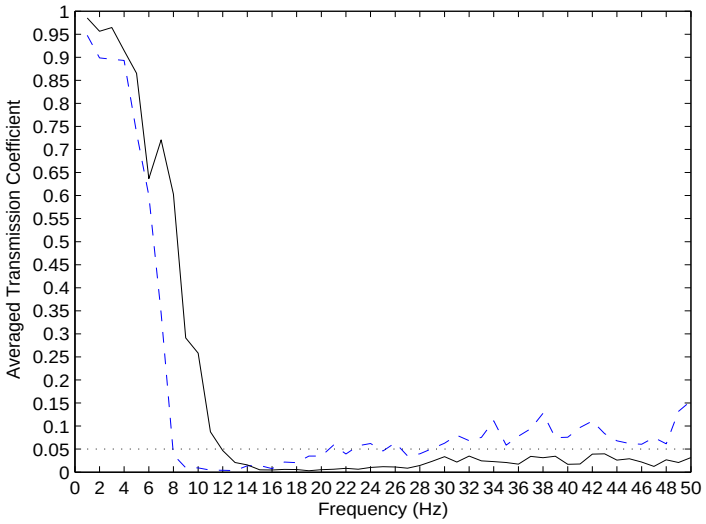

Figure 4.45: Influence of inclusion shape difference with randomness on wave propagation (Solid line: *small perturbation* randomness case; Dashed line: *randomness* circle inclusion case; Dotted line: indicates the position of 5% along frequency)

randomness in a direction perpendicular to the wave propagation front is more significant than randomness in the direction parallel to the wave propagation front in the low frequency range. Furthermore, randomness added into both horizontal and vertical directions can practically remove the second pass band even with a low level of randomness.

The gradient elasticity formulation for the 2D material has also been analysed from the position of wave propagation. The simulation process was the same as the *deterministic* case but with homogenised material. The simulation result is shown in Figure 4.37, and the result at each frequency was averaged and compared to the *deterministic* case (shown in Figure 4.38). The results indicate that the gradient elasticity formulation can predict the lower bound of the stop band but cannot predict the second pass band. This result is consistent with the stop band prediction based on gradient elasticity in the 1D case.

Chapter 5

Conclusions

In this study, analysis of wave propagation through a heterogeneous material with periodic and random microstructure situation was performed from the position of the stop band phenomenon. The finite element method was used to simulate the wave propagation, here a longitudinal wave propagating through a finite domain of a medium. Stop or pass bands were predicted, based on the value of a transmission coefficient which links the amplitudes of initial wave and the wave after it had passed through the medium domain. The gradient elasticity theory was introduced in this study and applied to predicting the stop band both analytically and numerically for the first time.

The study started with a wave propagating through 1D periodic laminate material. The laminate material has two components. The influence of the Young's modulus and mass density contrast of the two components on the stop band was analysed. The simulation results indicated that:

- a) By increasing the Young's modulus contrast of the two material phases, the frequency of the lower bound of the first stop band becomes lower and the transmission coefficient in the pass band drops;
- b) By increasing the density contrast of the two material phases, the width of the first stop band increases and the transmission coefficient associated with the second pass band decreases.

The study also focussed on the laminate material where the whole sample length was kept the same, but the unit cell size inside was varied. It was found that increasing the unit cell length whilst keeping the test specimen fixed gives rise to a stop-band at a lower frequency.

Following the analysis of the wave propagation in the *periodic* 1D laminate material, different levels of *randomness* were added to the laminate material in terms of both mechanical and geometrical properties. The simulation results suggest that when randomness is added to the material's mechanical properties, with different levels of randomness, the influence on the stop band is minor. However, when the randomness is added to a material's geometrical properties, even in the form of a small perturbation, the influence on the stop band is significant. With randomness added to the material's geometrical properties, the transmission coefficient in the second pass band was reduced

significantly and even changed into a stop band at some frequencies. When increasing the level of randomness, to avoid extremely large or small unit cells being generated, a *"Fibonacci"* randomness was introduced and named *"semi-random"*. This material can significantly reduce the transmission coefficient in the second pass band frequency range but retains a similar transmission coefficient in another frequency range compared to the *periodic* case. The picture changes, when analysing "*fully-random*" material; for some frequencies, the stop band turned into a pass band (although the transmission coefficient remained at a low level).

In this study, gradient theory was introduced and applied to predict the stop band, in a novel manner. Three different forms of gradient elasticity were discussed and dispersion analysis was performed based on these three methodologies. The dispersion analysis showed the stop band prediction potential of the gradient theory. The gradient theory was then applied to predict the stop band analytically for 1D homogenised material and the result showed good agreement with simulation results, based on classical elasticity with periodic laminate material. The gradient elasticity was applied to simulate the wave propagation in both 1D and 2D material as well. The simulation results also agreed well with simulation results based on periodic material.

The wave propagating through 2D material was researched in this study as well. Finite element simulation was used to test wave propagation through periodic 2D material with a "*chess board*" microstructure, **microstructure with circle inclusions**, and 2D materials with introduced randomness. Different levels of randomness were added to the material with "*chess board*" configuration in three ways:

- only in the horizontal direction;
- only in the vertical direction;
- in both horizontal and vertical directions.

The material with circular inclusions had randomness added to the radius of circles. The randomness was added into the material with "*chess board*" microstructure in two ways: one was set at the length of the unit cell following normal distribution ("*small perturbation* randomness") and another was picked from the parts off the "*Fibonacci bar*" ("*Fibonacci* randomness"). The levels of "*Fibonacci* randomness" were considered as follows:

- Lower levels of randomness are called "*small Fibonacci* randomness" which is equivalent to "*small perturbation* randomness".
- Higher levels of randomness are called "*large Fibonacci* randomness".

The simulation results of 2D material with "*a chess board*" microstructure indicate that the influence of "*small perturbation* randomness" and "*small Fibonacci* randomness" on wave propagation is similar in all three "*chess board*" configurations. Bringing together the simulation results, the following conclusion can be drawn:

1) With different levels of randomness added to the horizontal direction of the 2D material with "*chess board*" microstructure,

a) The stop band is extended.

b) The average transmission coefficient is reduced significantly at high frequency.

c) The "*large Fibonacci* randomness" has a larger influence on wave propagation compared to "*small perturbation* randomness".

2) With different levels of randomness added to the vertical direction of the 2D material **with "*chess board*" microstructure**,

a) The average transmission coefficient was reduced at the mid and high frequency range.

b) The average transmission coefficient was decreased at low frequency range.

3) With different levels of randomness added to both horizontal and vertical directions of the 2D material **with "*chess board*" microstructure**,

a) The second pass band is practically removed.

b) The averaged transmission coefficient is reduced slightly in the low frequency range.

c) The "*large Fibonacci* randomness" changed the stop band into a pass band, but the "*small perturbation* randomness" extended the stop band.

After comparing the simulation results gained from the same type of randomness added to 2D material **with "*chess board*" microstructure** in different ways, it can be concluded that randomness in the direction perpendicular to the wave front is more significant than randomness in the direction coinciding to front propagation at low frequency range.

The simulation results of the 2D material with circle inclusion in the microstructure compared to the simulation results of the 2D material with "*chess board*" microstructure indicate that the stop band exists in the composite material with different shapes of inclusion but the stop band range is different. The simulation results of randomness added to 2D material with circle inclusion in the microstructure compared to the simulation results of "*small perturbation* randomness" added to both horizontal and vertical directions of the 2D material with "*chess board*" microstructure indicated that randomness can maintain the transmission coefficient at a low level at medium and high frequency range despite the shape difference of the inclusion but the starting point of the stop band is different due to the shape difference of the inclusion.

The aims and objectives of this thesis were to analyse and be able to control the wave propagation through heterogeneous materials. These were met and an extensive list was complied, with information on the different material properties (periodic, random at

different degrees) and their influence on wave propagation.

After wave propagation behaviour in the heterogeneous material is understood, material with a stop band can be designed for specific requirements. For example, if a designer needs a 1D laminate material with large stop band, the density contrast between the two counterparts in the laminate material should be designed to be large enough.

Chapter 6

Future work

As a possible follow up to the current research, potential extensions of the work could be located in these areas: study the wave propagation in the 2D composite material with different shapes of inclusions; introduce randomness to the 2D composite material and study the influence of it with different shapes of inclusions; study the wave propagation in the 3D composite material with different shapes of inclusions; and undertake more work on applying gradient elasticity to predict the stop band.

In the present work, wave propagation through 2D composite material with square and circle inclusions was studied. In the future, the study could be carried out with inclusion shapes such as regular triangle, regular hexagon, or other shapes (even irregular shapes). Note that, in the present study, both square inclusions and circle inclusions in the composite material were full parts. In the future, the inclusion in the composite material could be designed to have hollows to test the influence of them on wave propagation. Randomness could be added to the above materials to test their influence to the wave propagation as well.

In the present work, the study has been limited to the 1D and 2D frames, but it could be extended to 3D in the future. With one more dimension, the simulation process will be more complicated and time consuming but the simulation results will carry more information as well. In 3D, the study could begin with wave propagation through composite material with regular shape inclusions periodically arranged in the material. Then randomness could be added to the composite material to test its influence on wave propagation. Similar to 2D, the shape of the inclusion could be different as well.

The gradient elasticity applied in the present work can only predict the first stop band frequency. It may be possible to predict second or other stop bands by adding higher-order space and/or time gradients into the gradient elasticity formulation. This work will be conducted in the future as well.

Bibliography

[1] L. Brillouin. *Wave propagation in periodic structures*. McGraw-Hill, 1946.

[2] Kushwaha M.S.; Halevi P.; Dobrzynski L. and Djafari R.B. Acoustic band structure of periodic elastic composites. *Phys. Rev. Lett.*, 71:2022–2025, 1993.

[3] Sigalas M.M. and Economou E.N. Elastic waves in plates with periodically placed inclusions. *J. Appl. Phys.*, 75:2845–2850, 1994.

[4] Vasseur J.O.; Djafari R.B.; Dobrzynski L.; Kushwaha M.S. and Halevi P. Complete acoustic band gaps in periodic fibre reinforced composite materials: the carbon/epoxy composite and some metallic systems. *J. phys.:Condens*, 6:8759–8770, 1994.

[5] Sigalas M.; Kushwaha M.S.; Economou E.N.; Kafesaki M.; Psarobas I.E. and Steurer W. Classical vibrational modes in phononic lattices: theory and experiment. *Z. Kristallogr.*, 220:765–809, 2005.

[6] Vasseur J.O.; Deymier P.A.; Chenni B.; Djafari R.B.; Dobrzynski L. and Prevost D. Experimental and theoretical evidence for the existence of absolute acoustic band gaps in two-dimensional solid phononic crystals. *Physical Review Letters*, 86:3012–3015, 2001.

[7] Kushwaha M.S. and Djafari R.B. Sonic stop-bands for periodic arrays of metallic rods: honeycomb structure. *Journal of Sound and Vibration*, 218(4):697–709, 1998.

[8] Vasseur J.O.; Deymier P.A.; Khelif A.; Lambin Ph.; Djafari R.B.; Dobrzynski L.; Akjouj A.; Fettouhi N. and Zemmouri J. Phononic crystal with low filling fraction and absolute acoustic band gap in the audible frequency range: A theoretical and experimental study. *Physical Review Letters*, 65:056608, 2002.

[9] Shen M.R. and Cao W.W. Acoustic band-gap engineering using finite-size layered structure of multiple periodicity. *Appl. Phys. Letters*, 75:3713–3715, 1998.

[10] Kushwaha M.S.; Halevi P. and Martinez G. Theory of acoustic band structure of periodic elastic composites. *Phys. Rev. B*, 49(4):2313–2322, 1994.

[11] Kushwaha M.S. and Halevi P. Band-gap engineering in periodic elastic composites. *Appl. Phys. Lett.*, 64:1085, 1994.

[12] Kushwaha M. S. and Halevi P. Giant acoustic stop bands in twodimensional periodic arrays of liquid cylinders. *Appl. Phys. Lett.*, 69:31, 1996.

[13] Kushwaha M.S. and Djafari-Rouhani B. Complete acoustic stop bands for cubic arrays of spherical liquid balloons. *J. Appl. Phys.*, 80:3191, 1996.

[14] Kushwaha M.S. Stop-bands for periodic metallic rods: Sculptures that can filter the noise. *Appl. Phys. Lett.*, 70:3218, 1997.

[15] Kushwaha M.S. and Halevi P. Ultrawideband filter for noise control. *Jpn. J. Appl. Phys.*, 36:L 1043, 1997.

[16] Kushwaha M.S. and Halevi P. Stop bands for cubic arrays of spherical balloons. *J. Acoust. Soc. Am.*, 101:619, 1997.

[17] Kushwaha M.S.; Djafari-Rouhani B.; Dobrzynski L. and Vasseur J.O. Sonic stop-bands for cubic arrays of rigid inclusions in air. *Eur. Phys. J.*, B3:155, 1998.

[18] Kushwaha M.S.; Akjouj A.; Djafari-Rouhani B.; Dobrzynski L. and Vasseur J.O. Acoustic spectral gaps and discrete transmission in slender tubes. *Solid State Commun*, 106:659, 1998.

[19] Kushwaha M.S. and Djafari-Rouhani B. Giant sonic stop bands in two-dimensional periodic system of fluids. *J. Appl. Phys.*, 84:4677, 1998.

[20] Kushwaha M.S.; Djafari-Rouhani B. and Dobrzynski L. Sound isolation from cubic arrays of air bubbles in water. *Physics Letters*, A248:252, 1998.

[21] Economou E.N. and Sigalas M. Classical wave propagation in periodic structures: Cermet versus network topology. *Phys. Rev.*, B48:13434, 1993.

[22] Economou E.N. and Sigalas M. Stop bands for elastic waves in periodic composite materials. *J. Acoust. Soc. Am.*, 95:1734, 1994.

[23] Kinra V.K.; Henderson B.K. and Maslov K. Elastodynamic response of layers of spherical particals in hexagonal and square periodic arrangement. *J. Mech. Phys Solids*, 47:2147–2170, 1998.

[24] Kinra V.K.; Day N.A.; Maslov K.; Henderson B.K. and Diderich G. The transmissionof a longitudinal wave through a layer of spherical inclusions with random or periodic arrangement. *J. Mech. Phys Solids*, 46:153–165, 1998.

[25] Esquivel-Sirvent R. and Cocoletzi G.H. Band structure for the propagation of elastic waves in superlattices. *J. Acoust. Soc. Am.*, 95:86, 1994.

[26] Henderson B.K.; Maslov K. and Kinra V.K. Experimantal investigation of acoustic band structures in tetragonal periodic particulate composite structures. *J. Mech. Phys Solids*, 49:2369–2383, 2001.

[27] Martinez-Sala R.; Sanchez J.V.; Gomez V.; Llinares J. and Meseguer F. Sound attenuation by sculpture. *Nature*, 378:241, 1995.

[28] Cervera F.; Sanchis L.; Sanchez-Perez J.V.; Martinez-Sala R.; Rubio C. Meseguer F.; Lopez C.; Caballero D. and Sanchez-Dehesa J. Refractive acoustic devices for airborne sound. *Phys. Rev. Lett.*, 88:023902, 2002.

[29] Khelif A.; Choujaa A.; Djafari-Rouhani B.; Wilm M.; Ballandras S. and Laude V. Trapping and guiding of acoustic waves by defect modes in a full-band-gap ultrasonic crystal. *Phys. Rev.*, B68:214301, 2003.

[30] Liu Z.; Chan C.T.; Sheng P.; Goertzen A.L. and Page J.H. Elastic wave scattering by periodic structures of spherical objects: Theory and experiment. *Physhical Review B*, 62(4):2446(12), 2000.

[31] Hodges C.H. and Woodhouse J. Vibration isolation from irregularity in a nearly periodic structure – theory and measurements. *J. Acoust. Soc. Am.*, 74:894, 1983.

[32] He S. and Maynard J.D. Detailed measurements of inelastic scattering in anderson localization. *Phys. Rev. Lett.*, 57:3171, 1986.

[33] Belzons M.; Devillard P.; Dunlop F.; Guazzelli E.; Parodi O. and Souillard B. Localization of surface-waves on a rough bottom – theories and experiments. *Europhys. Lett.*, 4:909, 1987.

[34] Smith D.T.; Lorenson C.P.; Hallock R.B.; McCall K.R. and Guyer R.A. Third sound on substrates patterned with periodic and random disorder: Evidence for classical wave localization. *Phys. Rev. Lett.*, 61:1286, 1988.

[35] D.K. Ziolkowski R.W.; Lewis and Cook B.D. Evidence of localized wave transmission. *Phys. Rev. Lett.*, 62:147, 1989.

[36] Graham I.S.; Piche L. and Grant M. Experimental evidence for localization of acoustic waves in three dimensions. *Phys. Rev. Lett.*, 64:3135, 1990.

[37] Liu J.; Ye L.; Weitz D.A. and Sheng P. Novel acoustic excitations in suspensions of hard-sphere colloids. *Phys. Rev. Lett.*, 65:2602, 1990.

[38] Albada M.P.; van Tiggelen B.A.; Lagendijk A. and Tip A. Speed of propagation of classical waves in strongly scattering media. *Phys. Rev. Lett.*, 66:3132, 1991.

[39] Ye L.; Cody G.; Zhou M.; Sheng P. and Norris A.N. Observation of bending wave localization and quasi mobility edge in two dimensions. *Phys. Rev. Lett.*, 69:3080, 1992.

[40] Zhang S.; Hua J. and Cheng J. Experimental and theoretical evidence for the existence of broad forbidden gaps in the three-component composite. *Chin. Phys. Lett.*, 20(8):1303–1305, 2003.

[41] Condat C.A. and Kirkpatrick T.R. Third-sound propagation on a periodic substrate. *Phys. Rev.*, B32:4392, 1985.

[42] Sheng P. and Zhang Z. Q. Scalar-wave localization in a two-component composite. *Phys. Rev. Lett.*, 57:1879, 1986.

[43] Condat C.A. and Krikpatrick T.R. Observability of acoustical and optical localization. *Phys. Rev. Lett.*, 58:226, 1987.

[44] Condat C.A. and Krikpatrick T.R. Acoustic localization and resonant scattering. *J. Acoust. Soc. Am.*, 83:441, 1988.

[45] Feng S.; Kane C.; Lee P.A. and Stone A.D. Correlations and fluctuations of coherent wave transmission through disordered media. *Phys. Rev. Lett.*, 61:834, 1988.

[46] Makivic M.; Trivedi N. and Ullah S. Disordered bosons: Critical phenomena and evidence for new low energy excitations. *Phys. Rev. Lett.*, 71:2307, 1993.

[47] Nisamaneephong P.; Zhang L. and Ma M. Gaussian theory of superfluid-bose-glass phase transition. *Phys. Rev. Lett.*, 71:3830, 1993.

[48] Dong H. and Xiong S. Acoustic properties of a layered medium with randomly distributed layer thicknesses. *J. Phys.: Condens. Matter*, 5:8849, 1993.

[49] Weaver R.L. Anderson localization in the time domain: Numerical studies of waves in two-dimensional disordered media. *Phys. Rev.*, B49:58881, 1994.

[50] Sheng P.; Zhou M. and Zhang Z.Q. Phonon transport in strongscattering media. *Phys. Rev. Lett.*, 72:234, 1994.

[51] Nakashima K.; Biwa S. and Matsumoto E. Elastic wave transmission and stop band characteristics in unidirectional composites. *Journal of Solid Mechanics and Materials Engineering*, 2:1195–1206, 2008.

[52] James R.; Woodley S.M.; Dyer C.M. and Humphrey V.F. Sonic bands, bandgaps, and defect states in layered structures-theory and experiment. *J. Acoust. Soc. Am.*, 97:2041–2047, 1995.

[53] Vasseur J.O.; Deymier P.A.; Frantziskonis G.; Hong G.; Djafari-Rouhani B. and Dobrzynski L. Experimental evidence for the existence of absolute acoustic band gaps in two-dimensional periodic composite media. *J. Phys.: Condens. Matter*, 10:6051C6064, 1998.

[54] Robertson W.M. and Rudy J.F. Measurement of acoustic stop bands in two-dimensional periodic scattering arrays. *J. Acoust. Soc. Am.*, 104:694C699, 1998.

[55] Montero de Espinoza F.R.; Jimenez E. and Torres M. Ultrasonic band gap in a periodic two-dimensional composite. *Phys. Rev. Lett.*, 80:1208C1211, 1998.

[56] Torres M.; Montero de Espinoza F.R.; Garcia-Pablos D. and Garcia N. Sonic band gaps in finite elastic media: Surface states and localization phenomena in linear and point defects. *Phys. Rev. Lett.*, 82:3054C3057, 1999.

[57] K. Maslov and V. K. Kinra. Acoustic response of a periodic layer of nearly rigid spherical inclusions in an elastic solid. *J. Acoust. Soc. Am.*, 106:3081C3088, 1999.

[58] Maslov K.; Kinra V.K. and Henderson B.K. Lattice resonances of a planar array of spherical inclusions: An experimental study. *Mechanics of Materials*, 31:175C186, 1999.

[59] Lu Y.Q.; Zhu Y.Y.; Chen Y.F.; Zhu S.N.; Ming N.B. and Feng Y.J. Optical properties of an ionic-type phononic crystal. *Science*, 284:1822C1824, 1999.

[60] Meseguer F.; Holgado M.; Caballero D.; Benaches N.; Lopez C.; Sanchez-Dehesa J. and Llinares J. Two-dimensional elastic bandgap crystal to attenuate surface waves. *J. Lightwave Tech.*, 17:2196C2201, 1999.

[61] Meseguer F.; Holgado M.; Caballero D.; Benaches N.; Sanchez-Dehesa J.; Lopez C. and Llinares J. Rayleigh-wave attenuation by a semi-infinite two-dimensional elastic-band-gap crystal. *Phys. Rev.*, B59:12169C12172, 1999.

[62] Maslov K.; Kinra V.K. and Henderson B.K. Elastodynamic response of a coplanar periodic layer of elastic spherical inclusions. *Mechanics of Materials*, 32:785C795, 2000.

[63] Torres M.; Montero de Espinoza F.R. and Aragon J.L. Ultrasonic wedges for elastic wave bending and splitting without requiring a full band gap. *Phys. Rev. Lett.*, 86:4282–4285, 2001.

[64] T. Miyashita. Full band gaps of sonic crystals made of acrylic cylinders in air-numerical and experimental investigations. *Jpn. J. Appl. Phys.*, 41:3170C3175, 2002.

[65] J. Sanchis L.; Hakansson A.; Cervera F.and Sanchez-Dehesa. Acoustic interferometers based on two-dimensional arrays of rigid cylinders in air. *Phys. Rev.*, B67:035422, 2003.

[66] Lu T.; Gao G.; Ma S.; Jin F. and Kim T. Acoustic band gaps in two-dimensional square arrays of semi-hollow circular cylinders. *Sci China Ser E-Tech Sci*, 52:303–312, 2009.

[67] Yukihiro T.; Yoshinobu T. and Shin I.T. Band structure of acoustic waves in phononic lattices: Two-dimensional composites with large acoustic mismatch. *Physhical Review B*, 62(11):7387(6), 2000.

[68] Yeh J.Y. and Chen L.W. Wave propagations of a periodic sandwich beam by fem and the transfer matrix method. *Composite Structures*, 73:53–60, 2006.

[69] Cai L. and Patil S. Effects of randomness on band gap formation in models of fiber-reinforced composite panels having quasirandom fiber arrangements. *Journal of Vibration and Acoustics*, 129:663–671, 2007.

[70] Biwa S.; Yamamoto S.; Kobayashi F. and Ohno N. Computitional multiple scattering analysis for shear wave propagation in unidirectional composites. *International Journal of Solids and Structures*, 41:435–457, 2004.

[71] Kobayashi F.; Biwa S. and Ohno N. Wave transmission chatacteristics in periodic media of finite length: multilayers and fiber arrays. *International Journal of Solids and Structures*, 41:7361–7375, 2004.

[72] M.M. Chan C.T.; Datta S.; Yu Q.L.; Sigalas and K.M.; Ho. New structures and algorithms for photonic band gaps. *Physica*, A211:411, 1994.

[73] Chan C.T.; Yu Q.L. and K.M. Ho. Order-n spectral method for electromagnetic waves. *Phys. Rev.*, B51:16635, 1995.

[74] Fan S.; Villeneuve P.R. and Joannopoulos J.D. Large omnidirectional band gaps in metallodielectric photonic crystals. *Phys. Rev.*, B54:11245, 1996.

[75] Mekis A.; Chen J.C.; Kurland I.; Fan S.; Villeneuve P.R. and Joannopoulos J.D. High transmission through sharp bends in photonic crystal waveguides. *Phys. Rev. Lett.*, 77:3787, 1996.

[76] Sigalas M.M.; Biswas R.; Ho K.M.; Soukoulis C.M. and Crouch D.D. Waveguides in three-dimensional metallic photonic band-gap materials. *Phys. Rev.*, B60:4426, 1999.

[77] Clayton R. and Engquist B. Absorbing boundary conditions for acoustic and elastic wave. *Bull. Seism. Soc. Am.*, 67:1529, 1977.

[78] Zhou J. and Saffari N. Absorbing boundary conditions for elastic media. *Proc. R. Soc. London*, Part A 452:1609, 1996.

[79] Zhou J. and Saffari N. Constructing absorbing boundary conditions from prescribed elastic-wave incidences. *Bull. Seism. Soc. Am.*, 87:1324, 1997.

[80] Garcia P.D.; Sigalas M.; Montero E.F.R.; Torres M.; Kafesaki M. and Garcia N. Theory and experiments on elastic band gaps. *Physical Review Letters*, 84(19):4349(4), 2000.

[81] Aifantis E.C. On the role of gradients in the localization of deformation and fracture. *Int. J. Engng. Sci.*, 30:1279–1299, 1992.

[82] Bennett T.; Gitman I.M. and Askes H. Elasticity theories with higer-order gradients of inertia and stiffness for the modelling of wave dispersion in laminates. *Letters in fracture and micromechanics*, 148:185–193, 2007.

[83] Vasseur J.O. and Deymier P.A. Propagation of acoustic waves in periodic and random two-dimensional composite media. *Journal of Materials Research*, 12(8):2207–2212, 1997.

[84] Klaus-Jurgen Bathe. *Finite Element Procedure in Engineering Analysis*. Prentice-Hall, 1982.

[85] Berenger J.P. A perfect match layer for the absorbtion of electromegnetic waves. *Journal of Computional Physics*, 114:185–200, 1994.

[86] A.Cemal Eringen. *Nonlocal Continuum Field Theories*. Springer, 2001.

[87] Toupin R.A. Elastic materials with couple-stresses. *Archive for Rational Mechanics and Analysis*, 11:385–414, 1962.

[88] Muhlhaus H.B. and Oka F. Dispersion and wave propagation in discrete and continuous models for granular materials. *Int. J. Solids Struct.*, 33:2841–2858, 1996.

[89] Mindlin R.D. Micro-structure in linear elasticity. *Archive for Rational Mechanics and Analysis*, 16:51–78, 1964.

[90] Altan B.S. and Aifantis E.C. On some aspects in the special theory of gradient elasticity. *Journal of the Mechanical Behavior of Materials*, 8:231–282, 1997.

[91] Triantafyllidis N. and Aifantis E.C. A gradient approach to localization of deformation. i.hyperelastic materials. *Journal of Elasticity*, 16:225–237, 1986.

[92] Ru C.Q. and Aifantis E.C. A simple approach to solve boundary-value problems in gradient elasticity. *Acta Mechanica*, 101:59–68, 1993.

[93] Eringen A.C. On differential equations of nonlocal elasticity and solutions of screw dislocation and surface waves. *Journal of Applied Physics*, 54:4703–4710, 1983.

[94] Askes H. and Metrikine A.V. Higher-order continua derived from discrete media: continualisation aspects and boundary conditions. *Int. J. Solids Struct.*, 42:187–202, 2005.

[95] Gitman I.M.; Askes H. and Sluys L.J. Representative volume: existence and size determination. *Engineering Fracture Mechanics*, 74:2518–2534, 2007.

[96] Askes H. and Gutierrez M.A. Implicit gradient elasticity. *Int J Numer Methods Eng*, 67:400–416, 2006.

[97] Metrikine A.V. and Askes H. One-dimensional dynamically consistent gradient elasticity models derived from a discrete microstructure. part 1: generic formulation. *European Journal of Mechanics A/Solids*, 21:555–572, 2002.

[98] Gitman I.M.; Askes H. and Aifantis E.C. The representative volume size in static and dynamic micro-macro transitions. *International Journal of Fracture*, 135:L3–L9, 2005.

[99] Askes H. and Aifantis E.C. Gradient elasticity in statics and dynamics: An overview of formulations, length scale identification procedures, finite element implementations and new results. *International Journal of Solids and Structures*, 48:1962–1990, 2011.

[100] Chen W. and Fish J. A dispersive model for wave propagation in periodic heterogeneous media based on homogenization with multiple spatial and temporal scales. *ASME Journal of Applied Mechanics*, 68:153–161, 2001.

[101] Askes H. and Gitman I.M. Review and critique of the stress gradient elasticity theories of eringen and aifantis. *Advances in Mechanics and Mathematics*, 21:203–210, 2010.